



OPEN

Ectopic JAK-STAT activation enables the transition to a stem-like and multilineage state conferring AR-targeted therapy resistance

Su Deng^{1,11}, Choushi Wang^{1,11}, Yunguan Wang^{2,11}, Yaru Xu¹, Xiaoling Li¹, Nickolas A. Johnson¹, Atreyi Mukherji¹, U-Ging Lo³, Lingfan Xu⁴, Julisa Gonzalez¹, Lauren A. Metang¹, Jianfeng Ye⁵, Carla Rodriguez Tirado¹, Kathia Rodarte⁶, Yinglu Zhou⁴, Zhiqun Xie^{1,2}, Carlos Arana⁷, Valli Annamalai¹, Xihui Liu^{1,2}, Donald J. Vander Griend^{1,8}, Douglas Strand^{1,3}, Jer-Tsong Hsieh³, Bo Li^{1,5}, Ganesh Raj^{1,3}, Tao Wang^{1,2} and Ping Mu^{1,9,10}✉

Emerging evidence indicates that various cancers can gain resistance to targeted therapies by acquiring lineage plasticity. Although various genomic and transcriptomic aberrations correlate with lineage plasticity, the molecular mechanisms enabling the acquisition of lineage plasticity have not been fully elucidated. We reveal that Janus kinase (JAK)-signal transducer and activator of transcription (STAT) signaling is a crucial executor in promoting lineage plasticity-driven androgen receptor (AR)-targeted therapy resistance in prostate cancer. Importantly, ectopic JAK-STAT activation is specifically required for the resistance of stem-like subclones expressing multilineage transcriptional programs but not subclones exclusively expressing the neuroendocrine-like lineage program. Both genetic and pharmaceutical inhibition of JAK-STAT signaling resensitizes resistant tumors to AR-targeted therapy. Together, these results suggest that JAK-STAT are compelling therapeutic targets for overcoming lineage plasticity-driven AR-targeted therapy resistance.

Despite the clinical success surrounding targeted therapies directed toward driver oncogenes, resistance to these therapies often emerges quickly, resulting in poor clinical outcomes. One of the most salient examples of this phenomenon is metastatic castration-resistant prostate cancer (mCRPC), whereby resistance to androgen receptor (AR)-targeted therapies occurs rapidly, and subsequent disease progression is often inevitable¹. Several mechanisms have been revealed to confer resistance to AR-targeted therapy, such as restoration of the AR-driven transcriptional program or bypass of AR signaling through the activation of other transcription factors¹. Emerging evidence has demonstrated a third mechanism called lineage plasticity, whereby luminal prostate epithelial cells transition to a lineage-plastic state where survival is no longer dependent on AR². The acquisition of lineage plasticity may result in cells transitioning to a stem cell-like and multilineage state followed by redifferentiation to new lineages or possibly direct transdifferentiation to a different lineage, such as a neuroendocrine (NE)-like lineage².

Lineage plasticity has been observed in mCRPC and is characterized by various genomic and transcriptional aberrations^{3–13}, which parallels examples documented in EGFR-mutant lung adenocarcinoma, estrogen receptor-positive breast cancers and BRAF-mutant melanoma^{14–16}. One example of lineage plasticity-driven resistance occurs in mCRPC with concurrent loss of function of TP53 and

RB1, which is then accompanied by ectopic activation of SOX2 (refs. ^{4,5,17,18}). However, the molecular mechanism that promotes lineage plasticity in many mCRPC subtypes, especially in the context of TP53/RB1 deficiency, is not fully understood. Furthermore, although heterogenous subpopulations have been connected to prostate cancer (PCa) progression and AR therapy resistance^{19–24}, the key survival factor of lineage-plastic and stem-like cells has yet to be defined. Finally, therapeutic approaches targeting lineage plasticity-driven resistance are not currently available, underscoring the unmet clinical urgency to identify druggable targets that drive lineage plasticity.

Here, we reveal that the ectopic activation of Janus kinase (JAK)-signal transducer and activator of transcription (STAT) signaling is required for lineage plasticity-driven AR-targeted therapy resistance in mCRPC with TP53/RB1 deficiency and SOX2 upregulation. Single-cell RNA-sequencing (scRNA-seq) analysis revealed that JAK-STAT signaling is specifically required for AR therapy resistance of subclones expressing stem-like and multilineage transcriptional programs but not for AR therapy resistance of subclones exclusively expressing the NE-like lineage program. We demonstrate that both genetic and pharmaceutical inactivation of key components of the JAK-STAT pathway, including JAK1/JAK2 and STAT1/STAT3, resensitize resistant mCRPC to AR-targeted therapy. Collectively, these findings

¹Department of Molecular Biology, UT Southwestern Medical Center, Dallas, TX, USA. ²Quantitative Biomedical Research Center, Department of Population and Data Sciences, UT Southwestern Medical Center, Dallas, TX, USA. ³Department of Urology, UT Southwestern Medical Center, Dallas, TX, USA.

⁴Department of Pathology, Duke University School of Medicine, Durham, NC, USA. ⁵Lyda Hill Department of Bioinformatics, UT Southwestern Medical Center, Dallas, TX, USA. ⁶Department of Neuroscience, UT Southwestern Medical Center, Dallas, TX, USA. ⁷Wakeland Genomics Core, UT Southwestern Medical Center, Dallas, TX, USA. ⁸Department of Pathology, The University of Illinois at Chicago, Chicago, IL, USA. ⁹Hamon Center for Regenerative Science and Medicine, UT Southwestern Medical Center, Dallas, TX, USA. ¹⁰Harold C. Simmons Comprehensive Cancer Center, UT Southwestern Medical Center, Dallas, TX, USA. ¹¹These authors contributed equally: Su Deng, Choushi Wang, Yunguan Wang. ✉e-mail: ping.mu@utsouthwestern.edu

suggest that JAK–STAT signaling is a crucial executor driving lineage plasticity and could be a potential therapeutic target designed to overcome AR-targeted therapy resistance.

Results

The JAK–STAT pathway is altered concomitantly with TP53, RB1 and SOX2. To investigate the mechanisms of lineage plasticity in TP53/RB1-deficient mCRPC with SOX2 upregulation, we first inquired which transcriptional programs were altered concomitantly with both the loss of TP53 and RB1 and the upregulation of SOX2. By leveraging a series of LNCaP/AR cell lines we have previously—generated⁵, we profiled transcriptomic changes induced by TP53/RB1 deficiency and overexpression of SOX2 in four cell lines (control non-targeting short hairpin RNA (shNT), shTP53/RB1, shTP53/RB1/SOX2 and SOX2 overexpression (SOX2-OE)) before exposure to the AR therapy drug enzalutamide (Enz)²⁵. As expected, these genetic modifications led to global transcriptomic changes, and gene set enrichment analysis (GSEA) revealed significantly altered pathways (Fig. 1a and Supplementary Tables 1–6), including the duality of specific pathways, where they demonstrated upregulation in TP53/RB1 double-knockdown (shTP53/RB1) and SOX2-OE cells and, by contrast, downregulation in TP53/RB1/SOX2 triple-knockdown cells (Fig. 1a). To further decipher which of these transcriptional changes specifically contribute to AR therapy resistance, we investigated signaling pathways enriched following treatment with Enz compared to vehicle (Extended Data Fig. 1a and Supplementary Tables 1–6). Notably, the JAK–STAT signaling pathway was the sole cancer-related pathway that was concomitantly altered with TP53/RB1 loss and SOX2 upregulation (Extended Data Fig. 1b) and was also consistently upregulated in the sgTP53/RB1 Enz-resistant cells (Extended Data Fig. 1c–g). Interestingly, the JAK–STAT pathway was not significantly altered in shNT cells treated with Enz compared to cells treated with vehicle, suggesting that the JAK–STAT pathway has a specific role in the context of TP53/RB1 deficiency (Extended Data Fig. 1a).

JAK–STAT signaling regulates various biological processes, such as embryonic development, immune response, inflammation, cell fate decision, differentiation and hematopoiesis^{26,27}. Notably, numerous lines of evidence implicate JAK–STAT signaling in the regulation of stem cell self-renewal and multilineage differentiation²⁸. The consequence of JAK–STAT activation on tumorigenesis is complicated and considered a ‘double-edged sword’. On one hand, JAK–STAT signaling promotes antitumor immune surveillance and therapy-induced cell death and is associated with a favorable clinical outcome in various cancers^{29,30}. On the other hand, constitutive activation of JAK–STAT signaling has been correlated with poor clinical outcomes in hematological malignancies and many solid tumors, including PCa^{31–42}. In addition, JAK–STAT activation promotes epithelial-to-mesenchymal transition (EMT), invasion and metastasis of PCa^{43–47}, further indicating its role in regulating PCa lineage transition. Thus, the observed ectopic upregulation of JAK–STAT signaling in the TP53/RB1-deficient and SOX2-OE PCa cells raises the intriguing possibility that it may play a crucial role in acquiring lineage plasticity-driven AR therapy resistance.

JAK–STAT signaling is required for lineage plasticity and resistance. To examine the role of JAK–STAT signaling in Enz resistance, we first surveyed a series of PCa cell lines and determined the protein levels of TP53, RB1 and JAK1. Here, we observed a substantial accumulation of JAK1 in all three Enz-resistant cell lines (DU145, PC3 and H660; Extended Data Fig. 2a), which are all characterized by TP53/RB1 deficiency (deletion/mutation), compared to in Enz-sensitive cell lines (LNCaP/AR, CWR22Pc, MDA-PCa-2b, VCaP and CWR22Rv). To further dissect the role of JAK–STAT signaling, we generated a stable sgTP53/RB1 clone by knocking out TP53 and RB1 in LNCaP/AR cells with CRISPR guides *cis* linked

with red fluorescent protein (RFP). These sgTP53/RB1 cells proliferated significantly quicker after exposure to Enz than sgNT cells expressing green fluorescent protein (GFP; Extended Data Fig. 2b,c and Supplementary Fig. 1). sgTP53/RB1 cells displayed clear lineage plasticity, as they express significantly decreased levels of luminal lineage genes and increased levels of non-luminal lineage genes (Extended Data Fig. 2d). We also observed significant upregulation in the expression of canonical JAK–STAT signaling genes in sgTP53/RB1 cells, which was comparable to the levels of JAK–STAT signaling genes induced by SOX2 OE (Fig. 1b). Interestingly, only double knockout (KO) of TP53/RB1, but not individual KO of either TP53 or RB1, led to significant JAK–STAT activation and lineage plasticity (Extended Data Fig. 2e,f), suggesting that TP53 and RB1 cooperatively suppress ectopic JAK–STAT activation.

To determine whether sustained JAK–STAT signaling is required to maintain resistance, we knocked out key JAK–STAT signaling genes in sgTP53/RB1 cells and observed that only KO of JAK1 and STAT1 significantly blunted resistant growth of sgTP53/RB1 cells (Fig. 1c and Extended Data Fig. 3a–c). However, these results did not preclude the possibility that different JAK and STAT proteins may function within a cooperative network to regulate AR-targeted therapy resistance. Therefore, we knocked out various combinations of JAK and STAT proteins in the TP53/RB1 double-KO cells and observed that KO of JAK1 and JAK2 had a significantly more profound effect on inhibiting Enz-resistant growth of PCa cells than KO of JAK1 alone, suggesting a cooperative function of JAK2 and JAK1 in conferring Enz resistance (Fig. 1d). Similarly, KO of STAT1 and STAT3 had a significantly more profound effect on inhibiting Enz-resistant growth than KO of STAT1 alone (Fig. 1d), demonstrating how STAT3 and STAT1 function cooperatively to regulate resistance. These results were further validated in an additional Enz-sensitive PCa cell line, CWR22Pc (Extended Data Fig. 3d,e). Interestingly, KO of JAK–STAT genes in wild-type sgNT cells or in sgTP53/RB1-KO cells treated with vehicle did not influence tumor cell survival (Extended Data Fig. 3f,g), suggesting a specific role of JAK–STAT signaling in lineage plasticity-driven AR therapy resistance. These findings were validated *in vivo* in castrated severe combined immunodeficient (SCID) mice treated with Enz, where the depletion of JAK1 and STAT1 largely resensitized sgTP53/RB1 xenografted tumors to Enz (Fig. 1e,f).

To determine the connection between JAK–STAT signaling and lineage plasticity, we examined the expression of canonical lineage markers in sgTP53/RB1/JAK1 cells, which have suppressed JAK–STAT signaling (Extended Data Fig. 4a,b). We observed that JAK1 depletion largely attenuated the downregulation of AR signaling and the expression of luminal lineage genes (Fig. 2a,b) and upregulation of the expression of stem-like, basal, EMT and NE-like marker genes (Fig. 2c–e), which reinforces its crucial role in the acquisition of non-luminal and multilineage transcriptional programs. Immunofluorescence (IF) staining validated this transition from an exclusively AR-driven luminal lineage to an AR-independent, multilineage state after TP53/RB1 depletion (Extended Data Fig. 4c), which was largely reversed following JAK1 KO (Extended Data Fig. 4c). JAK1 KO also reversed the increased migratory and invasive abilities of sgTP53/RB1 cells (Fig. 2f–i), supporting the necessity of JAK–STAT signaling in the maintenance of an EMT lineage program. Furthermore, JAK1 or STAT1 KO also reversed the enhanced prostasphere formation of sgTP53/RB1 cells (Fig. 2j,k), which corroborates the role of JAK–STAT signaling in promoting a stem-like state.

JAK–STAT activation correlates with poor clinical outcomes. Given the prominent role of JAK–STAT signaling in promoting EMT and AR therapy resistance in our preclinical model, we examined the impact of JAK–STAT upregulation in various clinically relevant models and scenarios. We performed immunohistochemistry

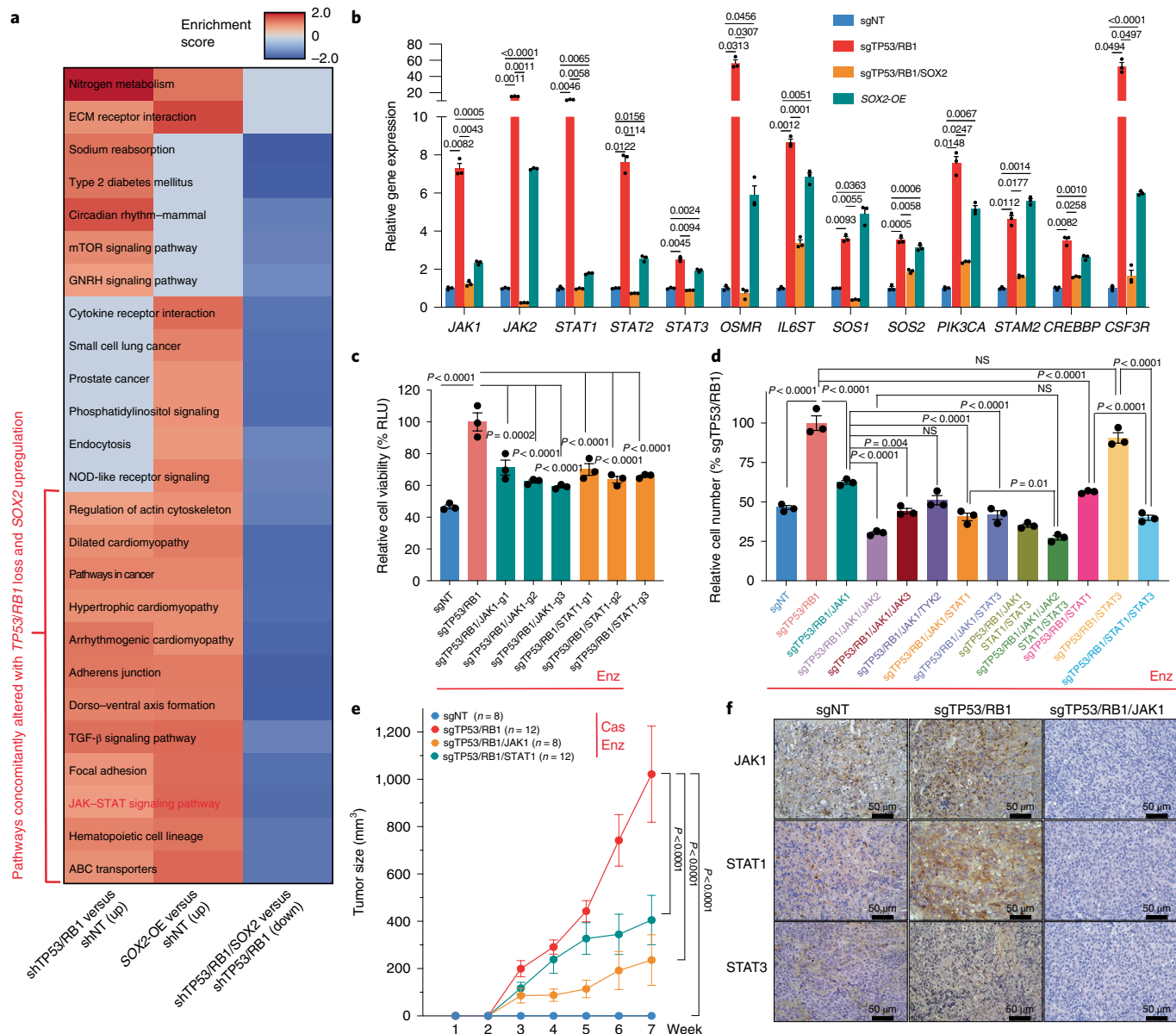


Fig. 1 | JAK-STAT signaling is required for Enz resistance in TP53/RB1-deficient mCRPC. **a**, Heat map representing the significantly changed signaling pathways in LNCaP/AR cell lines transduced with annotated shRNAs based on GSEA analysis. Three comparisons are presented. Reads from $n=3$ independently treated cell cultures in each group were used for analysis. Signaling pathways concomitantly altered with *TP53/RB1* loss and *SOX2* upregulation are labeled with a red bracket. **b**, Relative gene expression of canonical genes activated in the JAK-STAT signaling pathway in LNCaP/AR cells transduced with Cas9 and annotated guide RNAs; $n=3$ independently treated cell cultures. P values were calculated using a two-way ANOVA with a Bonferroni multiple-comparison test. **c**, Relative cell numbers of LNCaP/AR cells transduced with Cas9 and annotated CRISPR guide RNAs. Cells were treated with $10\text{ }\mu\text{M}$ Enz for 8 d, and cell numbers (viability) were measured using a CellTiter-Glo assay, with all values normalized to the sgTP53/RB1 group; $n=3$ independently treated cell cultures. P values were calculated by one-way ANOVA with a Bonferroni multiple-comparison test; RLU, relative light units. **d**, Relative cell numbers of LNCaP/AR cells transduced with Cas9 and annotated CRISPR guide RNAs. Cells were treated with $10\text{ }\mu\text{M}$ Enz for 8 d, and cell numbers (viability) were measured using a CellTiter-Glo assay, with all values normalized to the sgTP53/RB1 group; $n=3$ independently treated cell cultures. P values were calculated by one-way ANOVA with a Bonferroni multiple-comparison test; NS, not significant. **e**, Tumor growth curve of xenografted LNCaP/AR cells transduced with Cas9 and annotated guide RNAs in castrated mice. Cas denotes castration 2 weeks before grafting. Enz denotes Enz treatment at 10 mg kg^{-1} from day 1 of grafting; n = number of independent xenografted tumors in each group (two tumors per mouse); sgNT, $n=8$ tumors; sgTP53/RB1, $n=12$ tumors; sgTP53/RB1/JAK1, $n=8$ tumors; sgTP53/RB1/STAT1, $n=12$ tumors. P values were calculated by two-way ANOVA with a Bonferroni multiple-comparison test. **f**, IHC staining of JAK-STAT proteins on annotated xenografted tumor slides showing representative images of $n=2$ independent tumors.

(IHC) staining of key JAK-STAT proteins in a collection of de-identified human PCa samples and matched benign prostate tissues and validated the substantial augmentation of JAK-STAT signaling in human PCa samples, especially CRPC samples, compared to matched benign tissue (Fig. 3a). Consistent with the IHC results,

human PCa tumor samples exhibited a significant enhancement in the expression of JAK1 and STAT1 compared to that observed in benign tissues (Fig. 3b,c). We then treated seven independent human-derived explants (PDE) and observed an upregulation of JAK1 and STAT1 following Enz treatment (Fig. 3d-f)^{48,49}, further

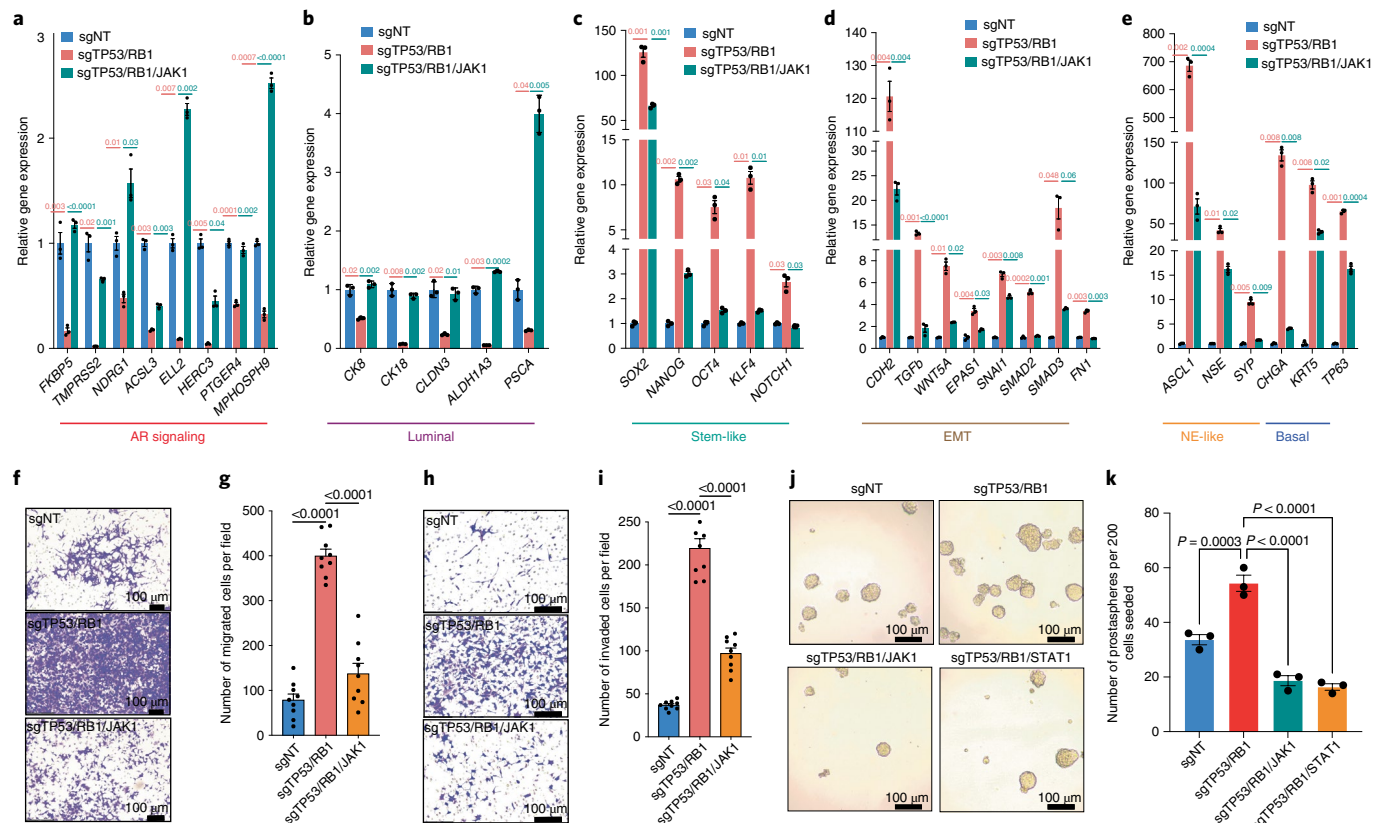


Fig. 2 | JAK1 KO stagnates the lineage transition to a stem-like and multilineage state. **a–e**, Relative expression of canonical AR target genes and lineage marker genes in LNCaP/AR cells transduced with Cas9 and annotated guide RNAs; $n=3$ independently treated cell cultures. P values were calculated by two-way ANOVA with a Bonferroni multiple-comparison test. **f**, Representative images of an LNCaP/AR cell transwell migration assay of three independent treated cell cultures. **g**, Quantification of the migrated cell numbers of nine representative images taken from three independent treated cell cultures for each of the cell lines. P values were calculated by one-way ANOVA with a Bonferroni multiple-comparison test. **h**, Representative images of an LNCaP/AR cell invasion assay of three independent treated cell cultures. **i**, Quantification of the numbers of invading cells of nine representative images taken from three independent treated cell cultures for each of the cell lines. P values were calculated by one-way ANOVA with a Bonferroni multiple-comparison test. **j**, Representative images of an LNCaP/AR cell prostasphere formation assay of three independent treated cell cultures. **k**, Quantification of the prostaspheres formed from three independent treated cell cultures for each of the cell lines. P values were calculated by one-way ANOVA with a Bonferroni multiple-comparison test. Unless otherwise noted, data are represented as mean \pm s.e.m.

demonstrating their role in mediating AR therapy resistance. Next, we investigated two human PCa cohorts (The Cancer Genome Atlas (TCGA) and SU2C) and hypothesized that reduced sensitivity to AR-targeted therapy would correlate with a higher frequency of copy number variations of JAK–STAT genes in mCRPC tumors than in hormone-sensitive primary tumors^{50–52}. Indeed, the frequencies of copy number amplifications and somatic mutations in JAK–STAT signaling genes were significantly higher in mCRPC (SU2C) than in hormone-naïve PCa (TCGA; Extended Data Fig. 5a,b). Finally, we examined both the pathological characteristics and the expression of JAK–STAT signaling genes in the TCGA cohort and discovered that individuals with regional lymph node metastasis (N1) or high-grade tumors (Gleason score of ≥ 8) had significantly higher JAK–STAT signaling gene expression than individuals lacking regional lymph node metastasis (N0) or with low-grade tumors (Gleason score of ≤ 7 ; Extended Data Fig. 5c,d).

To determine whether JAK–STAT signaling is specifically upregulated in human PCa with reduced *TP53/RB1* expression, we performed transcriptomic analysis of an existing human CRPC scRNA-seq dataset²⁴. Among the six individuals of this cohort, we identified two major clusters of PCa cell subpopulations expressing either high or low levels of both *TP53* and *RB1* in participant 1 (CRPC-adeno) and participant 5 (CRPC-NE;

Fig. 3g). Transcriptomic analysis revealed increased expression of JAK–STAT signaling genes, such as *JAK1*, *STAT1* and *IL6ST*, in the *TP53/RB1*-low subpopulation compared to in the *TP53/RB1*-high subpopulation in both individuals (Fig. 3g,h). Strikingly, the *TP53/RB1*-low subpopulations displayed substantially higher expression of stem-like (*TACSTD2*, *ATXN1*, *KRT4* and *CD55*) and EMT (*VIM*, *SNAI2* and *CDH11*) gene and lower AR target (*KLK3*, *PTGER4* and *ACSL3*) gene (Fig. 3g,i–k), which is consistent with the role of JAK–STAT signaling in promoting the transition from an AR-dependent state to an AR-independent, multilineage and stem-like state. Interestingly, an increase in NE-like lineage in the *TP53/RB1*-low cells was only observed in participant 1 (CRPC-adeno) but not in participant 5 (CRPC-NE; Fig. 3g,l). These data indicate that JAK–STAT may be dispensable for tumor cells exclusively expressing NE-like lineage. To further validate whether ectopic JAK–STAT is required for resistance in human PCa, we surveyed a series of three-dimensional (3D)-cultured human-derived organoid (PDO) models (Extended Data Fig. 6a)^{53–55} and observed ectopic upregulation of JAK–STAT signaling genes in PDOs with *TP53/RB1* deficiency (Extended Data Fig. 6b). Among those PDOs, MSKPCa8 and MSKPCa9 belong to a subclass defined by increased stem-like, EMT-like and interferon response-related transcriptional programs^{54,55}. Strikingly, JAK–STAT signaling inhibition

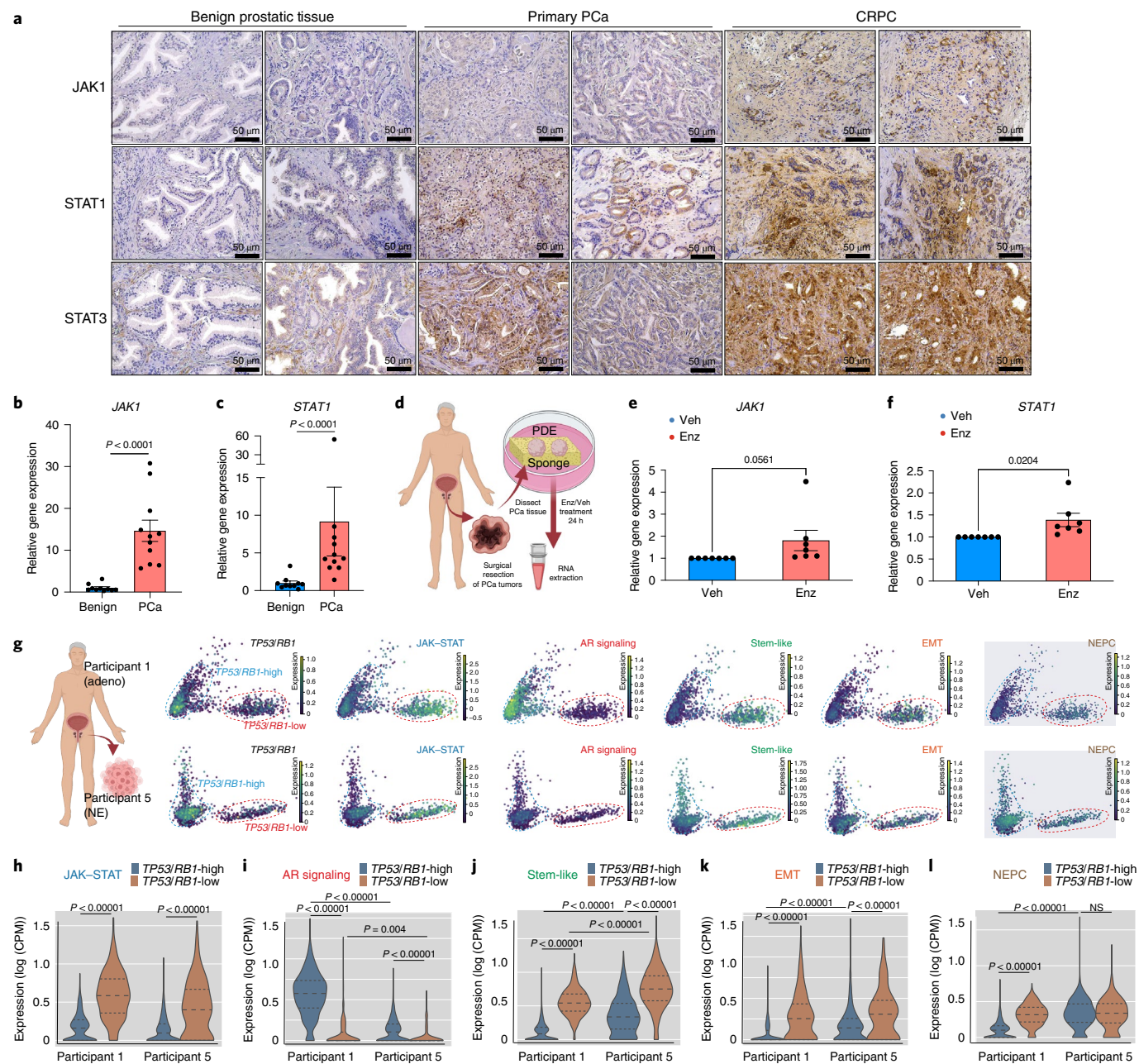


Fig. 3 | Ectopic JAK-STAT activation correlates with poor clinical outcomes. **a**, IHC staining of annotated JAK-STAT proteins on benign prostate tissues or PCa samples; $n=2$ independent tumors in each group. **b,c**, Relative expression of *JAK1* (**b**) and *STAT1* (**c**) in benign prostate tissues or PCa samples. The center line indicates the median, the box limits indicate upper and lower quartiles and the whiskers indicate maximum and minimum values. *P* values were calculated by a two-sided Mann-Whitney test; $n=10$ benign prostate samples; $n=11$ PCa tumors. **d**, Schematic figure representing the generation and examination of the PDE model. The figure was created with BioRender.com; Veh, vehicle. **e**, Relative expression of *JAK1* in a series of PDEs treated with vehicle (DMSO) or Enz (10 μ M) for 24 h. **f**, Relative expression of *STAT1* in a series of PDEs treated with vehicle (DMSO) or Enz (10 μ M) for 24 h. For **e** and **f**, $n=7$ independent PDEs, and data show mean \pm s.e.m. *P* values were calculated by two-sided *t*-test. **g**, Principal-component analysis (PCA) plots of human CRPC biopsy samples; participant 1, $n=2,691$ cells, CRPC-adeno; participant 5, $n=2,123$ cells, CRPC-NE. For each sample, single-cell transcriptomic profiles are colored by the expression (\log_2 CPM) of selected genes representing canonical signaling pathways and lineage-related transcriptional programs. The schematic figure was created with BioRender.com. **h-l**, Violin plots representing the expression scores of canonical JAK-STAT signaling, AR signaling and lineage marker genes in subclones with high versus low *TP53/RB1* expression in both participants 1 and 5. The center line indicates the median, upper and lower lines indicate upper and lower quartiles and violin limits indicate maximum and minimum values; *TP53/RB1*-high: participant 1 $n=2,215$ cells and participant 5 $n=1,796$ cells; *TP53/RB1*-low: participant 1 $n=476$ cells and participant 5 $n=327$ cells. *P* values were calculated by two-sided Mann-Whitney test.

by the JAK1 inhibitor filgotinib (Filg) largely resensitized these Enz-resistant PDOs (Extended Data Fig. 6c,d), supporting the crucial role of JAK-STAT in mediating AR therapy resistance.

JAK1 inhibition reverses lineage plasticity and resistance. Identification of JAK-STAT signaling as a crucial executor of lineage plasticity-driven resistance raises the hope that appropriate

therapeutic approaches targeting this pathway could overcome AR-targeted therapy resistance. Indeed, *in vitro* cell viability assays demonstrated that combination treatment of Filg and Enz significantly inhibited the growth of Enz-resistant sgTP53/RB1 LNCaP/AR cells (Fig. 4a). Dose-response measurements (half-maximum inhibitory concentration (IC_{50})) validated that sgTP53/RB1 cells exhibit less sensitivity to Enz than sgNT cells (Extended Data Fig. 7a), while the sgTP53/RB1 cells are more susceptible to Filg than sgNT cells (Extended Data Fig. 7b). These results were again validated in CWR22Pc cells, where Filg significantly inhibited the growth of Enz-resistant cells and attenuated the upregulation of non-luminal lineage programs (Extended Data Fig. 7c,d). Furthermore, Filg impaired the growth of DU145 and PC3 cells, two Enz-resistant PCa cell lines expressing ectopic levels of JAK1 (Extended Data Fig. 7e,f). These *in vitro* results are further supported by *in vivo* xenograft experiments, as the combination treatment of Enz and Filg stagnated the growth of Enz-resistant sgTP53/RB1 tumors and induced more tumor regression than either drug alone (Fig. 4b).

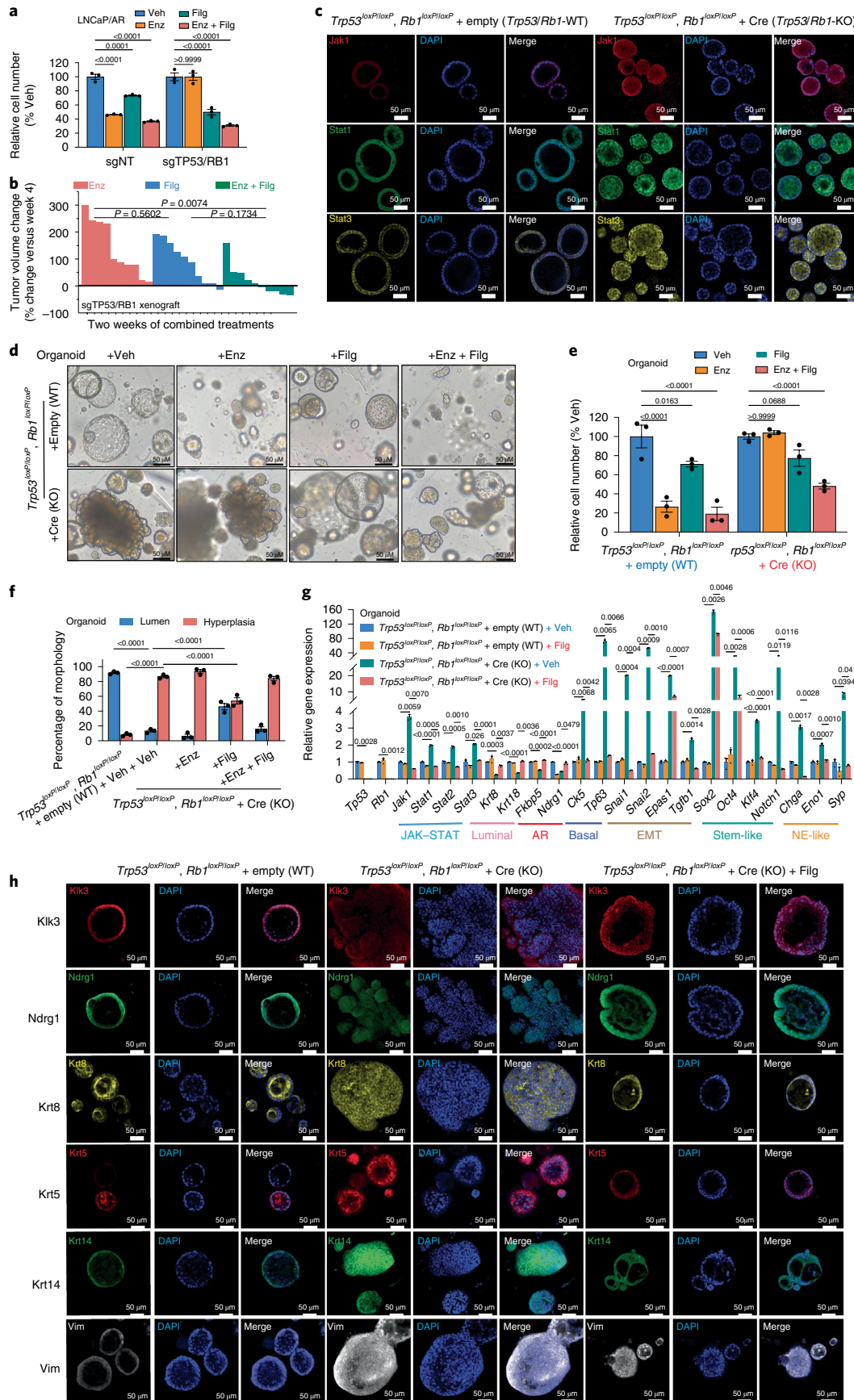
To further explore the effect of JAK1 inhibition in a genetically defined model, we used the previously established mouse prostate organoids derived from *Trp53*^{loxP/loxP}*Rb1*^{loxP/loxP} mice, followed by infection with Cre or empty lentivirus⁵. In contrast to the typical lumen structure, which the *Trp53*^{loxP/loxP}*Rb1*^{loxP/loxP} + empty (*Trp53/Rb1*-wildtype (WT)) organoids formed in 3D culture, *Trp53*^{loxP/loxP}*Rb1*^{loxP/loxP} + Cre (*Trp53/Rb1*-KO) organoids displayed a hyperplastic morphology, where the organoid cells formed a solid ball with protrusive structures invading the surrounding Matrigel (Fig. 4c,d). The *Trp53/Rb1*-KO organoids expressed significantly elevated levels of JAK-STAT proteins compared to *Trp53/Rb1*-WT organoids (Fig. 4c and Extended Data Fig. 8a). Although these *Trp53/Rb1*-KO organoids were significantly more resistant to Enz than *Trp53/Rb1*-WT controls (Fig. 4d,e), they responded well to the combination of Enz and Filg (Fig. 4d,e). Remarkably, we also observed that a substantial number of *Trp53/Rb1*-KO organoids reestablished a classic lumen-like structure when treated with Filg (Fig. 4d,f), indicating that JAK1 inhibition impairs the acquisition of non-luminal programs and restores the luminal program. Consistent with this hypothesis, the percentage of lumen-like organoids in the *Trp53/Rb1*-KO group significantly receded when treated with Enz and Filg (Fig. 4d,f), suggesting that Enz sensitivity was restored in those lumen-like organoids. The reversal of the lineage plasticity within Filg-treated organoids is supported by quantitative PCR (qPCR) results and IF staining, which demonstrated attenuated downregulation of AR and luminal gene expression and upregulation of non-luminal gene expression (Fig. 4g,h and Extended Data Fig. 8b).

As JAK1/JAK2 and STAT1/STAT3 may cooperatively mediate lineage plasticity and resistance (Fig. 1d), we examined the

inhibitory effects of various pharmaceutical inhibitors targeting different JAK and STAT proteins, including ruxolitinib (JAK1/JAK2 inhibitor), fludarabine (STAT1 inhibitor) and niclosamide (STAT3 inhibitor). Interestingly, the dual JAK1/JAK2 inhibitor ruxolitinib had a greater inhibitory effect on *TP53/RB1*-KO cells than Filg (Extended Data Fig. 8c). Similarly, combined administration of fludarabine and niclosamide achieved a more profound inhibitory effect on Enz-resistant growth than fludarabine or niclosamide alone (Extended Data Fig. 8c), supporting the cooperative roles of both JAK1/JAK2 and STAT1/STAT3. To further examine whether JAK-STAT signaling mediates lineage plasticity-driven resistance in a broader fashion, we surveyed a series of xenograft-derived, Enz-resistant cell lines with *CHD1* loss, which display clear lineage plasticity¹², and identified three cell lines with ectopic JAK-STAT signaling (Extended Data Fig. 8d). JAK-STAT inhibition through both Filg and ruxolitinib largely resensitized xenograft-derived resistant cells to Enz (Extended Data Fig. 8e-g), suggesting that PCa cells may hijack JAK-STAT signaling as a general avenue to promote lineage plasticity and resistance.

SOX2 promotes JAK-STAT signaling in a positive feedback fashion. We next sought to reveal the mechanism through which JAK-STAT signaling is upregulated. Interestingly, SOX2 KO in the *TP53/RB1*-deficient cells impaired the upregulation of JAK-STAT signaling genes (Fig. 1b), indicating a critical role of SOX2 in activation of JAK-STAT signaling. SOX2 chromatin immunoprecipitation (ChIP)-qPCR analysis supports this hypothesis by demonstrating a significant augmentation of SOX2 binding at JAK-STAT gene loci in cells with *TP53/RB1* KO or ectopic SOX2 expression (Fig. 5a-d). Consistent with these SOX2 ChIP-qPCR results, an increase in histone 3 lysine 27 (H3K27) acetylation (H3K27ac) and a decrease in H3K27 trimethylation (H3K27me3) at the *JAK1* gene locus following *TP53/RB1* KO or SOX2 OE were also identified, indicating a transcriptional upregulation of *JAK1* by SOX2 (Extended Data Fig. 9a,b). This hypothesis was further supported by analyzing an existing SOX2 ChIP-seq dataset generated from another mCRPC cell line with ectopic SOX2 expression⁵⁶, CWR-R1, which demonstrated PCa-specific SOX2 binding sites in JAK-STAT genes compared to canonical SOX2 binding sites in the embryonic stem cell line WA01 (Extended Data Fig. 9c,d). To explore whether JAK and STAT are required for SOX2-promoted lineage plasticity and resistance, we knocked out *JAK1* and *STAT1* in the SOX2-OE cells and observed significantly impaired resistant growth of those cells, as shown in cell proliferation assays (Fig. 5e) and CellTiter-Glo viability assays (Fig. 5f). Furthermore, *JAK1* and *STAT1* KO in the SOX2-OE cells largely attenuated the acquisition of lineage plasticity (Fig. 5g). JAK1 inhibition by Filg significantly resensitized SOX2-OE cells to

Fig. 4 | JAK1 inhibitor restores Enz sensitivity. **a**, Relative cell number of LNCaP/AR cells transduced with Cas9 and annotated CRISPR guide RNAs and treated with annotated treatments in CSS medium and normalized to the vehicle group; Enz, 10 μ M Enz; Filg, 5 μ M Filg; Enz + Filg, combination of Enz and Filg; vehicle, DMSO treatment with equal volume as Enz. Cells were treated for 8 d, and cell numbers were measured by a CellTiter-Glo assay. **b**, Waterfall plot displaying changes in tumor size of xenografted LNCaP/AR-sgTP53/RB1 cells after 2 weeks of treatments. All animals were treated with Enz at 10 mg kg⁻¹ orally 1 d after grafting. Beginning from week 3 of xenografting, animals were randomized into three groups and treated with Enz only at 10 mg kg⁻¹ orally, Filg only at 20 mg kg⁻¹ orally twice daily or a combination of Enz plus Filg; n = the number of independent xenografted tumors in each group (two tumors per mouse); Enz, n = 10 tumors; Filg, n = 10 tumors; Enz + Filg, n = 10 tumors. P values were calculated by one-way ANOVA with a Bonferroni multiple-comparison test. **c**, IF staining of the *Trp53*^{loxP/loxP}*Rb1*^{loxP/loxP} + empty (*Trp53/Rb1*-WT) and *Trp53*^{loxP/loxP}*Rb1*^{loxP/loxP} + Cre (*Trp53/Rb1*-KO) organoids in 3D with annotated antibodies; representative images of n = 2 independent treated cell cultures are shown. **d**, Brightfield images of annotated organoids treated with DMSO (vehicle), 1 μ M Enz, 5 μ M Filg or Enz and Filg (Enz + Filg) for 6 d; representative images of n = 3 independent treated cell cultures are shown. **e**, Relative cell numbers of annotated organoids treated with annotated treatments for 6 d normalized to the vehicle group. Treatments are the same as described in **d**. **f**, Percentage of organoids that display lumen or hyperplasia morphology. Treatments are the same as described in **d**. **g**, Relative expression of JAK-STAT and lineage marker genes in organoids treated with the treatments annotated in **d**. **h**, IF staining of the annotated organoids with antibodies targeting the proteins encoded by AR target genes and lineage marker genes; representative images of n = 2 independent treated cell cultures are shown. Unless otherwise noted, n = 3 independent treated cell cultures, and data represent mean \pm s.e.m. P values were calculated by two-way ANOVA with a Bonferroni multiple-comparison test.



Enz (Extended Data Fig. 9e) and attenuated the acquisition of lineage plasticity in these cells (Extended Data Fig. 9f).

To reveal whether JAK-STAT activation is sufficient to promote lineage plasticity, we overexpressed *JAK1* and *STAT1* (*JAK1*-OE and *STAT1*-OE) in LNCaP/AR cells and observed significantly upregulated expression of stem-like, EMT, basal and NE-like marker genes (Fig. 5h). Notably, the observed upregulation of SOX2 in *JAK1*-OE and *STAT1*-OE cells (Fig. 5h) suggests positive feedback regulation between SOX2 and JAK-STAT activation. Consistent with this feedback model, *JAK1* inhibition through either CRISPR-mediated KO or Filg treatment in sgTP53/RB1 cells led to a ~30% reduction of SOX2 expression (Fig. 5i,j). Furthermore, combination of KO or pharmaceutical inhibition of various JAK and STAT proteins led to a more profound downregulation of SOX2 expression (Fig. 5i,j), suggesting that various JAK and STAT proteins cooperatively regulate SOX2 in a similar feedback fashion. Finally, to further decipher the dynamic of this SOX2- and JAK-STAT-regulated lineage plasticity, we used an inducible shRNA-transduced LNCaP/AR model, where doxycycline (Dox)-inducible *TP53/RB1* knockdown led to upregulation of JAK-STAT signaling genes as soon as 12 h following Dox administration (Fig. 5k). Remarkably, stem-like and EMT-like programs were spontaneously upregulated with JAK-STAT signaling as soon as 12 h after Dox induction, while NE-like programs were not upregulated until 24 h after Dox administration (Fig. 5k). Furthermore, although stem-like and EMT-like programs were simultaneously reversed to wild-type levels following the downregulation of JAK-STAT signaling after Dox removal, NE-like programs were not fully restored (Fig. 5k), suggesting that NE-like programs were retained in a subset of cells. These results may suggest that JAK-STAT signaling is required for therapy resistance of stem-like and multilineage cells rather than cells exclusively expressing NE-like lineage.

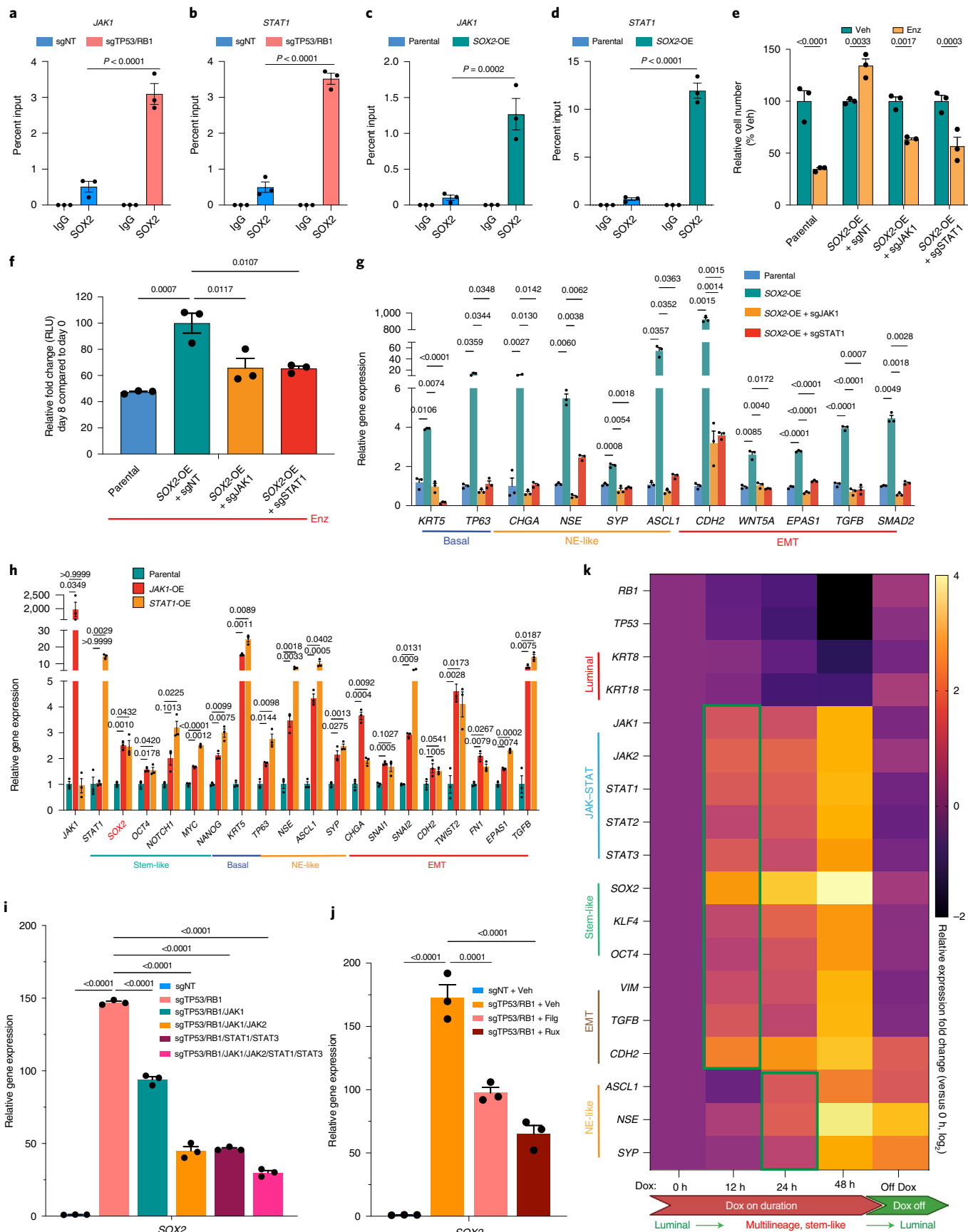
Single-cell transcriptomics reveal lineage heterogeneity. To examine the role of JAK-STAT in heterogeneous cell subpopulations, we performed scRNA-seq and transcriptomic analysis using the series of LNCaP/AR cell lines treated with Enz or vehicle. As expected, clustering of the sequenced cells was primarily driven by genetic and treatment perturbations (Fig. 6a–c). Interestingly, the majority of both the sgNT and sgTP53/RB1/JAK1 cells were clearly separated by different treatments (Fig. 6a,c), while sgTP53/RB1 cells did not display a similar separation (Fig. 6b). These data support the observation that a majority of the sgTP53/RB1 cells exhibit Enz resistance. Because AR antagonists can promote PCa cell cycle arrest⁵⁷, we performed cell cycle prediction analysis and observed a dramatically increased cell cycle arrest occurring in the sgNT cells treated with Enz (Fig. 6a,d). By contrast, Enz treatment did not increase the population of sgTP53/RB1 cells in G1 phase, suggesting that the majority of sgTP53/RB1 cells are resistant to Enz (Fig. 6b,d). Remarkably, *JAK1* KO substantially increased the percentage of cells entering G1 after Enz treatment compared to

that observed in the vehicle-treated group (Fig. 6c,d). These data validate the specific role of JAK-STAT in mediating AR-targeted therapy resistance. To further assess the dynamics of resistance, we investigated whether AR signaling was restored in resistant subclones. Not surprisingly, the sgNT + vehicle group consisted of the greatest number of cells expressing canonical AR score genes (Supplementary Table 7), and inhibition of their expression was subsequently verified after Enz exposure (Extended Data Fig. 10a–f). By contrast, both sgTP53/RB1 vehicle and sgTP53/RB1 Enz groups lacked expression of AR genes, supporting the emergence of AR-independent transcriptional programs (Extended Data Fig. 10a–f). The expression of AR targets was largely reestablished in many cells belonging to the sgTP53/RB1/JAK1 + vehicle group (two-thirds of AR score genes; Supplementary Table 7) compared to that observed in the sgTP53/RB1 + vehicle group (Extended Data Fig. 10a–f). These data suggest a partial restoration of AR signaling and AR dependency among the sgTP53/RB1/JAK1 cells.

To characterize lineage-specific tumor heterogeneity in resistant PCa cells, we performed unsupervised graph clustering (uniform manifold approximation and projection (UMAP))⁵⁸ and identified six distinct cell subsets labeled as clusters 0–5, with further partitioning to 13 subclusters (Fig. 6e,f). Consistent with transcriptomic changes caused by TP53/RB1/JAK1 modification, five of the six clusters (clusters 0–4) predominantly overlapped with the clusters identified by genetic and treatment perturbations (Fig. 6g), while cluster 5 is a mixture of a small fraction of cells from five groups (Fig. 6e–g). To examine the cell proliferation state of these clusters, we overlapped the transcriptomic-based clustering with cell cycle prediction (Fig. 6h). Interestingly, cells within clusters 0, 1, 3 and 5 remain proliferative (termed the ‘winner’ clusters; Fig. 6i), whereas cluster 2 contains a much higher percentage of cells in cell cycle arrest (termed the ‘loser’ cluster; Fig. 6i). Lastly, cells within cluster 4 express elevated levels of cell cycle phase heterogeneity (Fig. 6h), a finding that will be expounded on later.

JAK-STAT signaling is required for stem-like and multilineage clones. We next probed the well-established AR score and five lineage-specific gene signatures (Supplementary Table 7)^{5,24,59–61} and analyzed the expression of genes (*z* score) comprising these signatures across all clusters and samples (Fig. 7a–c). In congruence with the luminal epithelial cell lineage of LNCaP/AR cells, cluster 2 and cluster 3, which consist of cells originating from the sgNT groups, represent the two clusters expressing the highest level of luminal genes (Fig. 7a–d). Most of cluster 2 cells, while retaining their luminal lineage, displayed loss of AR signaling gene expression and entered cell cycle arrest following Enz administration (Fig. 7a–e). Notably, the most substantial proportions of clusters 0 and 1, consisting primarily of cells originating from the sgTP53/RB1 groups, expressed the lowest levels of the luminal gene signature and relatively high levels of non-luminal and multilineage gene signatures (Fig. 7a–i). Surprisingly, clusters 0 and 1 also contained a proportion

Fig. 5 | SOX2 enables JAK-STAT activation in a positive feedback fashion. **a–d**, SOX2 ChIP-qPCR of *JAK1* (a,c) and *STAT1* (b,d) genomic loci in LNCaP/AR cells transduced with annotated CRISPR guide RNAs or overexpressing constructs. **e**, Relative cell numbers of LNCaP/AR cells transduced with annotated constructs and treated with Enz or vehicle, normalized to the vehicle group; Enz, 10 μ M Enz; vehicle, DMSO treatment with equal volume as Enz. Cells were treated for 6 d, and cell numbers were measured by cell proliferation assay. **f**, Relative cell number fold change of LNCaP/AR cells transduced with annotated constructs. Data are normalized to the SOX2-OE + sgNT group; Enz, 10 μ M Enz treatment for 8 d. Cell numbers were measured by a CellTiter-Glo assay. *P* values were calculated by one-way ANOVA with a Bonferroni multiple-comparison test. **g**, Relative expression of canonical lineage marker genes in LNCaP/AR SOX2-OE cells transduced with annotated constructs. **h**, Relative expression of canonical lineage marker genes in LNCaP/AR cells transduced with *JAK1* or *STAT1* cDNA constructs. SOX2 expression is highlighted in red. **i**, Relative expression of SOX2 in LNCaP/AR cells transduced with annotated guide RNAs. **j**, Relative expression of SOX2 in LNCaP/AR cells treated with 5 μ M Filg or 5 μ M ruxolitinib (Rux) or DMSO for 8 d. *P* values in **i** and **j** were calculated by one-way ANOVA with a Bonferroni multiple-comparison test. **k**, Relative gene expression levels of canonical JAK-STAT signaling and lineage marker genes in the inducible shTP53/RB1 LNCaP/AR cells treated with Dox for various lengths of time. Data are normalized to 0 h. Unless otherwise noted, $n=3$ independent treated cell cultures, and data represent mean \pm s.e.m. *P* values were calculated by two-way ANOVA with a Bonferroni multiple-comparison test.



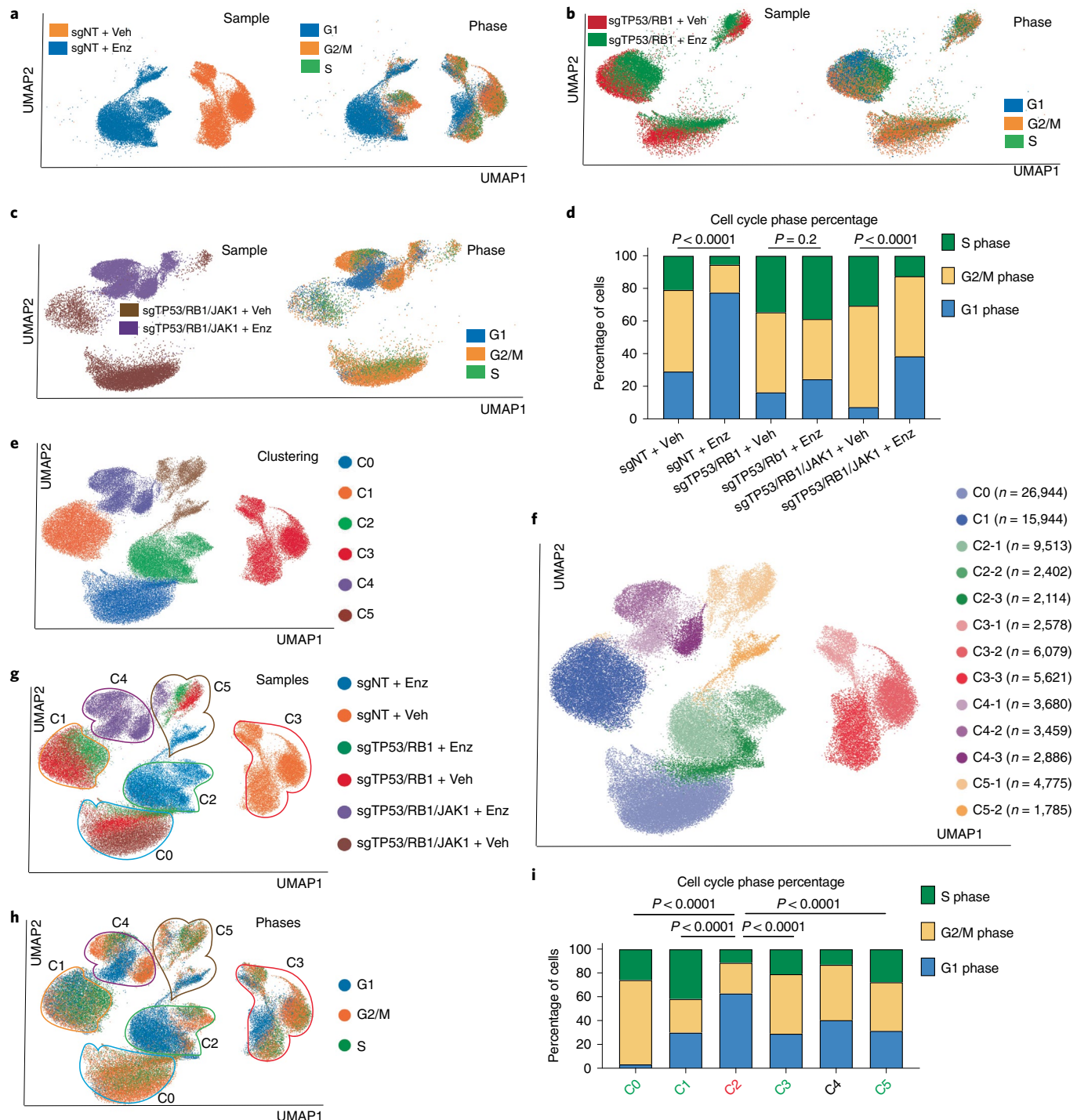


Fig. 6 | JAK-STAT is required for AR therapy resistance of heterogeneous subclones. **a-c**, UMAP plots of single-cell transcriptomic profiles of LNCaP/AR cells transduced by annotated CRISPR guide RNAs and treated with vehicle (DMSO) or 10 μ M Enz for 5 d; sgNT (Veh, $n=14,268$ cells; Enz, $n=15,149$ cells; **a**); sgTP53/RB1 (Veh, $n=12,267$ cells; Enz, $n=9,850$ cells; **b**); sgTP53/RB1/JAK1 (Veh, $n=25,200$ cells; Enz, $n=11,096$ cells; **c**). Cells on the left are colored according to sample origin, while cells on the right are colored by predicted cell cycle phase. **d**, Bar plot presenting the percent distribution of single cells in different cell cycle phases in each sample. The numbers of cells (n) are the same as in **a-c**. P values were calculated by two-sided Fisher's exact test.

e, Single-cell profile of LNCaP/AR cells based on clustering. A UMAP plot of single cells colored by unsupervised clustering of six subsets is presented; cluster 0 (C0), $n=26,944$ cells; C1, $n=15,994$ cells; C2, $n=14,029$ cells; C3, $n=14,278$ cells; C4, $n=10,025$ cells; C5, $n=6,560$ cells. **f**, Single-cell profile of LNCaP/AR cells based on subclustering. A UMAP plot of single cells colored by unsupervised clustering of 13 subclusters is presented; C0, $n=26,944$ cells; C1, $n=15,994$ cells; C2-1, $n=9,513$ cells; C2-2, $n=2,402$ cells; C2-3, $n=2,114$ cells; C3-1, $n=2,578$ cells; C3-2, $n=6,079$ cells; C3-3, $n=5,621$ cells; C4-1, $n=3,680$ cells; C4-2, $n=3,459$ cells; C4-3, $n=2,886$ cells; C5-1, $n=4,775$ cells; C5-2, $n=1,785$ cells.

g, Single-cell profile of LNCaP/AR cells transduced with annotated CRISPR guide RNAs and treated with vehicle or Enz. A UMAP plot of single cells colored by samples is represented. The area and number of clusters in **e** are highlighted with colored circles. **h**, Single-cell profile of LNCaP/AR cells based on cell cycle states. A UMAP plot of single cells colored by cell cycle prediction is presented. The area and number of clusters in **e** are highlighted with colored circles. **i**, Bar plot presenting the percent distribution of single cells in different cell cycle phases in each of the six clusters. The number of cells (n) in each sample is the same as in **e**. P values were calculated by two-sided Fisher's exact test.

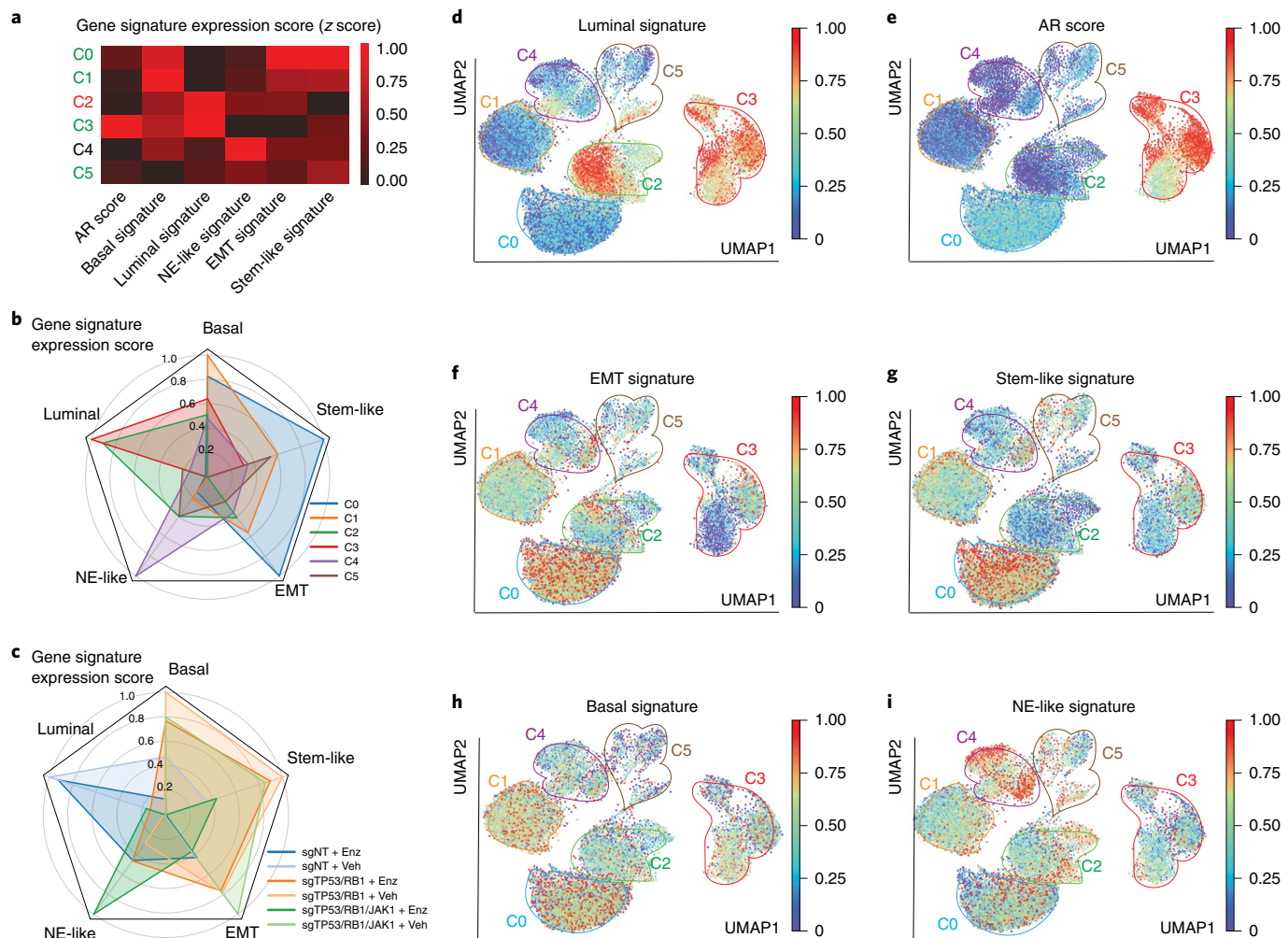
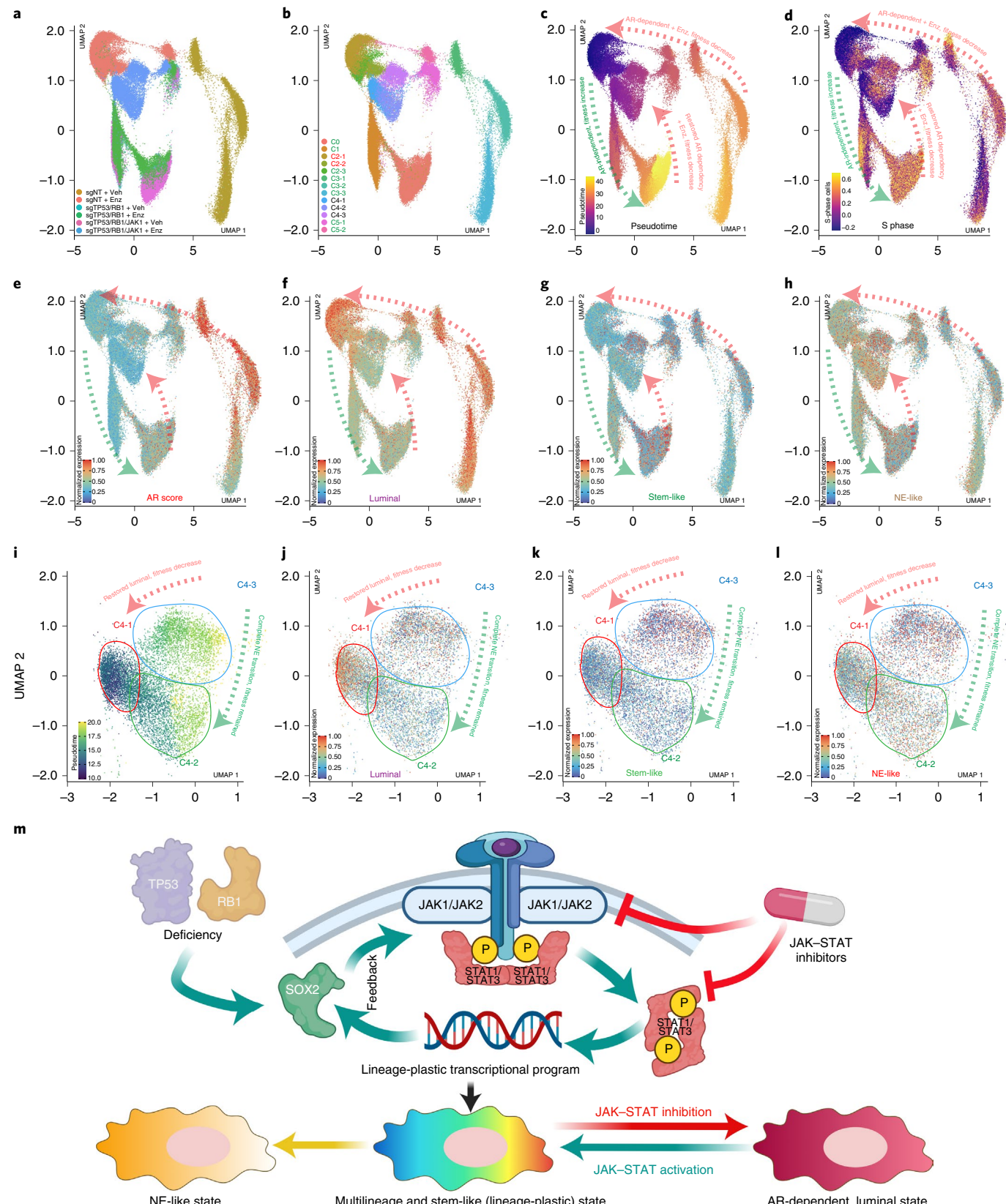


Fig. 7 | JAK-STAT is required for stem-like and multilineage subclones. **a**, Heat map representing the lineage scores of canonical lineage marker gene signatures in cell clusters. Winner clusters (without increased cell cycle arrest) are highlighted in green, and the loser cluster (with increased cell cycle arrest) is highlighted in red. **b**, Radar plot representing the lineage scores and distribution of different cell clusters. **c**, Radar plot representing the lineage scores and distribution of different samples. In **a–c**, lineage scores were scaled from 0 to 1 across all clusters. **d**, UMAP plot of single-cell transcriptomic profiles colored by AR gene signature score (z score) for each cell (dot). **e**, UMAP plot of single-cell transcriptomic profiles colored by EMT gene signature score (z score) for each cell (dot). **f**, UMAP plot of single-cell transcriptomic profiles colored by stem cell-like gene signature score (z score) for each cell (dot). **g**, UMAP plot of single-cell transcriptomic profiles colored by basal gene signature score (z score) for each cell (dot). **h**, UMAP plot of single-cell transcriptomic profiles colored by NE-like gene signature score (z score) for each cell (dot). In **d–i**, distribution areas of each cluster are labeled in color circles. The color density of each cell is scaled by the color bar. For all data, the numbers (n) of cells in each sample and cluster are the same as in Fig. 6, and lineage scores were scaled from 0 to 1 across all cells.

of cells from the sgTP53/RB1/JAK1 + vehicle group, which maintained non-luminal programs (Fig. 7b–i), supporting the hypothesis that JAK-STAT inhibition does not impair the survival of those subclones in the absence of Enz (Figs. 6i and 7b,c). However, Enz dramatically diminished the survival of sgTP53/RB1/JAK1 subclones and the expression of stem-like and multilineage programs, suggesting that JAK-STAT inactivation restored AR dependency and impaired lineage plasticity (Fig. 7b,c). This hypothesis is further supported by restored AR signaling in sgTP53/RB1/JAK1 subclones (Extended Data Fig. 10a–f). Interestingly, JAK1 KO did not substantially impair the resistance of subclones only expressing an NE-like lineage program (Fig. 7b,c,i), indicating that JAK-STAT signaling is specifically required for the transition to a stem-like and multilineage state rather than the transition to an exclusive NE-like state.

To decipher the dynamics of lineage plasticity, we performed pseudotime reconstructing trajectory analysis (Fig. 8a–c). We started

with the transcriptional landscape of the only loser cluster, cluster 2, and tracked the changes of cell proliferation and lineage states. The increased pseudotime correlated with cell fitness, as reflected by an increased percentage of cells with active cell cycle and proliferation (Fig. 8c,d). Because clusters 2 and 3 predominantly contain wild-type sgNT cells (Fig. 7e,f), Enz treatment caused a substantial decrease of both cell fitness and pseudotime of the luminal and AR-dependent cells in those two clusters (Fig. 8c,d). Genetic perturbation of TP53/RB1 KO (clusters 0 and 1) led to the transition to a multilineage and stem-like state, which confers an increase in cell fitness and pseudotime (Fig. 8a–d,f–h). Interestingly, JAK1 KO did not immediately impair fitness nor reduce pseudotime of multilineage subclones but rather restored AR signaling in those cells (Fig. 8e). Indeed, Enz substantially impaired the fitness of those JAK1 KO subclones and led to a decrease in pseudotime (Fig. 8c,d), supporting the hypothesis that JAK-STAT inhibition restored AR dependency.



of those cells. Notably, the subclones only expressing NE-like lineage maintained both high fitness and pseudotime (Fig. 8h), suggesting that JAK-STAT signaling is inessential for those subclones.

We continued to explore the lineage heterogeneity of the subclusters of cluster 4 (Fig. 6f and Extended Data Fig. 10g), which

contain cells originating from the sgTP53/RB1/JAK1 + Enz group (Fig. 6e,g). The three subclusters of cluster 4 expressed diverse levels of the JAK-STAT signaling genes (Extended Data Fig. 10i-r), presumably because JAK-STAT signaling was not fully deactivated in a proportion of JAK1-KO cells due to compensatory signaling driven

Fig. 8 | Dynamics of lineage plasticity driven by ectopic JAK-STAT activation. **a**, UMAP plots represent the reconstructive trajectory of single cells in each of the samples. **b**, UMAP plots represent the reconstructive trajectory of single cells in each of the subclusters. **c**, UMAP plots represent the pseudotime reconstructive trajectory of single cells. Color intensity represents the pseudotime estimation of each single cell. Arrows and the dotted line represent the direction of pseudotime flow. **d**, UMAP plots represent the S phase score per cell in each single cell within the pseudotime reconstructive trajectory. **e–h**, UMAP plots represent the AR signaling and lineage scores per cell in each single cell within the pseudotime reconstructive trajectory. **i**, UMAP plots represent the pseudotime reconstructive trajectory of single cells of cluster 4. Color intensity represents the pseudotime estimation of each single cell. Arrows and the dotted line represent the direction of pseudotime flow. **j–l**, UMAP plots represent lineage scores per cell in each single cell within the pseudotime reconstructive trajectory of single cells of cluster 4. **m**, Schematic figure illustrating that SOX2 ectopically activates JAK-STAT signaling, which enables the transition of mCRPC to a stem-like and multilineage state. Figure created with [BioRender.com](https://biorender.com). The numbers (*n*) of cells in each sample and cluster are the same as in Fig. 6.

by JAK2 (Extended Data Fig. 10j). Cluster 4-3 contained the ‘outlier’ cells, which partially maintain JAK-STAT signaling, likely driven by JAK2 (Figs. 6f and 8i and Extended Data Fig. 10j). Remarkably, the cells within cluster 4-3 maintained expression of multilineage programs as well as the highest level of cell fitness, regardless of treatment conditions (Fig. 8i–k and Extended Data Fig. 10h). The other two subclusters of cluster 4 demonstrated two contrasting fates following deactivation of JAK-STAT signaling. Cluster 4-1 cells, which lose the multilineage and stem-like programs, restored the exclusive expression of the luminal program (Fig. 8j). Thus, cells of this subcluster were highly responsive to Enz (Extended Data Fig. 10h), which caused a substantial diminishment in cell fitness (Fig. 8i). By contrast, the cells of cluster 4-2, which exclusively express NE-like lineage programs, maintained cell fitness even in the absence of JAK-STAT signaling (Fig. 8l and Extended Data Fig. 10h), supporting the hypothesis that JAK-STAT signaling is not required for the cells fully differentiated to an NE-like state. The juxtaposition between different subclusters of cluster 4 further supports the crucial role of ectopic JAK-STAT signaling in maintaining AR therapy resistance of stem-like and multilineage subclones rather than subclones exclusively expressing an NE-like lineage (Fig. 8m).

Discussion

Emerging evidence demonstrates that lineage plasticity represents an important mechanism for conferring targeted therapy resistance in various cancers, particularly prominent in cancers where the molecular target of therapies are lineage-specific survival factors². In the case of PCa, however, it is not fully understood whether differentiated luminal tumor cells acquire lineage plasticity through reverting back (dedifferentiating) to a multilineage, stem cell-like state and then redifferentiating to alternative lineages or through direct transdifferentiation to a distinctively new lineage. Another intriguing feature of lineage plasticity-driven resistance is the elevated levels of intratumoral heterogeneity⁶², which increases the difficulty to dissect the molecular mediators required either for multilineage plasticity or for a specific lineage program, such as NE-like lineage, through the analysis of bulk cell population. Thus, the identification of lineage heterogeneous TP53/RB1-deficient tumor cell subpopulations through single-cell transcriptomic analyses illuminates these once hidden details and represents a major insight into this work. Here, we showed that a vast majority of the TP53/RB1-deficient tumor cells acquire lineage plasticity by transitioning to a stem-like, multilineage and AR-independent state. Importantly, our data acquired from the Dox-inducible model, as well as the pseudotime trajectory analysis, suggested that ectopic JAK-STAT activation is required for AR therapy resistance of those stem-like cells expressing multilineage programs rather than cells having undergone complete transition to an exclusive NE-like lineage.

Various genetic and transcriptional aberrations have been connected to lineage plasticity in PCa^{3,6–9,12,13,18,61}. Interestingly, many of those cases involve the ‘hijacking’ of stem-like, pluripotency or epigenetic regulation programs^{4,5,7,8,10,63}. Although the role of the

JAK-STAT signaling pathway in regulating cell fate decision, stem cell self-renewal and multilineage differentiation has been well documented^{27,28}, its potential function in mediating lineage plasticity remains largely unclear. Furthermore, the consequence of constitutive activation of STAT proteins in tumorigenesis is highly context specific^{29,30}. Our results revealed that SOX2 regulates the ectopic induction of JAK-STAT signaling in a positive feedback and cell-autonomous fashion. Consequently, JAK-STAT activation, in a JAK1/JAK2- and STAT1/STAT3-dependent manner, is required for the transition to a stem-like, multilineage and EMT state but not for the tumor cells that have completely redifferentiated to an NE-like lineage. The results of combinatorial KO and pharmaceutical inhibition of various JAK-STAT signaling proteins suggests that those proteins, specifically JAK1/JAK2 and STAT1/STAT3, may function in a collaborative and compensatory network to confer lineage plasticity. Our results also reveal that ectopic JAK-STAT expression enables an EMT lineage program that promotes a metastatic phenotype.

Despite the clinical success of AR-targeted therapies, resistance to these treatments universally develops and largely impairs the clinical outcome of individuals with mCRPC. Although lineage plasticity has been suggested as a substantial mechanism conferring resistance, effective therapeutic approaches targeting lineage plasticity are still not available². Here, we demonstrated that various pharmaceutical inhibitors targeting different JAK and STAT proteins have combinatorial effects when administered with Enz. These results may provide a rationale for future clinical trials designed to target JAK-STAT signaling for overcoming lineage plasticity-driven AR-targeted therapy resistance. Finally, it is crucial to place our model of how JAK-STAT signaling promotes lineage plasticity-driven resistance within the context of TP53 and RB1 deficiency. Although the connection between JAK-STAT activation and TP53/RB1 alterations are well documented in various cancers^{64,65}, an inverse correlation between wild-type TP53 and JAK-STAT activation is also widely reported^{66,67}. These results are consistent with our finding that the inactivation of JAK-STAT signaling impairs proliferation of resistant cells with TP53/RB1 deficiency while not affecting cells with intact TP53/RB1. Therefore, it is critical to consider the genomic state of TP53/RB1 when correlating JAK-STAT activation with the clinical outcome of AR therapy responses, as JAK-STAT activation in individuals with wild-type TP53/RB1 may not be a consequence of lineage hijacking but rather a cytokine-induced immune response.

Methods

Ethics statement. All animals were housed under humidity- and temperature-controlled conditions with a 12-h light/12-h dark cycle in the pathogen-free facilities at UT Southwestern Medical Center by the Animal Resource Center and were monitored closely to minimize discomfort, distress, pain or injury throughout the course of the *in vivo* experiments. Animals were removed from the study and killed if any signs of pain and distress were detected or if the tumor volume reached 2,000 mm³. The maximal tumor size was not exceeded in all reported studies. All procedures were performed in accordance with the recommendations of the Panel on Euthanasia of the American Veterinary Medical Association, and the

animal protocol was approved by Institutional Animal Care and Use Committee of UT Southwestern Medical Center (protocol 2019-102493). Male C.B-*lgh-1^b*/IcrTac-*Prkdc^{scid}* SCID mice were obtained from Taconic Biosciences.

Cell lines and organoid culture. Information and requests for resources and reagents should be directed to and will be fulfilled by the corresponding author. All cell lines, plasmids and other reagents generated in this study are available from the corresponding author with a completed materials transfer agreement if there is potential for commercial application. Parental LNCaP/AR and CWR22Pc PCa cell lines were obtained from the laboratory of C. Sawyers at Memorial Sloan Kettering Cancer Center (MSKCC)³, and DU145 (HTB-81) and PC3 (CRL-1435) cell lines were purchased from ATCC. LNCaP/AR, CWR22Pc and PC3 cells were cultured in RPMI 1640 medium supplemented with 10% fetal bovine serum (FBS), 1% L-glutamine, 1% penicillin-streptomycin, 1% HEPES and 1% sodium pyruvate. DU145 cells were cultured in DMEM high-glucose medium supplemented with 10% FBS, 1% L-glutamine and 1% penicillin-streptomycin. LNCaP/AR, PC3 and DU145 cells were passaged at a 1:6 ratio every 3–5 d, and CWR22Pc cells were passaged at a 1:3 ratio every 3–5 d. When treated with 10 μ M Enz and/or 5 μ M Filg, LNCaP/AR cells were cultured in RPMI 1640 medium supplemented with 10% charcoal-stripped serum (CSS medium). All cell cultures were assessed for mycoplasma monthly via a MycoAlert Plus Mycoplasma Detection kit (Lonza, LT07-710), and all results were negative. Cell line identification was validated through human short tandem repeat profiling cell authentication and was compared to ATCC cell line profiles every year. *Trp53^{loxP/loxP} Rb1^{loxP/loxP}* mouse organoids were generated from *Trp53^{loxP/loxP} Rb1^{loxP/loxP}* mice³. Human organoids were obtained from the laboratory of Y. Chen at MSKCC^{4,5}. Organoids were cultured in 3D Matrigel according to the previously described protocol^{13,68}. Organoids were split at a 1:10 (mouse) or 1:3 (human) ratio every 5 d.

CRISPR and shRNA. Lentiviral-based constructs were used for CRISPR-based KO or shRNA-based knockdown of all genes modified in the manuscript¹³. LNCaP/AR cells were seeded at 400,000 cells per well in 2 ml of medium in six-well plates. Medium was replaced with medium containing 50% virus, 50% fresh culture medium and 5 μ g ml⁻¹ polybrene the next day. The lentiviral virus-containing medium was replaced with normal culture medium after 24 h. Cells were selected with 2 μ g ml⁻¹ puromycin for 4 d or 5 μ g ml⁻¹ blasticidin for 5 d. For cells with double colors, transduced cells were further sorted with a flow cytometer. Human DYKDDDDK (Flag)-tagged SOX2 expression lentivirus (337402) was purchased from Qiagen and used for direct cell transduction, following the manufacturer's instruction. The All-In-One lentiCRISPRv2 (Addgene plasmid 52961), LentiCRISPRv2GFP (Addgene plasmid 82416), LentiCRISPRv2-mCherry (Addgene plasmid 99154), pLKO5_sgRNA.EFS.RFP (Addgene plasmid 57823), pLKO5_sgRNA.EFS.GFP and lentiCas9-Blast (Addgene plasmid 52962) plasmids were used to generate the CRISPR and guide RNAs. Guide RNA constructs with an empty space holder served as the sgNT control. Guide RNAs were designed using the Benchling guide RNA designing tool (<https://benchling.com>). shRNA constructs SGEP (pRRL-GFP-miRE-PGK-PuroR) and LT3GEP (pRRL-TRE 3G-GFP-miRE-PGK-PuroR-IRES-rtTA3) were originally obtained from the laboratory of J. Zuber at the Research Institute of Molecular Pathology. Sequences of sgRNAs and shRNAs are listed in Supplementary Table 8.

In vivo xenograft experiment. All animal experiments were performed in compliance with the guidelines of the Animal Resource Center of UT Southwestern. LNCaP/AR in vivo xenograft experiments were performed by subcutaneous injection of 2 \times 10⁶ cells, which were suspended in 100 μ l in 50% Matrigel and 50% growth medium, into the flanks of castrated male C.B-Igh-1b/IcrTac-*Prkdc^{scid}* SCID mice on both sides. For the experiment depicted in Fig. 1e, daily gavage treatment with 10 mg kg⁻¹ Enz or vehicle (1% carboxymethyl cellulose, 0.1% Tween 80 and 5% DMSO) was started 1 d after the injection. Tumor size was measured weekly by digital caliper because tumors were noticeable. For experiments depicted in Fig. 4b, 10 mg kg⁻¹ Enz (daily) and/or 20 mg kg⁻¹ Filg (twice daily) were given after 3 weeks of Enz-only administration when tumors averaged around 200 mm³ in size.

Cell dose-response curve, growth, viability and fluorescence-activated cell sorting-based competition assays. For the viability assay and dose-response curve, 4,000 LNCaP/AR cells were seeded in each well of a 96-well plate and treated with the annotated treatments for 8 d before conducting the assay. Cell viability was then measured by CellTiter-Glo luminescent cell viability assay (Promega, 7570) according to manufacturer's protocol by using a SpectraMax iD3 automatic plate reader¹³. For the cell growth assay, LNCaP/AR (10,000 cells per well) or CWR22Pc (50,000 cells per well) cells were seeded in a 24-well plate in FBS medium (CWR22Pc) or CSS medium (LNCaP/AR) and treated with Enz (10 μ M for LNCaP/AR and 1 μ M for CWR22Pc) or vehicle (DMSO) for 7 d (LNCaP/AR) or 4 d (CWR22Pc). Cell numbers were counted by a Countess II FL automatic cell counter (Invitrogen). For the organoid growth assay, 2,000 mouse organoid cells were seeded in 3D Matrigel (per 50- μ l sphere) in murine organoid medium with Enz and/or Filg for 6 d. Matrigel was washed away with cell recovery medium (Corning, 354253), and organoids were separated into single-cell

suspensions by treatment with trypsin. Cell numbers were counted, and the relative cell growth (treatments/vehicle) was calculated. For fluorescence-activated cell sorting (FACS)-based competition assays, the competition cell mixture of sgTP53/RB1-RFP cells and sgNT-GFP cells was treated with Enz (10 μ M), and the percentages of RFP-positive cells were measured on day 0, day 4 and day 8 by FACS. LNCaP/AR cells were first gated based on SSC-H/FSC-A \rightarrow FSC-H before measuring the RFP/GFP signals. Relative cell number fold change was calculated and normalized to the vehicle-treated group, as previously described¹³. Attune NxT (version 4.2.1627.1) and FlowJo (version 10.8.0) were used for FACS data analysis.

Chemicals. Enz was purchased from the Organic Synthesis Core Facility at MSKCC. Filg and ruxolitinib are commercially available from MedChem Express (Filg, HY-18300; ruxolitinib, HY-50856). Fludarabine and niclosamide are commercially available from Selleck Chemicals (fludarabine, S1491; niclosamide, S3030).

Migration, invasion and prostasphere assays. For the migration assay, 20,000 LNCaP/AR cells were resuspended in serum-free RPMI and seeded in the upper transwell insert (Corning, 353097)⁴⁹. RPMI with 10% serum was added to the lower chamber as a chemoattractant. After 60 h of incubation, cells that migrated to the lower side of the transwell insert were fixed with paraformaldehyde and stained with 1% crystal violet. Images were acquired on a Leica DMi8 inverted microscope. Nine representative images of each group were used to quantify the migrated cell numbers. For the invasion assay, inserts were coated with extracellular matrix gel (Corning, 354234) before plating. Stock Matrigel (10 mg ml⁻¹) was thawed overnight at 4 °C and diluted in serum-free RPMI to 30 μ g per insert. Each insert was then coated with 100 μ l of diluted Matrigel and incubated for 1 h at 37 °C with 5% CO₂. Cells were then seeded at the same density as the migration assay. Cells were fixed and stained with 1% crystal violet after 60 h, and the invading cell numbers were quantified by using ImageJ, as in the migration assay. The prostasphere assay method was adapted from previous reports⁵⁰. Two hundred cells were seeded into each well of a 96-well ultralow attachment plate. For each condition, three wells were prepared for statistical analysis. Prostaspheres were imaged at one picture/well and quantified 7 d after seeding. Culture medium used in this experiment was basic organoid medium supplemented with 20 ng ml⁻¹ epidermal growth factor and 10 ng ml⁻¹ basic fibroblast growth factor. All images were quantified by using ImageJ (version 2.0.0).

PDE and PDO experiments. PDE models were established in the Raj laboratory, as previously described^{48,49}. PDEs of ~1 mm³ were cultured in a sponge with RPMI 1640 medium with 10% FBS, 1× penicillin-streptomycin (PS) solution, 0.01 mg ml⁻¹ hydrocortisone and 0.01 mg ml⁻¹ insulin. PDEs were treated with 10 μ M Enz or DMSO for 24 h before RNAs were collected. PDO models were established in the Chen laboratory^{51–55}. PDOs were cultured in 3D Matrigel with typical human organoid medium according to the previously published protocol⁵³. Organoids were split at a 1:3 ratio every 7 d by using trypsin or a sterile glass pipette. When treated with 1 μ M Enz and/or 5 μ M Filg, these organoids were cultured in typical human organoid medium supplemented with drugs.

Gene and protein expression detection by qPCR and western blotting. Total RNA from cells was extracted by using Trizol (Ambion, 15596018), and cDNA was made using SuperScript IV VILO Master Mix with eZDNase enzyme (Thermo Fisher, 11766500) with 200 ng μ l RNA template. cDNA was amplified with 2× PowerUp SYBR Green Master Mix (Thermo Fisher, A25778). For western blotting, proteins were extracted from cell lysates using RIPA buffer and measured with a Pierce BCA Protein Assay kit (23225). Protein lysates were boiled at 95 °C for 5 min and run on NuPAGE 4–12% Bis-Tris gels (Invitrogen, NP0323). Transfer was conducted for 1 h at 100 V at 4 °C. Membranes were then blocked for 15 min in 5% non-fat milk before incubation with primary antibody and washed with 1× TBST (10× stock from Teknova, T9511). The following antibodies were used for western blotting: JAK1 (Cell Signaling Technology, 3332S), STAT1 (Cell Signaling Technology, 9172S), p-STAT1(58D6) (Cell Signaling Technology, 9167S), Rb1(4H1) (Cell Signaling Technology, 5230), P53(DO1) (Leica Biosystems, NCL-p53-DO1), actin(8H10D10) (Cell Signaling Technology, 3700), JAK2(C-10) (Santa Cruz, sc-390539), JAK3 (Cell Signaling Technology, 3775), STAT2(D9J7L) (Cell Signaling Technology, 72604), STAT3(D1B2J) (Cell Signaling Technology, 30835), vimentin(D21H3) (Cell Signaling Technology, 5741), ASCL1(EPR19840) (Abcam, ab211327), peroxidase AffiniPure goat anti-mouse IgG (H + L) (AB_10015289; Jackson ImmunoResearch, 115-035-003) and peroxidase AffiniPure goat anti-rabbit IgG (H + L) (AB_2313567; Jackson ImmunoResearch, 111-035-003). Dilutions of all primary antibodies were 1:1,000. Dilutions of all secondary antibodies were 1:5,000. Human and mouse qPCR primers are listed in Supplementary Table 9.

IF and IHC staining. Tumors were collected and fixed in 4% paraformaldehyde and embedded in paraffin by the UT Southwestern Tissue Management Shared Resource core. Tumors were then sectioned at 5 μ m, and hematoxylin and eosin and IHC staining were performed using standard protocols. Images were acquired on a Leica DMi8 microscope. Deidentified human PCa formalin-fixed paraffin-embedded slides were purchased from the UT Southwestern Tissue

Management Shared Resource core, and IHC staining was performed using a standard protocol. Three-dimensional cultured organoids were washed with PBS and fixed in 4% paraformaldehyde for 90 min. Organoids were embedded in 2% agarose, and the agarose plug was sent to the UT Southwestern Tissue Management Shared Resource core for paraffin embedding. The paraffin-embedded organoids were then sectioned at 5 μ m and stained following a standard IHC protocol. For 3D-cultured organoid IF staining⁷¹, organoids were fixed in 4% paraformaldehyde, permeabilized with 0.5% Triton X-100, blocked with 3D blocking buffer (2% bovine serum albumin, 0.1% Triton X-100 and 0.05% Tween 20) and incubated with Alexa Fluor 647-conjugated or unconjugated primary antibody at 37 °C for 48 h. Organoids were then washed in 3D IF buffer (PBS, 0.1% Triton X-100 and 0.05% Tween 20) and incubated with Alexa Fluor 647-conjugated secondary antibody and DAPI at 37 °C overnight. After washing with PBS, stained organoids were placed on slides, and images were acquired on a confocal microscope. For LNCaP/AR cell IF staining, cells were seeded on round glass coverslips. Twenty-four hours after seeding, cells were fixed with 4% paraformaldehyde and permeabilized with 0.5% Triton X-100. After blocking with 3% bovine serum albumin/PBS, cells were incubated with primary antibody at 4 °C overnight, and Alexa Fluor-labeled secondary antibodies were incubated with cells for 1 h at room temperature. DAPI was used for nuclei staining. Images were captured on a Zeiss LSM 700 confocal laser-scanning microscope. The following antibodies were used for IHC and IF staining: Jak1 (Cell Signaling Technology, 3332), Stat1 (Cell Signaling Technology, 14994), Stat3(D1B2J) (Cell Signaling Technology, 30835), Alexa Fluor 647 anti-cytokeratin 8(EP1628Y) (Abcam, ab192468), Alexa Fluor anti-cytokeratin 18(E431-1) (Abcam, ab194125, GR-200266-1), Alexa Fluor 647 anti-cytokeratin 5(EP1601Y) (Abcam, ab193895, GR-219431-2), Alexa Fluor 647 anti-cytokeratin 14(EP1612Y) (Abcam, ab192056), Nkx3.1(4H4) (Abcam, ab96482), PSA/KLK3(D6B1) (Cell Signaling Technology, 5365), NDRG1(D8G9) (Cell Signaling Technology, 9485), vimentin(D21H3) (Cell Signaling Technology, 5741), synaptophysin(D8F6H) (Cell Signaling Technology, 36406), Alexa Fluor 647-conjugated AffiniPure goat anti-mouse IgG (H + L) (AB_2338902; Jackson ImmunoResearch, 115-605-003), Alexa Fluor 647-conjugated AffiniPure goat anti-rabbit IgG (H + L) (AB_2338078; Jackson ImmunoResearch, 111-605-144), donkey anti-mouse IgG antibody (biotin-SP (long spacer)) (AB_2307438; Jackson ImmunoResearch, 715-065-150) and donkey anti-rabbit IgG antibody (biotin-SP (long spacer)) (AB_2340593; Jackson ImmunoResearch, 711-065-152). Dilutions of all primary antibodies were 1:200 except for JAK1 (1:100). Dilutions of all secondary antibodies were 1:1,000.

ChIP-qPCR and SOX2 ChIP-seq. Cultured cells were cross-linked with 1% formaldehyde and quenched with 0.125 M glycine. Cells were then rinsed with cold 1× PBS twice and lysed in 1% SDS containing buffer supplemented with 1× protease and phosphatase inhibitors. Chromatin was sonicated to an average length of 500 base pairs and centrifuged at 14,000 r.p.m. to remove debris. One percent of the supernatant was saved as input, and the rest was added with ChIP-grade antibody overnight. Then, 20 μ l of agarose/protein A or G beads was added and incubated for 4 h. Beads were washed with standard wash buffers (low-salt, high-salt and LiCl) and finally with TE. The immunoprecipitated chromatin was eluted in elution buffer and decross-linked by NaCl at 65 °C overnight. Proteins were then digested by proteinase K, and DNA was purified with a MinElute PCR purification kit (Qiagen, 28006) and eluted with 10 μ l of water. Antibodies used included Sox2(D9B8N) (Cell Signaling Technology, 230645), anti-histone H3 (acetyl K27) antibody ChIP-grade (Abcam, ab4729) and tri-methyl-histone H3 (Lys 27) (C36B11) rabbit monoclonal antibody (Cell Signaling Technology, 9733S). Dilutions of all antibodies were 1:100. Primer sequences are listed in Supplementary Table 9. SOX2 ChIP-seq data generated from the CWR-R1 and WA01 cells were described in Wet et al., and the SOX2 ChIP-seq data were downloaded from [GSE166185](https://www.ncbi.nlm.nih.gov/assembly/GCF_000001405.26) (ref. ⁵⁶).

Bulk RNA-seq preparation and analysis. LNCaP/AR cells were treated with Enz or vehicle for 6 d before total RNA was extracted using Trizol (Ambion, 15596018). RNA-seq libraries were prepared using the stranded Illumina TruSeq mRNA kit starting from 500 ng of total RNA with 10 cycles of PCR amplification. Barcoded RNA-seq libraries were run as paired-end, 50-nucleotide reads on an Illumina HiSeq 2500 and filtered by poly(A) selection. Alignment, quantification and differential analysis were performed using the QBRC_BulkRnaSeqDE pipeline (https://github.com/QBRC/QBRC_BulkRnaSeqDE). Briefly, alignment of reads to the human reference genome (GRCh38, https://www.ncbi.nlm.nih.gov/assembly/GCF_000001405.26) was done using STAR (v2.7.2b)⁷². FeatureCounts (v1.6.4)⁷³ was used for gene counts, biotype counts and rRNA estimation. Differential expression analysis was performed using the R package DEseq2 (v1.26)⁷⁴. Cutoff values of an absolute fold change greater than 2 and a false discovery rate of <0.1 were used to select for differentially expressed genes. GSEA was performed with the R package fgsea (v1.14.0) using the 'KEGG' and 'Hallmark' libraries from MsigDB.

scRNA-seq preparation and analysis. LNCaP/AR cells were treated with Enz or vehicle for 5 d before the cells were collected. Single cells were sorted into 1.5-ml tubes, and the concentration was adjusted to 900–1,100 cells per μ l.

Cells were loaded between 10,000 and 17,000 cells per chip position using the Chromium Single Cell 5' Library, Gel Bead & Multiplex kit and Chip kit (10x Genomics, V1 barcoding chemistry). Single-cell gene expression libraries were generated according to the manufacturer's instructions, and single-cell expression sequencing was run on a NovaSeq 6000 (Novogene). The 10x scRNA-seq data were preprocessed using Cell Ranger software (5.0.0). We used the 'mkfastq', 'count' and 'aggr' commands to process the 10x scRNA-seq output into one cell by gene expression count matrix using default parameters. scRNA-seq data analysis was performed with the Scanpy (1.6.0) package in Python⁷⁵. Genes expressed in fewer than three cells were removed from further analysis. Cells expressing less than 100 and more than 7,000 genes were also removed from further analysis. In addition, cells with a high (≥ 0.15) mitochondrial genome transcript ratio were removed. For downstream analysis, we used count per million (CPM) normalization to control for library size differences in cells and transformed those into log (CPM + 1) values. After normalization, we used the 'pp.highly_variable_genes' command in Scanpy to find highly variable genes across all cells using default parameters except for 'min_mean = 0.01'. The data were then z-score normalized for each gene across all cells. We then used the 'tl.pca (n_comps=50, use_highly_variable=True)', the 'pp.neighbors (n_pcs=25, n_neighbors=15)' and the 'tl.leiden (resolution = 0.75)' commands in Scanpy to partition the single cells into six distance clusters. Briefly, these processes first identified 50 principal components in the data based on the previously found highly variable genes to reduce the dimensions in the original data and built a nearest neighbor graph based on the top 25 principal components, and a partition of the graph that maximizes modularity was found with the Leiden algorithm⁷⁶. To evaluate the activity of lineage-specific transcriptional programs in those cells, we used a custom library of genes based on the well-established gene signatures for AR target genes (AR score) and NE, luminal, basal, stem-like and EMT lineages. The AR score gene signature was adapted from Hieronymus et al.⁵⁹, and luminal, basal and NE gene signatures were defined by combining the signature genes from refs. ^{5,24,60,61}. EMT and stem-like gene signatures were adapted from the signature genes of Dong et al.²⁴ plus canonical lineage marker genes (Supplementary Table 7). The activation score was calculated based on the overall expression of genes in each gene list using the 'tl.score_genes' function of the Scanpy package. To evaluate and model lineage plasticity as a function of cell genotype, we performed trajectory analysis using the R package 'Monocle 3'⁷⁷. We provided the single-cell gene expression matrix containing only the highly variable genes defined as previously discussed as input and used principal-component analysis and UMAP during preprocessing steps. The trajectory was built using default parameters, with the root defined from the loser cluster. Human CRPC tumor biopsy single-cell data were downloaded from [GSE137829](https://www.ncbi.nlm.nih.gov/geo/query/acc.cgi?acc=GSE137829) (ref. ²⁴). We analyzed these data in a similar manner using the 'scipy' Python package. Briefly, we kept only epithelial cells from the data, performed CPM normalization and a principal-component analysis and evaluated gene expression representing key signaling pathways and lineage-specific translational programs.

Statistics and reproducibility. Statistical details of all experiments can be found in the respective figure legends. A two-sided *t*-test was used and adjusted for multiple comparisons (Welch's correction) when applicable when two groups of independent datasets that fit normality and homoscedasticity were compared. When normality and homoscedasticity were not satisfied, a Mann–Whitney *U*-test (non-parametric Wilcoxon rank-sum test) was used when comparing gene expressions between two groups. For in vitro cell line studies, data distribution was assumed to be normal, but this was not formally tested. One-way or two-way analysis of variance (ANOVA) and Kruskal–Wallis non-parametric ANOVA were used as appropriate to compare more than two groups. The mean \pm s.e.m. values were reported, and *P* values were calculated and adjusted for multiple comparisons (Bonferroni or Benjamini correction) when applicable. *P* values were calculated by non-linear regression with an extra sum-of-squares *F*-test for the dose–response curve. A two-sided Fisher's exact test was used to compare the numbers of tumors with genomic alterations between different groups and the percentages of cell populations. A two-sided chi-squared test with Yates correction was used to compare the exact cell numbers of different clusters of single-cell subclones. For in vivo experiments, no statistical method was used to predetermine sample size, but our sample sizes were selected based on and are similar to those reported in previous studies^{5,12,78–80}. No data were excluded from the analyses. For in vivo studies, the tumor xenografting, measurement and analysis were performed by different researchers to ensure that the studies were run in a blinded manner. Mice were randomized into each group. For in vitro studies, randomization and blinding of cell lines was not possible; however, all cell lines were treated identically without prior designation. Graph Pad Prism (V9.3.1) was used for data graphing and statistical analysis.

Reporting summary. Further information on research design is available in the Nature Research Reporting Summary linked to this article.

Data availability

All the described bulk and scRNA-seq data that support the findings of this study have been deposited in the Gene Expression Omnibus under the accession number [GSE175975](https://www.ncbi.nlm.nih.gov/geo/query/acc.cgi?acc=GSE175975). The human CRPC tumor biopsy single-cell data were downloaded

from and are available in the Gene Expression Omnibus under the accession number [GSE137829](#) (ref. ²⁴). Human genomic and transcriptomic data were derived from the TCGA research network and the SU2C cohort, which were queried using cBioPortal (http://www.cbioperl.org/study/summary?id=prad_su2c_2019) and the Genomic Data Commons Data Portal (<https://portal.gdc.cancer.gov/>). SOX2 ChIP-seq data were downloaded from and are available under the accession number [GSE166185](#) (ref. ⁵⁶). RNA-seq reads were aligned to the human reference genome (GRCh38, https://www.ncbi.nlm.nih.gov/assembly/GCF_000001405.26). Source data are provided with this paper. All other data supporting the findings of this study are available from the corresponding author on reasonable request.

Code availability

All analyses in this work were done using open-source software. Bulk RNA-seq analysis was done using the QBRC Bulk RNA-seq pipeline (https://github.com/QBRC/QBRC_BulkRnaSeqDE). Briefly, reads were aligned to a reference (GRCh38) with 'STAR' (v2.7.2b). Gene counts were quantified with 'FeatureCounts' (v1.6.4). Differential gene expression analysis was performed using the R package 'DESeq2' (v1.26). GSEA statistical analysis was performed with the R package 'gSEA' (v1.14.0). Demultiplexing, alignment and read counting of the scRNA-seq data were performed using the 10x Genomics Cell Ranger 5.0.0 software. scRNA-seq data analysis was performed with the 'Scanpy' (v1.6.0) package in Python. Custom codes for the analysis in the paper have been deposited to GitHub and can be accessed at <https://doi.org/10.5281/zenodo.6888969>.

Received: 30 January 2022; Accepted: 2 August 2022;

Published online: 5 September 2022

References

- Watson, P. A., Arora, V. K. & Sawyers, C. L. Emerging mechanisms of resistance to androgen receptor inhibitors in prostate cancer. *Nat. Rev. Cancer* **15**, 701–711 (2015).
- Beltran, H. et al. The role of lineage plasticity in prostate cancer therapy resistance. *Clin. Cancer Res.* **25**, 6916–6924 (2019).
- Bishop, J. L. et al. The master neural transcription factor BRN2 is an androgen receptor-suppressed driver of neuroendocrine differentiation in prostate cancer. *Cancer Discov.* **7**, 54–71 (2017).
- Ku, S. Y. et al. Rb1 and Trp53 cooperate to suppress prostate cancer lineage plasticity, metastasis, and antiandrogen resistance. *Science* **355**, 78–83 (2017).
- Mu, P. et al. SOX2 promotes lineage plasticity and antiandrogen resistance in TP53- and RB1-deficient prostate cancer. *Science* **355**, 84–88 (2017).
- Dardenne, E. et al. N-Myc induces an EZH2-mediated transcriptional program driving neuroendocrine prostate cancer. *Cancer Cell* **30**, 563–577 (2016).
- Cyrtà, J. et al. Role of specialized composition of SWI/SNF complexes in prostate cancer lineage plasticity. *Nat. Commun.* **11**, 5549 (2020).
- Zou, M. et al. Transdifferentiation as a mechanism of treatment resistance in a mouse model of castration-resistant prostate cancer. *Cancer Discov.* **7**, 736–749 (2017).
- Zhang, X. et al. SRRM4 expression and the loss of REST activity may promote the emergence of the neuroendocrine phenotype in castration-resistant prostate cancer. *Clin. Cancer Res.* **21**, 4698–4708 (2015).
- Davies, A. et al. An androgen receptor switch underlies lineage infidelity in treatment-resistant prostate cancer. *Nat. Cell Biol.* **23**, 1023–1034 (2021).
- Adams, E. J. et al. FOXA1 mutations alter pioneering activity, differentiation and prostate cancer phenotypes. *Nature* **571**, 408–412 (2019).
- Zhang, Z. et al. Loss of CHD1 promotes heterogeneous mechanisms of resistance to AR-targeted therapy via chromatin dysregulation. *Cancer Cell* **37**, 584–598 (2020).
- Bluemn, E. G. et al. Androgen receptor pathway-independent prostate cancer is sustained through FGF signaling. *Cancer Cell* **32**, 474–489 (2017).
- Garraway, L. A. et al. Integrative genomic analyses identify MITF as a lineage survival oncogene amplified in malignant melanoma. *Nature* **436**, 117–122 (2005).
- Sequist, L. V. et al. Genotypic and histological evolution of lung cancers acquiring resistance to EGFR inhibitors. *Sci. Transl. Med.* **3**, 75ra26 (2011).
- Xu, G. et al. ARID1A determines luminal identity and therapeutic response in estrogen-receptor-positive breast cancer. *Nat. Genet.* **52**, 198–207 (2020).
- Park, J. W. et al. Reprogramming normal human epithelial tissues to a common, lethal neuroendocrine cancer lineage. *Science* **362**, 91–95 (2018).
- Nyquist, M. D. et al. Combined TP53 and RB1 loss promotes prostate cancer resistance to a spectrum of therapeutics and confers vulnerability to replication stress. *Cell Rep.* **31**, 107669 (2020).
- Cheng, Q. et al. Pre-existing castration-resistant prostate cancer-like cells in primary prostate cancer promote resistance to hormonal therapy. *Eur. Urol.* **81**, 446–455 (2022).
- Chen, S. et al. Single-cell analysis reveals transcriptomic remodellings in distinct cell types that contribute to human prostate cancer progression. *Nat. Cell Biol.* **23**, 87–98 (2021).
- Song, H. et al. Single-cell analysis of human primary prostate cancer reveals the heterogeneity of tumor-associated epithelial cell states. *Nat. Commun.* **13**, 141 (2022).
- Brady, L. et al. Inter- and intra-tumor heterogeneity of metastatic prostate cancer determined by digital spatial gene expression profiling. *Nat. Commun.* **12**, 1426 (2021).
- Brady, N. J. et al. Temporal evolution of cellular heterogeneity during the progression to advanced AR-negative prostate cancer. *Nat. Commun.* **12**, 3372 (2021).
- Dong, B. et al. Single-cell analysis supports a luminal-neuroendocrine transdifferentiation in human prostate cancer. *Commun. Biol.* **3**, 778 (2020).
- Tran, C. et al. Development of a second-generation antiandrogen for treatment of advanced prostate cancer. *Science* **324**, 787–790 (2009).
- Thomas, S. J., Snowden, J. A., Zeidler, M. P. & Danson, S. J. The role of JAK/STAT signalling in the pathogenesis, prognosis and treatment of solid tumours. *Br. J. Cancer* **113**, 365–371 (2015).
- Beebe, K., Lee, W.-C. & Micchelli, C. A. JAK/STAT signaling coordinates stem cell proliferation and multilineage differentiation in the *Drosophila* intestinal stem cell lineage. *Dev. Biol.* **338**, 28–37 (2010).
- Singh, S. R., Chen, X. & Hou, S. X. JAK/STAT signaling regulates tissue outgrowth and male germline stem cell fate in *Drosophila*. *Cell Res.* **15**, 1–5 (2005).
- Owen, K. L., Brockwell, N. K. & Parker, B. S. JAK–STAT signaling: a double-edged sword of immune regulation and cancer progression. *Cancers* **11**, 2002 (2019).
- Meissl, K., Macho-Maschler, S., Müller, M. & Strobl, B. The good and the bad faces of STAT1 in solid tumours. *Cytokine* **89**, 12–20 (2017).
- Spiozzo, M. T. & Chung, T. D. K. STAT3 mediates IL-6-induced neuroendocrine differentiation in prostate cancer cells. *Prostate* **42**, 186–195 (2000).
- Zhu, Y. et al. Interleukin-6 induces neuroendocrine differentiation (NED) through suppression of RE-1 silencing transcription factor (REST). *Prostate* **74**, 1086–1094 (2014).
- Kim, J., Adam, R. M., Solomon, K. R. & Freeman, M. R. Involvement of cholesterol-rich lipid rafts in interleukin-6-induced neuroendocrine differentiation of LNCaP prostate cancer cells. *Endocrinology* **145**, 613–619 (2004).
- Lee, S. O., Chun, J. Y., Nadiminty, N., Lou, W. & Gao, A. C. Interleukin-6 undergoes transition from growth inhibitor associated with neuroendocrine differentiation to stimulator accompanied by androgen receptor activation during LNCaP prostate cancer cell progression. *Prostate* **67**, 764–773 (2007).
- Lee, S. O. et al. Interleukin-6 promotes androgen-independent growth in LNCaP human prostate cancer cells. *Clin. Cancer Res.* **9**, 370–376 (2003).
- Lee, S. O., Lou, W., Johnson, C. S., Trump, D. L. & Gao, A. C. Interleukin-6 protects LNCaP cells from apoptosis induced by androgen deprivation through the Stat3 pathway. *Prostate* **60**, 178–186 (2004).
- Baratianian, M. et al. H3K9 methylation drives resistance to androgen receptor-antagonist therapy in prostate cancer. *Proc. Natl. Acad. Sci. USA* **119**, e2114324119 (2022).
- Rojas, A. et al. IL-6 promotes prostate tumorigenesis and progression through autocrine cross-activation of IGF-IR. *Oncogene* **30**, 2345–2355 (2011).
- DeMiguel, F. et al. Stat3 enhances the growth of LNCaP human prostate cancer cells in intact and castrated male nude mice. *Prostate* **52**, 123–129 (2002).
- Lee, S. O. et al. RNA interference targeting *Stat3* inhibits growth and induces apoptosis of human prostate cancer cells. *Prostate* **60**, 303–309 (2004).
- Malilas, W. et al. Cancer upregulated gene 2, a novel oncogene, enhances migration and drug resistance of colon cancer cells via STAT1 activation. *Int. J. Oncol.* **43**, 1111–1116 (2013).
- Khodarev, N. N. et al. STAT1 is overexpressed in tumors selected for radioresistance and confers protection from radiation in transduced sensitive cells. *Proc. Natl. Acad. Sci. USA* **101**, 1714–1719 (2004).
- Liu, C. et al. Niclosamide suppresses cell migration and invasion in enzalutamide resistant prostate cancer cells via Stat3-AR axis inhibition. *Prostate* **75**, 1341–1353 (2015).
- Liu, C. et al. Inhibition of constitutively active Stat3 reverses enzalutamide resistance in LNCaP derivative prostate cancer cells. *Prostate* **74**, 201–209 (2014).
- Luo, Y. et al. Enzalutamide-resistant progression of castration-resistant prostate cancer is driven via the JAK2/STAT1-dependent pathway. *Frontiers Mol. Biosci.* **8**, 652443 (2021).
- Cho, K. H. et al. STAT3 mediates TGF-β1-induced TWIST1 expression and prostate cancer invasion. *Cancer Lett.* **336**, 167–173 (2013).
- Sun, M. et al. Inhibition of Stat3 activation by sanguinarine suppresses prostate cancer cell growth and invasion. *Prostate* **72**, 82–89 (2012).
- Raj, G. V. et al. Estrogen receptor coregulator binding modulators (ERXs) effectively target estrogen receptor positive human breast cancers. *eLife* **6**, e26857 (2017).
- Mohammed, H. et al. Progesterone receptor modulates estrogen receptor-α action in breast cancer. *Nature* **523**, 313–317 (2015).

50. Abida, W. et al. Genomic correlates of clinical outcome in advanced prostate cancer. *Proc. Natl Acad. Sci. USA* **116**, 11428–11436 (2019).

51. Network, C. G. A. R. The molecular taxonomy of primary prostate cancer. *Cell* **163**, 1011–1025 (2015).

52. Liu, J. et al. An integrated TCGA pan-cancer clinical data resource to drive high-quality survival outcome analytics. *Cell* **173**, 400–416 (2018).

53. Gao, D. et al. Organoid cultures derived from patients with advanced prostate cancer. *Cell* **159**, 176–187 (2014).

54. Tang, F. et al. Chromatin profiles classify castration-resistant prostate cancers suggesting therapeutic targets. *Science* **376**, eabe1505 (2022).

55. Mao, N. et al. Defining the therapeutic selective dependencies for distinct subtypes of PI3K pathway-altered prostate cancers. *Nat. Commun.* **12**, 5053 (2021).

56. Wet, L.d. et al. SOX2 mediates metabolic reprogramming of prostate cancer cells. *Oncogene* **41**, 1190–1202 (2022).

57. Hessenkemper, W. et al. A natural androgen receptor antagonist induces cellular senescence in prostate cancer cells. *Mol. Endocrinol.* **28**, 1831–1840 (2014).

58. McInnes, L., Healy, J. & Melville, J. UMAP: uniform manifold approximation and projection for dimension reduction. *J. Open Source Softw.* **3**, 861 (2018).

59. Hieronymus, H. et al. Gene expression signature-based chemical genomic prediction identifies a novel class of HSP90 pathway modulators. *Cancer Cell* **10**, 321–330 (2006).

60. Zhang, D. et al. Stem cell and neurogenic gene-expression profiles link prostate basal cells to aggressive prostate cancer. *Nat. Commun.* **7**, 10798 (2016).

61. Beltran, H. et al. Divergent clonal evolution of castration-resistant neuroendocrine prostate cancer. *Nat. Med.* **22**, 298–305 (2016).

62. Dagozo-Jack, I. & Shaw, A. T. Tumour heterogeneity and resistance to cancer therapies. *Nat. Rev. Clin. Oncol.* **15**, 81–94 (2017).

63. Kwon, O.-J., Zhang, L., Jia, D. & Xin, L. Sox2 is necessary for androgen ablation-induced neuroendocrine differentiation from *Pten* null Sca-1⁺ prostate luminal cells. *Oncogene* **40**, 203–214 (2021).

64. Offin, M. et al. Concurrent RB1 and TP53 alterations define a subset of EGFR-mutant lung cancers at risk for histologic transformation and inferior clinical outcomes. *J. Thorac. Oncol.* **14**, 1784–1793 (2019).

65. Wong, G. S. et al. Periostin cooperates with mutant p53 to mediate invasion through the induction of STAT1 signaling in the esophageal tumor microenvironment. *Oncogenesis* **2**, e59 (2013).

66. Girardot, M. et al. Persistent STAT5 activation in myeloid neoplasms recruits p53 into gene regulation. *Oncogene* **34**, 1323–1332 (2015).

67. Park, H. J. et al. Cytokine-induced megakaryocytic differentiation is regulated by genome-wide loss of a uSTAT transcriptional program. *EMBO J.* **35**, 580–594 (2016).

68. Karthaus, W. R. et al. Identification of multipotent luminal progenitor cells in human prostate organoid cultures. *Cell* **159**, 163–175 (2014).

69. Ritch, S. J., Brandhagen, B. N., Goyeneche, A. A. & Telleria, C. M. Advanced assessment of migration and invasion of cancer cells in response to mifepristone therapy using double fluorescence cytochemical labeling. *BMC Cancer* **19**, 376 (2019).

70. Lin, C.-J. et al. The paracrine induction of prostate cancer progression by caveolin-1. *Cell Death Dis.* **10**, 834 (2019).

71. Dow, LukasE. et al. Apc restoration promotes cellular differentiation and reestablishes crypt homeostasis in colorectal cancer. *Cell* **161**, 1539–1552 (2015).

72. Dobin, A. et al. STAR: ultrafast universal RNA-seq aligner. *Bioinformatics* **29**, 15–21 (2013).

73. Liao, Y., Smyth, G. K. & Shi, W. featureCounts: an efficient general purpose program for assigning sequence reads to genomic features. *Bioinformatics* **30**, 923–930 (2014).

74. Love, M. I., Huber, W. & Anders, S. Moderated estimation of fold change and dispersion for RNA-seq data with DESeq2. *Genome Biol.* **15**, 550 (2014).

75. Wolf, F. A., Angerer, P. & Theis, F. J. SCANPY: large-scale single-cell gene expression data analysis. *Genome Biol.* **19**, 15 (2018).

76. Traag, V. A., Waltman, L. & Eck, N. J. V. From Louvain to Leiden: guaranteeing well-connected communities. *Sci. Rep.* **9**, 5233 (2019).

77. Qiu, X. et al. Reversed graph embedding resolves complex single-cell trajectories. *Nat. Methods* **14**, 979–982 (2017).

78. Chen, C. D. et al. Molecular determinants of resistance to antiandrogen therapy. *Nat. Med.* **10**, 33–39 (2003).

79. Arora, V. K. et al. Glucocorticoid receptor confers resistance to antiandrogens by bypassing androgen receptor blockade. *Cell* **155**, 1309–1322 (2013).

80. Zhang, Z. et al. Tumor microenvironment-derived NRG1 promotes antiandrogen resistance in prostate cancer. *Cancer Cell* **38**, 279–296 (2020).

Acknowledgements

We thank C.L. Sawyers at MSKCC for providing the parental LNCaP/AR and CWR22Pc cell lines. We thank Y. Chen and C. Lee at MSKCC for providing the human organoid models. We thank K. O'Donnell, M. Buszczak and J. Wu at UT Southwestern Medical Center for helpful discussion. This work was supported, or partially supported, by the National Cancer Institute/National Institutes of Health (5R00CA218885 and 1R37CA258730 to P.M., 1P30CA142543 and 1R01CA258584 to T.W., 1R01CA245318 to B.L., R01CA178431 to D.J.V.G. and T32C124334 to C.R.T.), the Department of Defense (W81XWH-18-1-0411 and W81XWH21-1-0520 to P.M., W81XWH-16-1-0474 to J.-H.W. and W81XWH2110418 to X. Li), the Cancer Prevention Research Institute (RRI170050 and RP220473 to P.M., RP190208 to T.W., RR170079 to B.L. and RP160157 to K.R.), the Prostate Cancer Foundation (17YOUN12 to P.M.), the Welch Foundation (I-2005-20190330 to P.M.), the UTSW Deborah and W.A. Tex Moncrief, Jr., Scholar in Medical Research Award (P.M.), the UTSW Harold C. Simmons Cancer Center Pilot Award (P.M.) and the UTSW CCSG Data Science Shared Resources (D.S. and T.W.).

Author contributions

S.D. and P.M. conceived the project. S.D., C.W., Y.W. and P.M. designed and conducted experiments and interpreted data. S.D. and P.M. co-wrote the manuscript. L.A.M. and N.A.J. edited the manuscript. S.D., C.W., A.M. and X. Li conducted all genetic and pharmaceutical inactivation of JAK–STAT signaling in all the in vitro assays. S.D., C.W. and N.A.J. performed all in vivo xenograft experiments. Y.X., J.G. and S.D. performed all ChIP experiments. Y.X. and S.D. performed migration, invasion and prostasphere formation assays. S.D., C.W., X. Li, C.R.T., A.M. and V.A. performed all qPCR and western blotting experiments. X. Li, K.R. and P.M. performed all mouse and human organoid experiments. C.W., X. Li, X. Liu and G.R. performed all human explant experiments. C.W., X. Li and D.S. performed tumor sample IHC and qPCR. X. Li and S.D. performed all cell line and organoid IF and IHC staining. Y.W. and P.M. performed the analysis for cell line and human scRNA-seq. U.-G.L., L.X., J.-T.H., Y.Z. and P.M. performed clinical data analysis. B.L. and J.Y. conducted the library preparation and sequencing for the scRNA-seq experiment. T.W. and P.M. oversaw the bioinformatic analysis. D.J.V.G. performed the SOX2 ChIP-seq experiment and analysis. Z.X. conducted the deposit of bioinformatic data. P.M. is the corresponding author of this manuscript.

Competing interests

G.R. holds issued and pending patents, which have been licensed to EtiraRx. G.R. serves or has served in an advisory role to Bayer, Johnson and Johnson, Myovant, EtiraRx, Amgen, Pfizer and Astellas. G.R. has or has had grant support from Bayer, EtiraRx and Johnson and Johnson. All other authors declare that they have no competing interests.

Additional information

Extended data is available for this paper at <https://doi.org/10.1038/s43018-022-00431-9>.

Supplementary information The online version contains supplementary material available at <https://doi.org/10.1038/s43018-022-00431-9>.

Correspondence and requests for materials should be addressed to Ping Mu.

Peer review information *Nature Cancer* thanks Christopher Barbieri and Hua Yu for their contribution to the peer review of this work.

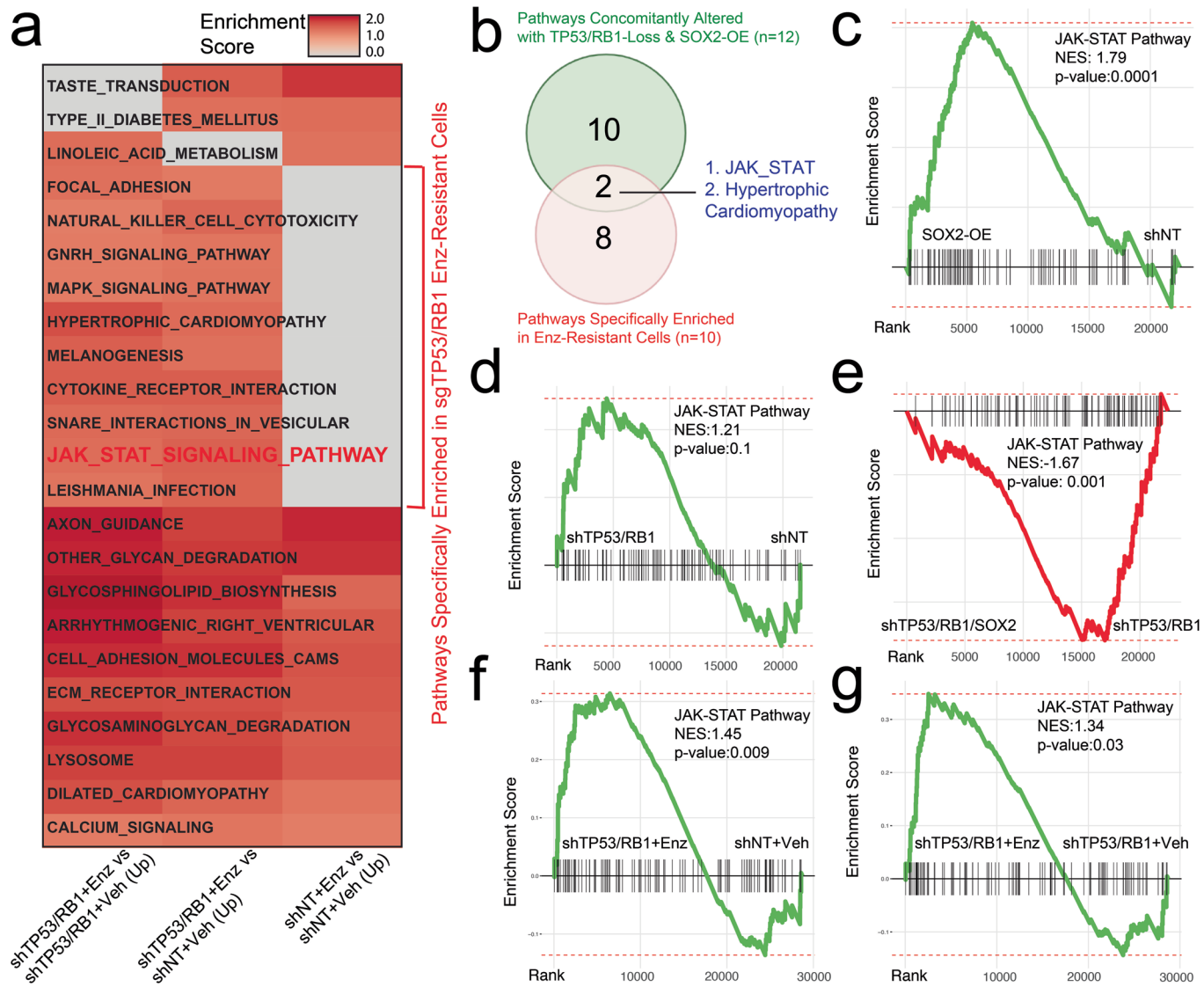
Reprints and permissions information is available at www.nature.com/reprints.

Publisher's note Springer Nature remains neutral with regard to jurisdictional claims in published maps and institutional affiliations.

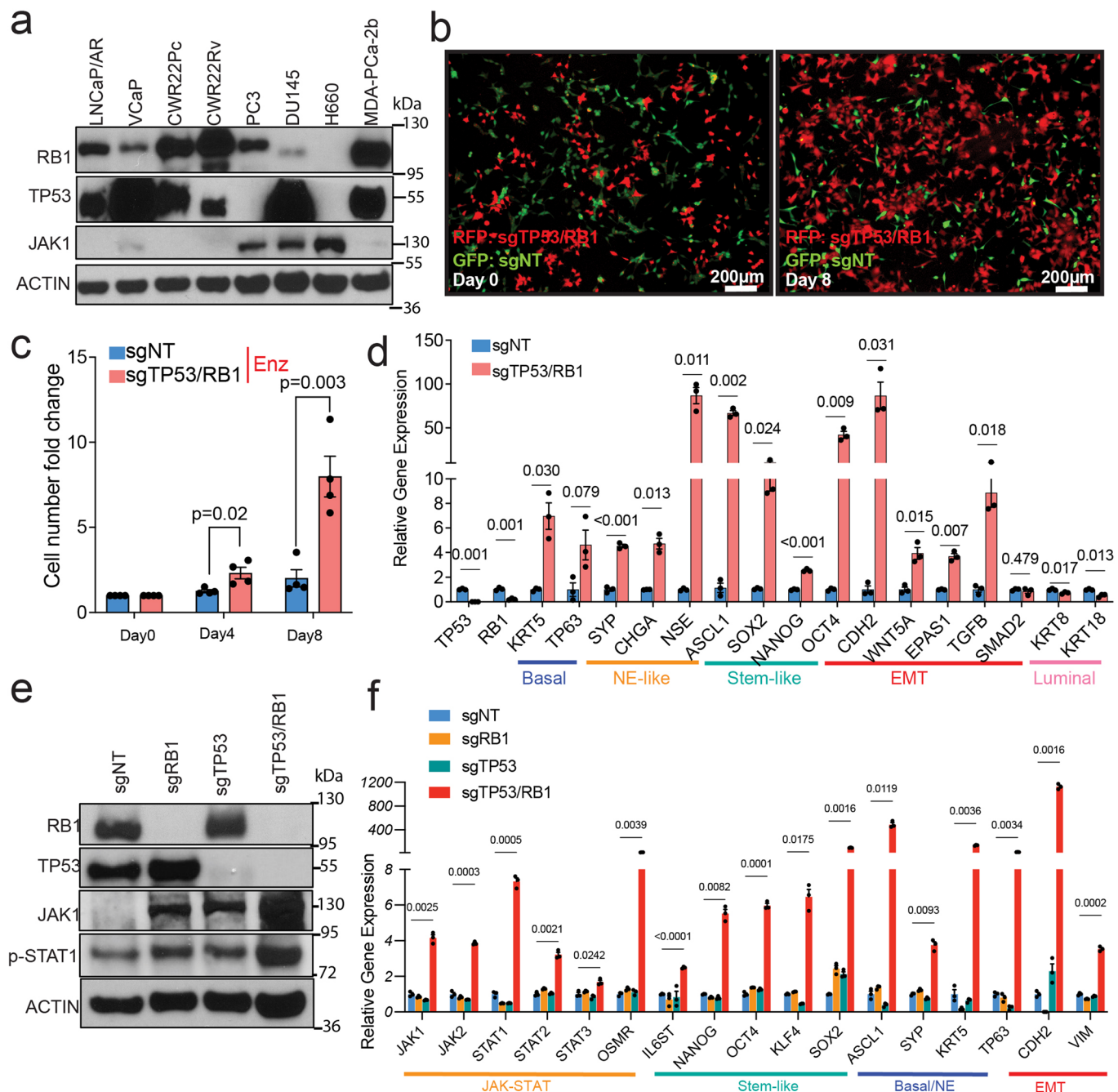


Open Access This article is licensed under a Creative Commons Attribution 4.0 International License, which permits use, sharing, adaptation, distribution and reproduction in any medium or format, as long as you give appropriate credit to the original author(s) and the source, provide a link to the Creative Commons license, and indicate if changes were made. The images or other third party material in this article are included in the article's Creative Commons license, unless indicated otherwise in a credit line to the material. If material is not included in the article's Creative Commons license and your intended use is not permitted by statutory regulation or exceeds the permitted use, you will need to obtain permission directly from the copyright holder. To view a copy of this license, visit <http://creativecommons.org/licenses/by/4.0/>.

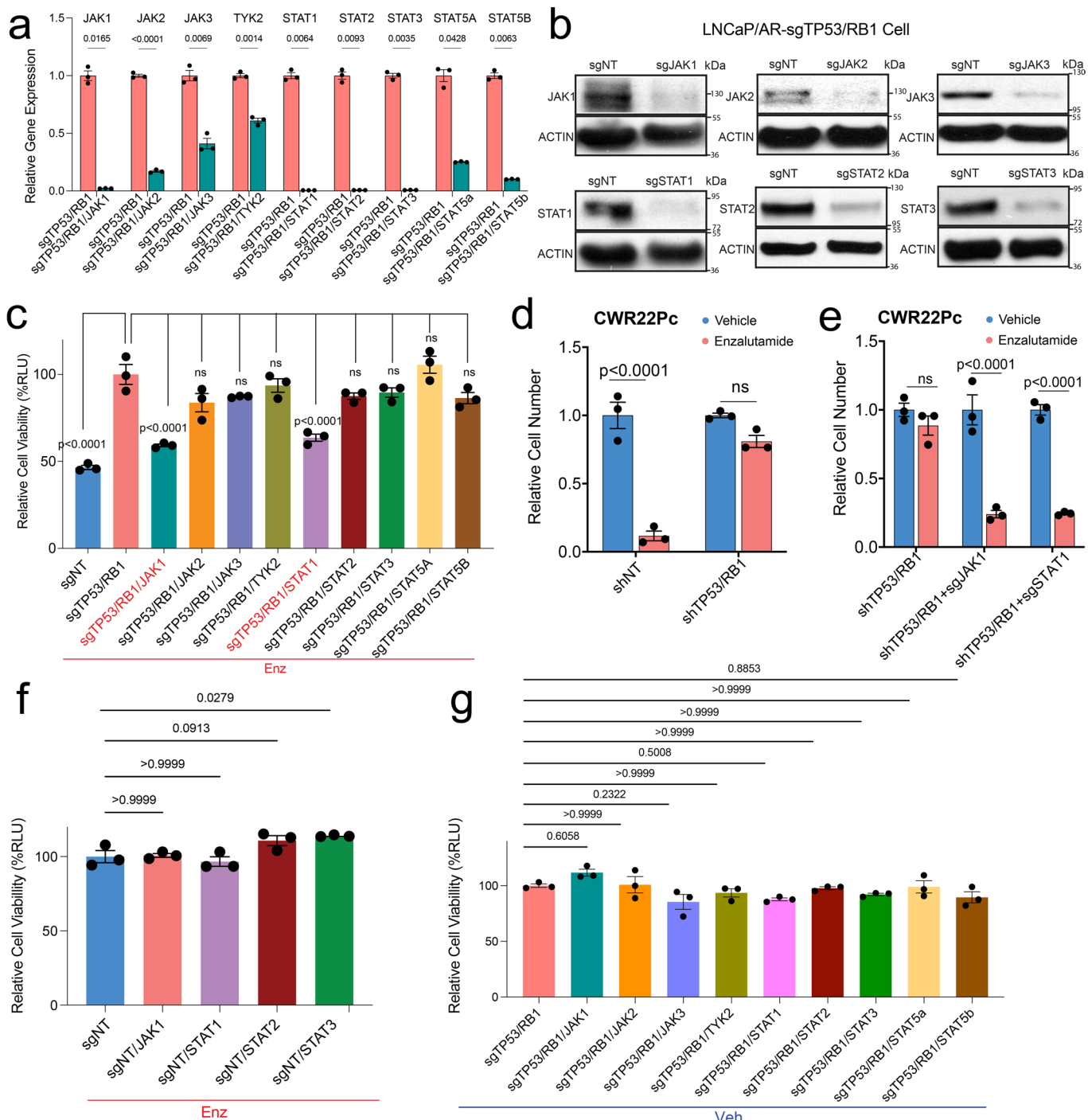
© The Author(s) 2022, corrected publication 2022



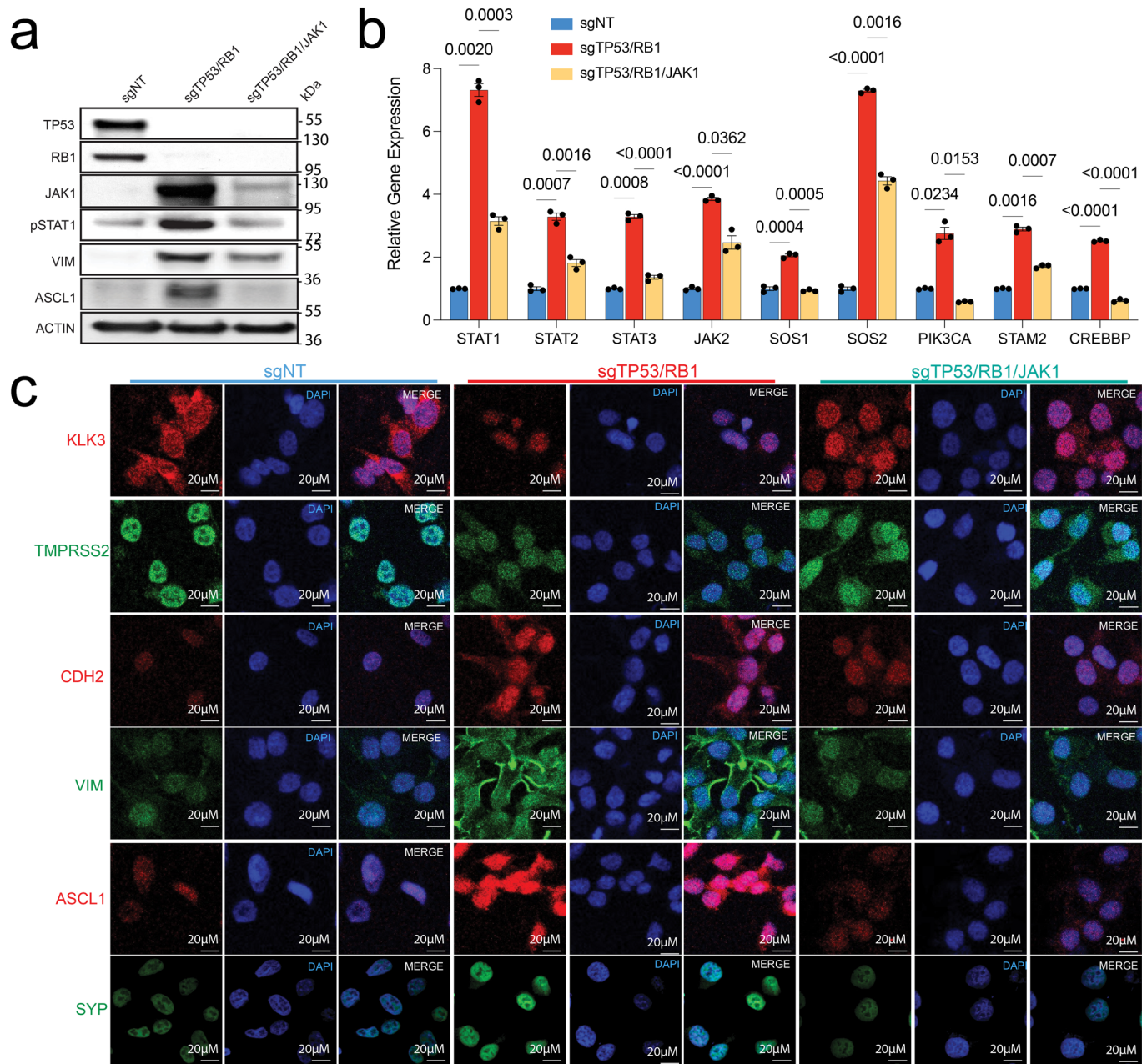
Extended Data Fig. 1 | JAK-STAT signaling pathway is enriched in Enz resistant mCRPC with TP53/RB1-deficiency. a, Heat map represents the significantly changed signaling pathways in LNCaP/AR cell lines transduced with annotated shRNAs and treated with Enz or vehicle, based on GSEA analysis. Signaling pathways specifically enriched in shTP53/RB1 Enz-resistant cells are labeled with red bracket. Three comparisons are presented and reads from $n=3$ independently treated cell cultures were used for analysis. b, Venn diagram represents the signaling pathways concomitantly altered with TP53/RB1-Loss and SOX2-OE, while also specifically enriched in shTP53/RB1 Enz-resistant cells. c-g, GSEA analysis of JAK-STAT signaling pathway (KEGG_JAK_STAT_Signaling_Pathway) expression in: (c) SOX2-OE group compared to shNT group; (d) shTP53/RB1 group compared to shNT group; (e) shTP53/RB1 group compared to shTP53/RB1/SOX2 group; (f) shTP53/RB1+Enz group compared to shNT-Veh group; (g) shTP53/RB1+Enz group compared to shTP53/RB1+Veh group. For panel c-g, reads from $n=3$ independently treated cell cultures were used for analysis. GSEA p-values were calculated with two-sided permutation test by simulations.



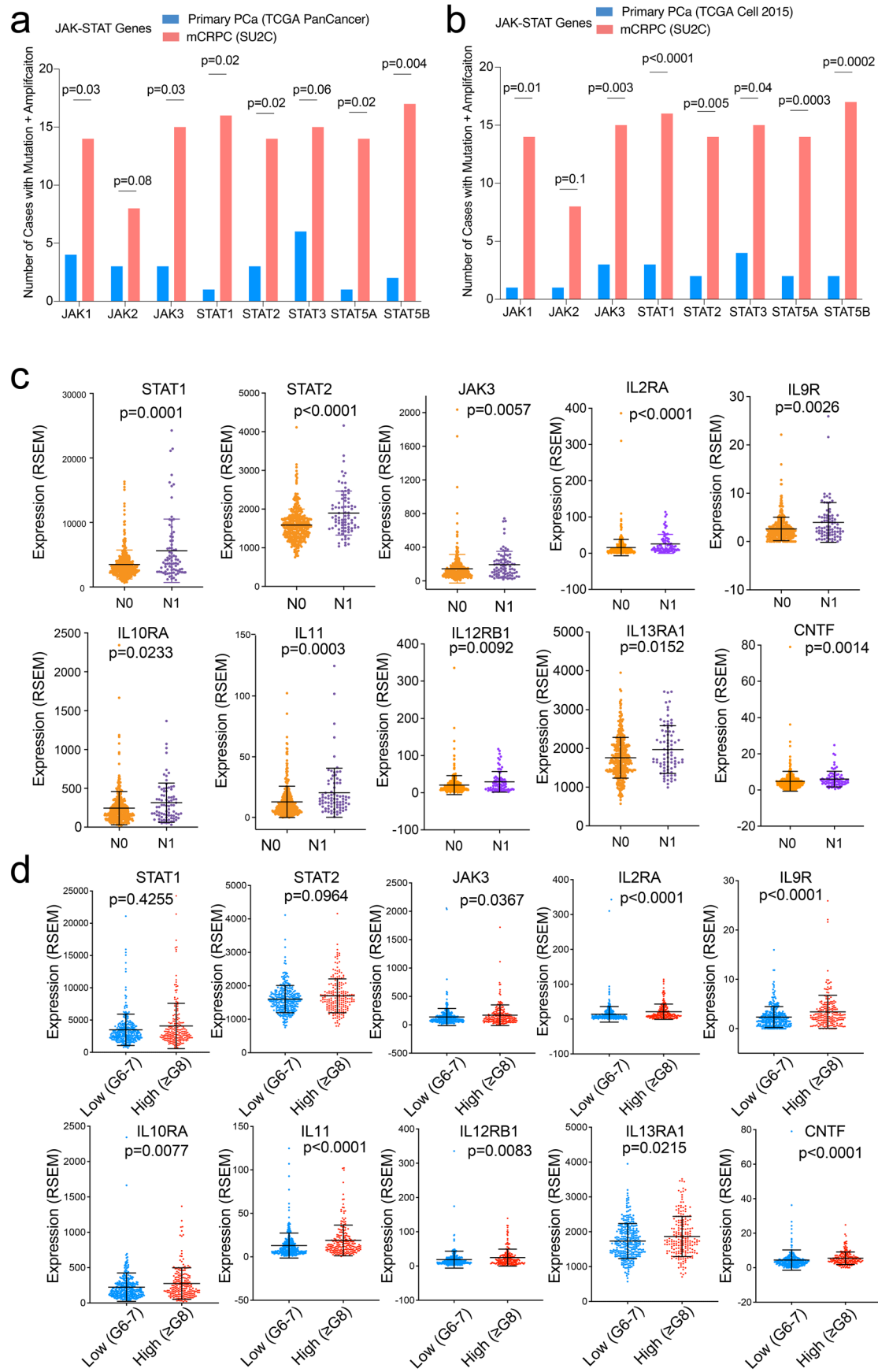
Extended Data Fig. 2 | LNCaP/AR-sgTP53/RB1 is a highly resistant and lineage plastic cell line model. **a**, Western Blot represents the level of RB1, TP53, JAK1 and ACTIN proteins in a series of human PCa cell line models; representative pictures of 2 repeats with similar results were shown. **b**, Fluorescence microscope imaging shows the cell mixtures of sgTP53/RB1-RFP cells (red) and sgNT-GFP cells (green) on Day 0 and Day 8 of the competition assay cultured in CSS medium and 10 μM Enz; representative pictures of $n=4$ independently treated cell cultures were shown. **c**, Relative cell number fold change of LNCaP/AR cells transduced with Cas9 and annotated guide RNAs measured in the competition assay. The cell mixtures of sgNT-GFP and sgTP53/RB1-RFP were treated in CSS medium with 10 μM Enz for 8 days and the number of GFP/RFP positive cells were measured by FACS on Day 0, 4 and 8. $n=4$ independently treated cell cultures. **d**, Relative expression of canonical lineage marker genes in LNCaP/AR cells transduced with Cas9 and annotated guide RNAs. For panel (c-d), p-values were calculated using two-tailed multiple t-test with Welch's correction and annotated in figure. **e**, Western Blot represents the level of RB1, TP53, JAK1, p-STAT1 and ACTIN proteins in LNCaP/AR cells transduced with Cas9 and annotated guide RNAs; representative of 2 repeats with similar results were shown. **f**, Relative expression of canonical JAK-STAT signaling and lineage marker genes in LNCaP/AR mCRPC cells transduced with Cas9 and annotated guide RNAs. p-values were calculated using two-way ANOVA with Bonferroni multiple-comparison test and annotated in figure. For all panels unless otherwise noted, $n=3$ independently treated cell cultures and mean \pm s.e.m. is represented.



Extended Data Fig. 3 | JAK-STAT signaling is specifically required for AR therapy resistance. a, Relative expression of JAK-STAT genes in LNCaP/AR-sgTP53/RB1 cells transduced with Cas9 and annotated guide RNAs. p-values were calculated using two-tailed multiple t-test with Welch's correction. b, Western blot of JAK1-3 and STAT1-3 proteins in LNCaP/AR cells transduced with Cas9 and annotated guide RNAs; representative pictures of 2 repeats with similar results were shown. c, Relative cell number of LNCaP/AR cells transduced with annotated CRISPR guide RNAs. Cells were treated with 10 μM enzalutamide (Enz) for 8 days, and cell numbers (viability) were measured using CellTiter-Glo assay, all normalized to sgTP53/RB1 group. p-values were calculated using one-way ANOVA with Bonferroni multiple-comparison test. d, Relative cell number of CWR22Pc cells transduced with annotated shRNAs. e, Relative cell number of CWR22Pc cells transduced with annotated shRNAs and/or Cas9 and CRISPR guide RNAs. For panel d-e, cell numbers were measured by cell proliferation assay, normalized to Veh condition, and p-values were calculated using two-way ANOVA with Bonferroni multiple-comparison. f, Relative cell number of LNCaP/AR-sgNT cells transduced with Cas9 annotated CRISPR guide RNAs. Cells were treated with 10 μM enzalutamide (Enz) for 8 days and cell number was measured using CellTiter-Glo assay, all normalized to sgNT group. p-values were calculated using one-way ANOVA with Bonferroni multiple-comparison test. g, Relative cell number of LNCaP/AR-sgTP53/RB1 cells transduced with Cas9 annotated CRISPR guide RNAs. Cells were treated with DMSO for 8 days and cell number was measured using CellTiter-Glo assay, all normalized to sgTP53/RB1 group. p-values were calculated using one-way ANOVA with Bonferroni multiple-comparison test. For all panels unless otherwise noted, n=3 independently treated cell cultures and mean ± s.e.m. is represented. p-values were annotated in figures.

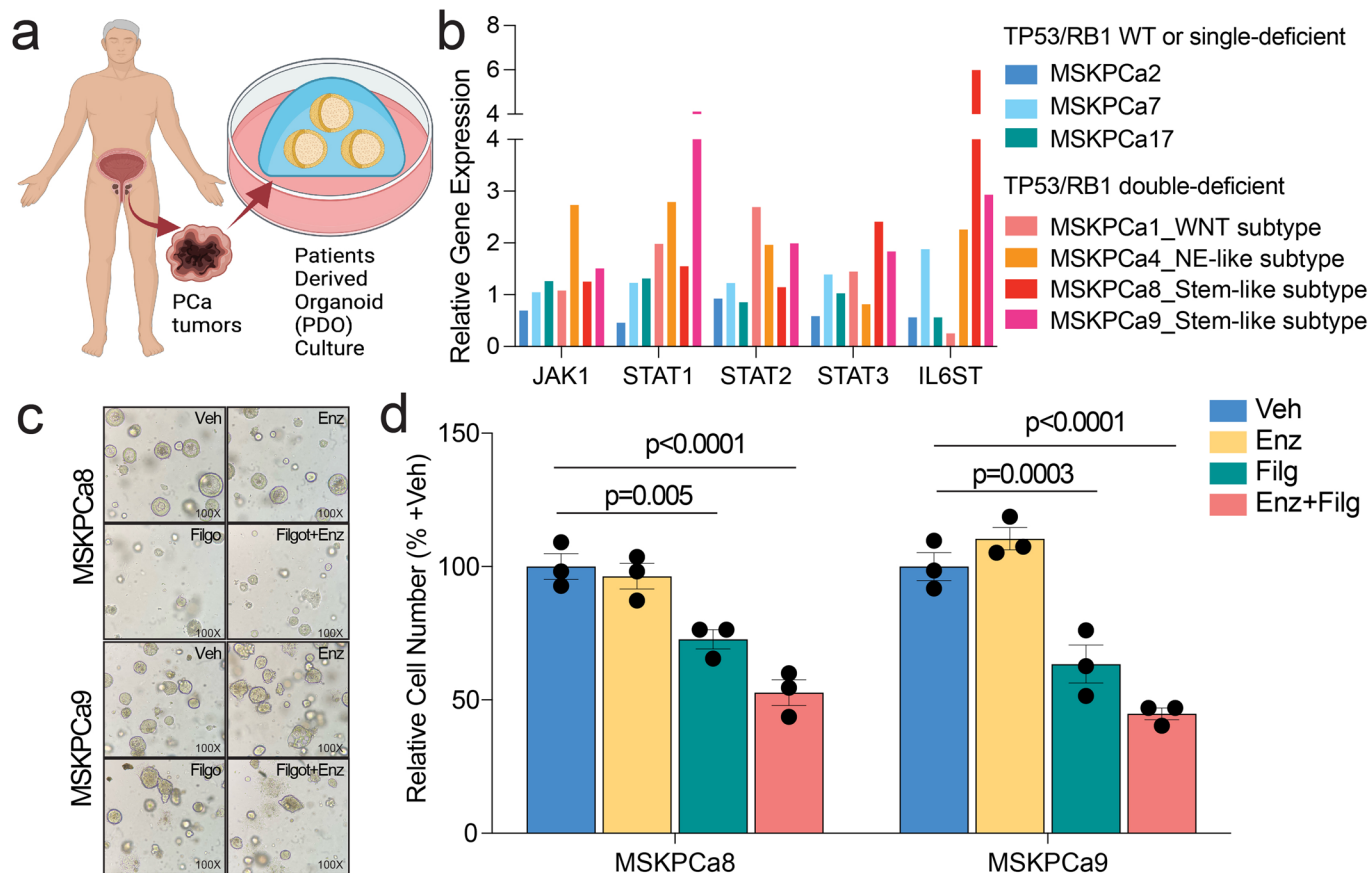


Extended Data Fig. 4 | JAK1-KO reversed the acquisition of lineage plasticity. **a**, Western blot of JAK1, pSTAT1 and lineage marker proteins in LNCaP/AR cells transduced with Cas9 and annotated guide RNAs; representative pictures of 2 repeats with similar results were shown. **b**, Relative expression of canonical JAK-STAT genes in LNCaP/AR mCRPC cells transduced with Cas9 and annotated guide RNAs. $n=3$ independently treated cell cultures and mean \pm s.e.m. is represented. p -values were calculated using two-way ANOVA with Bonferroni multiple-comparison test and annotated in figure. **c**, IF staining of LNCaP/AR cells transduced with Cas9 and annotated guide RNAs with annotated antibodies; representative pictures of $n=2$ independent treated cell cultures were shown.

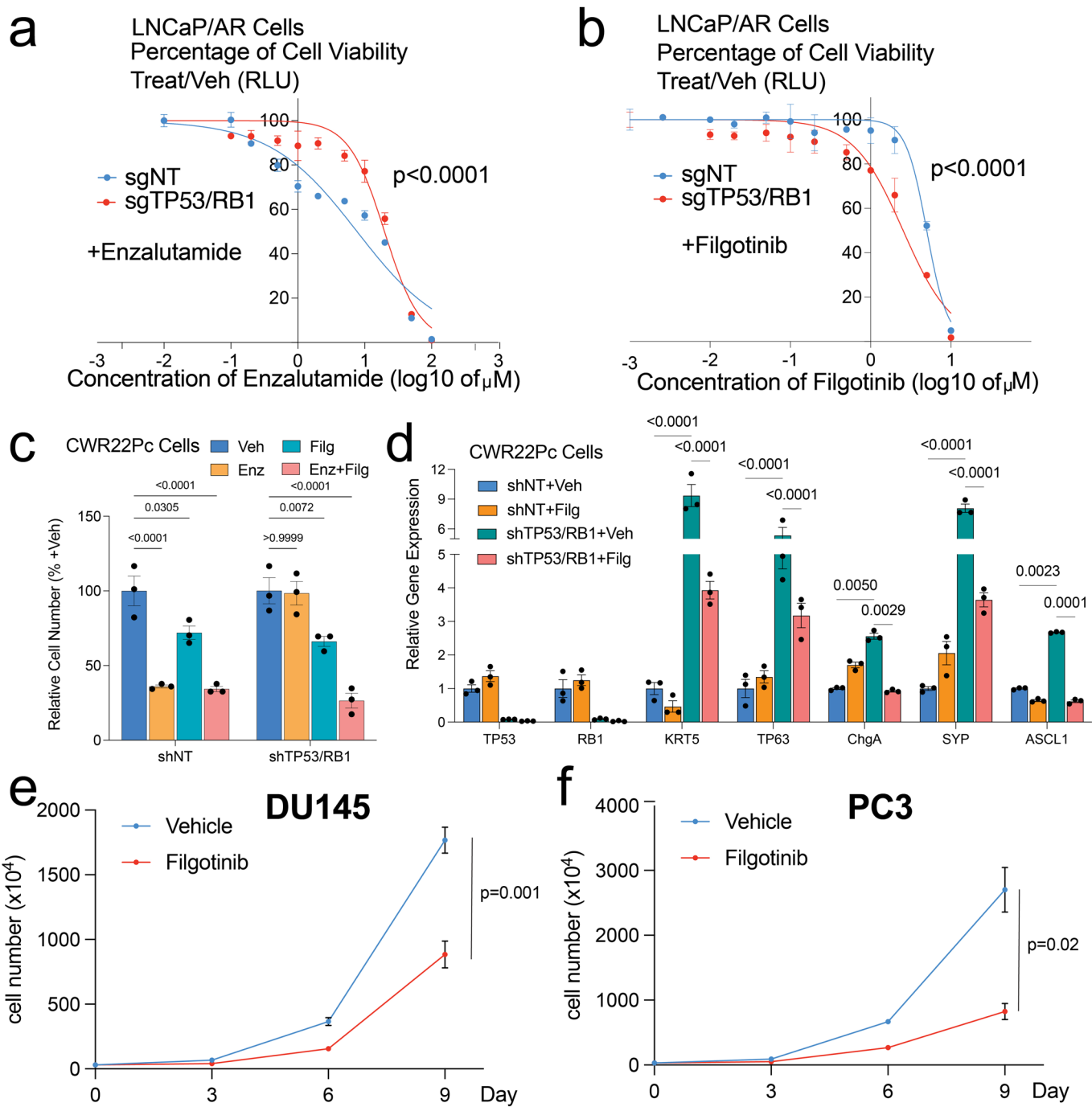


Extended Data Fig. 5 | See next page for caption.

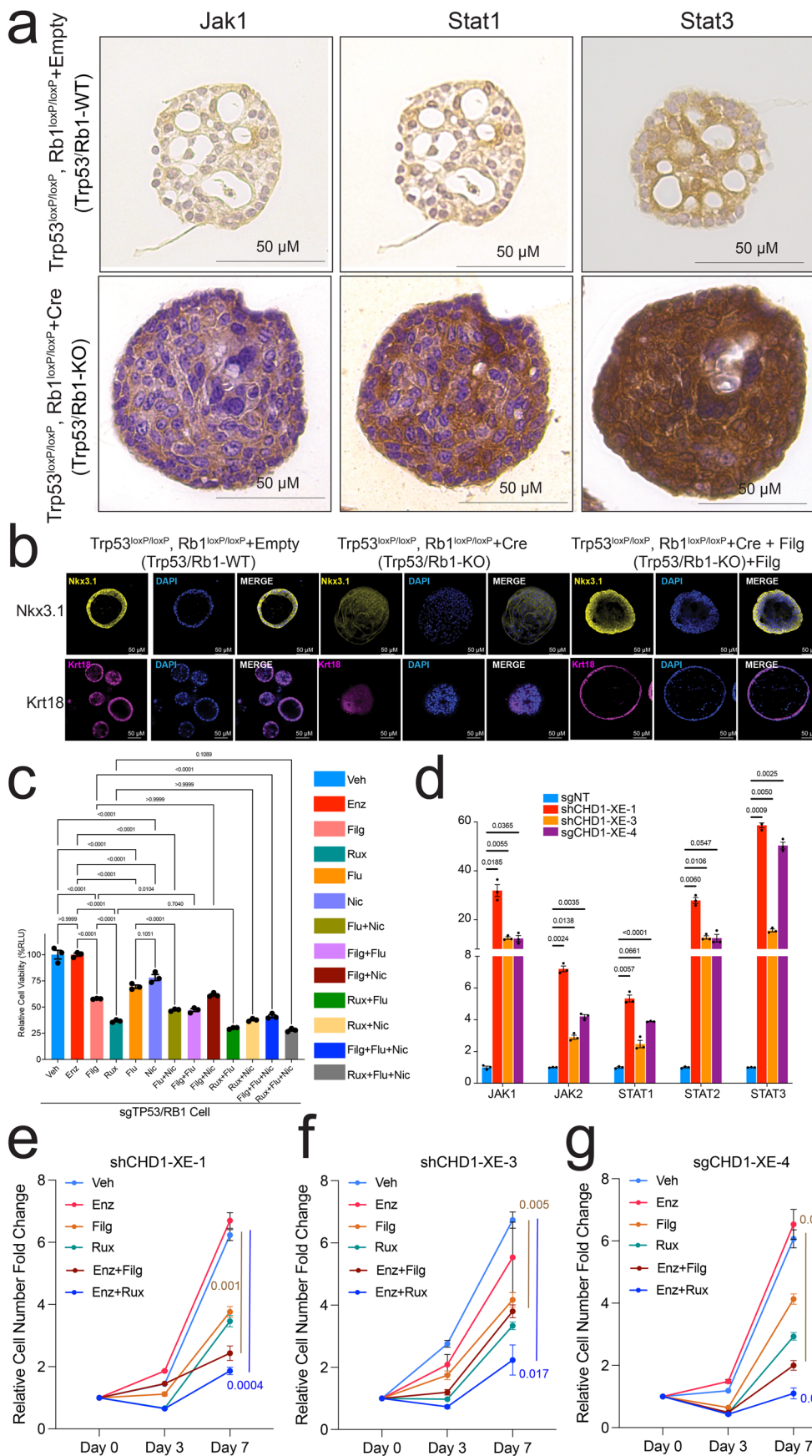
Extended Data Fig. 5 | JAK1 and STAT1 genomic alterations is correlated with poor outcome of patients with mCRPC. a, Number of PCa cases with genomic alterations (amplification or mutation) in the loci of key JAK-STAT signaling genes in the mCRPC tumors of the SU2C cohort, compared to the number in the primary tumors of the TCGA PanCancer cohort. TCGA PanCancer = 489 tumors, SU2C = 444 tumors. b, Number of PCa cases with genomic alterations (amplification or mutation) in the loci of key JAK-STAT signaling genes in the mCRPC tumors of the SU2C cohort, compared to the frequency in the primary tumors of the TCGA Cell 2015 cohort. TCGA Cell 2015 = 333 tumors, SU2C = 444 tumors. For panel (a-b), p-values were calculated using two-tails Fisher's exact test and annotated in figures. c, Expression (RSEM) of JAK-STAT signaling genes in patients with regional lymph nodes metastasis (N1, n = 80 tumors) compared to patients without regional lymph nodes metastasis (N0, n = 345 tumors). d, Expression (RSEM) of JAK-STAT signaling genes in the high-grade tumors (Gleason score ≥ 8 , n = 206 tumors) compared to the low-grade tumors (Gleason score ≤ 7 , n = 292 tumors). For panel (c-d), mean \pm s.d. is represented and p-values were calculated using two-sided Mann-Whitney test and annotated in figures.



Extended Data Fig. 6 | JAK-STAT inhibition reversed the lineage plasticity-driven AR therapy resistance in PDO. a, Schematic figure represents the generation and examination of patient-derived organoid (PDO) model. Figure was created with BioRender.com. b, Relative expression of JAK-STAT genes in a series of PDOs based on RNA-seq results (see Methods). c, Bright field pictures of PDO MSKPCa8 and MSKPCa9 cultured in 3D matrigel and treated with DMSO (Veh), 10 μ M enzalutamide (Enz), 5 μ M filgotinib (Filg) or the combination of Enz and Filg (Enz + Filg) for 6 days, representative pictures of $n=3$ independent treated cell cultures. d, Relative cell number of PDO MSKPCa8 and MSKPCa9 treated with annotated treatments for 6 days, normalized to “Veh” group. Treatment’s denotation is same as panel (c). $n=3$ independently treated cell cultures and mean \pm s.e.m. is represented. p-values were calculated using two-way ANOVA with Bonferroni multiple-comparison test and annotated in figure.

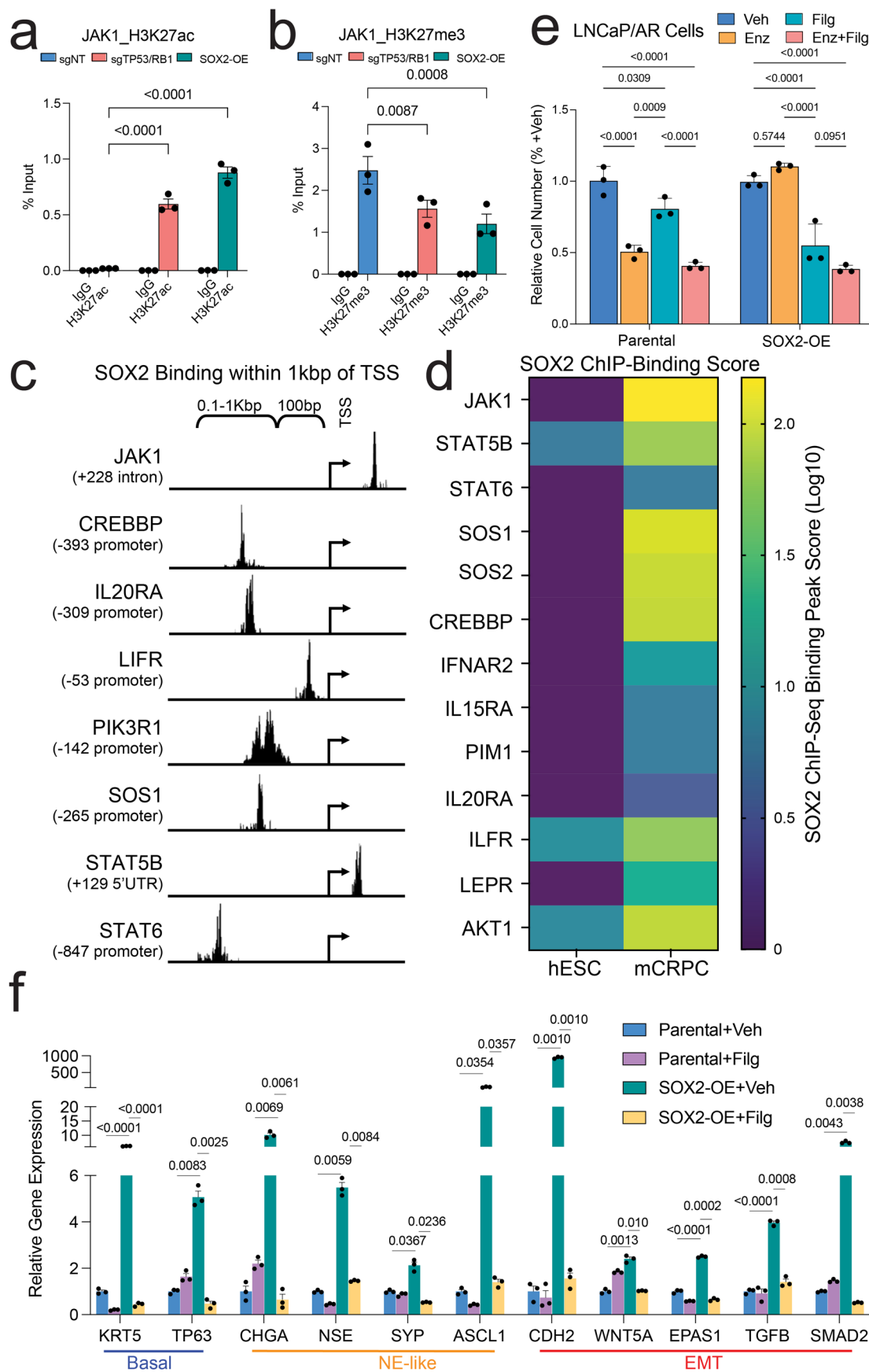


Extended Data Fig. 7 | JAK inhibitor impairs lineage plasticity and restores Enz sensitivity. a, Enz dose-response curve of LNCaP/AR cells transduced with Cas9 and annotated CRISPR guide RNAs. b, Filg dose-response curve of LNCaP/AR cells transduced with annotated Cas9 and CRISPR guide RNAs. For panel (a-b), p-values were calculated by non-linear regression with two-sided extra sum-of-squares F test. c, Relative cell number of CWR22Pc cells transduced with annotated shRNAs and treated with various treatments, normalized to “Veh” group. Enz denotes 1 μ M Enz, Filg denotes 5 μ M filgotinib, Enz + Filg denotes the combination of Enz and Filg and Veh denotes DMSO treatment with equal volume as Enz. Cells were treated for 4 days and cell numbers were counted. d, Relative expression of canonical lineage marker genes in CWR22Pc cells transduced with annotated shRNAs and treated with vehicle or Filg, normalized to “shNT + Veh” group. Filg denotes 5 μ M filgotinib, and Veh denotes DMSO treatment with equal volume as Filg. e, Cell number of DU145 cells upon treatment administration, measured by cell proliferation assay. f, Cell number of PC3 cells upon treatment administration, measured by cell proliferation assay. For e-f panels, Filg denotes 5 μ M Filgotinib and Veh denotes DMSO treatment for 9 days. For all panels unless otherwise noted, n=3 independently treated cell cultures and mean \pm s.e.m. is represented; p-values were calculated using two-way ANOVA with Bonferroni multiple-comparison test and were annotated in figures.



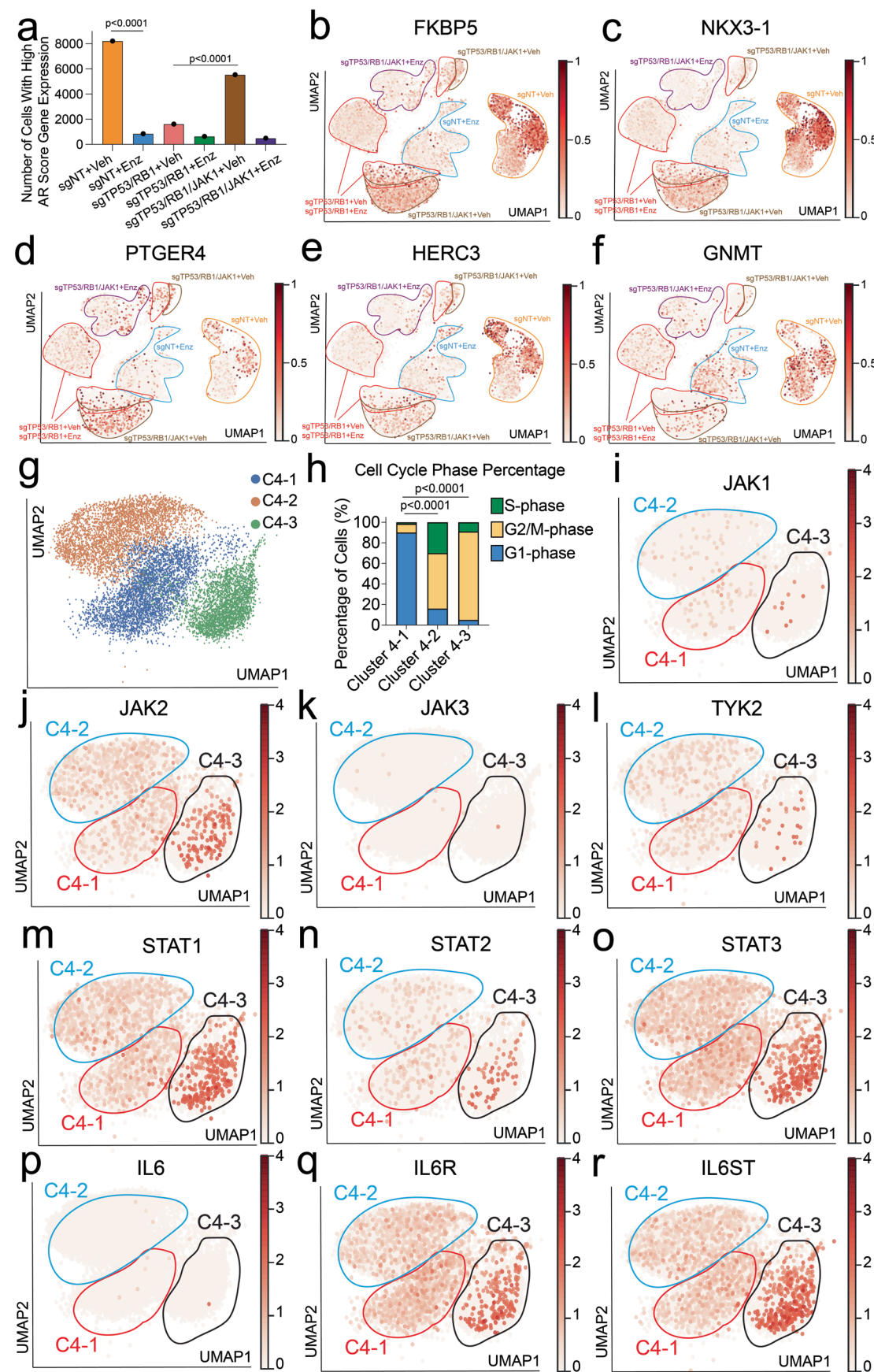
Extended Data Fig. 8 | See next page for caption.

Extended Data Fig. 8 | JAK-STAT inhibitors have combined inhibitory effect on PCa cells with lineage plasticity. a, IHC of the $\text{Trp53}^{\text{loxP/loxP}}, \text{Rb1}^{\text{loxP/loxP}}$ + Empty (TP53/RB1-WT) and $\text{Trp53}^{\text{loxP/loxP}}, \text{Rb1}^{\text{loxP/loxP}} + \text{Cre}$ (TP53/RB1-KO) organoids cultured in 3D, with annotated antibodies. b, IF of annotated organoids cultured in 3D, with annotated antibodies targeting canonical AR target genes and lineage marker genes. For panels a and b, representative pictures of $n=2$ independent treated cell cultures were shown. c, Relative cell number of LNCaP/AR cells treated with annotated treatment: 10 μM enzalutamide (Enz), 5 μM filgotinib (Filg), 5 μM ruxolitinib (Ruxo), 1 μM fludarabine (Flu), 0.2 μM niclosamide (Nic) and DMSO for 8 days and cell numbers (viability) were measured using CellTiter-Glo assay, all normalized to vehicle group. p-values were calculated using one-way ANOVA with Bonferroni multiple-comparison test. d, Relative gene expression of JAK-STAT genes in xenograft-derived Enz resistant cell lines with CHD1-deficiency. e-g, Cell number of xenografted-derived Enz resistant cells upon treatment administration, measured by cell proliferation assay. For panels (e-g), Enz denotes 10 μM enzalutamide, Filg denotes 5 μM filgotinib, Rux denotes 5 μM ruxolitinib and Veh denotes DMSO treatment for 7 days. For all panels unless otherwise noted, $n=3$ independently treated cell cultures and mean \pm s.e.m. is represented. p-values were calculated using two-way ANOVA with Bonferroni multiple-comparison test and annotated in figures.



Extended Data Fig. 9 | See next page for caption.

Extended Data Fig. 9 | Canonical JAK-STAT genes are among the prostate cancer-specific gene targets of SOX2 in mCRPC. a, H3K27ac ChIP-qPCR of the JAK1 genomic locus in LNCaP/AR cells transduced with annotated constructs. b, H3K27me3 ChIP-qPCR of the JAK1 genomic locus in LNCaP/AR cells transduced with annotated constructs. For panels (a,b), p-values were calculated using one-way ANOVA with Bonferroni multiple-comparison test. c, Representative SOX2 binding sites in the genomic loci of JAK-STAT signaling genes in the mCRPC CWR-R1 cell line based on ChIP-seq analysis. d, SOX2 binding peak score in the genomic loci of JAK-STAT signaling genes in the mCRPC CWR-R1 cell (prostate cancer specific binding) compared to human ESC cell line WA01. Reads from $n=3$ independent cell cultures and matching input controls were used for analysis. e, Relative cell numbers of LNCaP/AR cells transduced with annotated constructs and treated with various treatments in CSS medium for 8 days, normalized to "Veh" group. Enz denotes 10 μ M enzalutamide, Filg denotes 5 μ M filgotinib, Enz + Filg denotes the combination of Enz and Filg, Veh denotes DMSO treatment with equal volume as Enz, for 8 days and cell numbers were counted, normalized to Veh group. f, Relative expression of canonical lineage marker genes in LNCaP/AR-SOX2-OE cells treated with annotated treatments. Filg denotes 5 μ M filgotinib, and Veh denotes DMSO treatment with equal volume as Filg. Cells were treated for 6 days. p-values were calculated using two-way ANOVA with Bonferroni multiple-comparison test. For all panels unless otherwise noted, $n=3$ independently treated cell cultures and mean \pm s.e.m. is represented; p-values were annotated in figures.



Extended Data Fig. 10 | See next page for caption.

Extended Data Fig. 10 | AR signaling partially restored in the subclones with TP53/RB1/JAK1-KD and vehicle treatment. a, Bar plot presents the number of single cells expressing high level (expression level in the top 20% of all single cells of all samples) of AR targeted genes (partial AR Score genes as shown in Supplemental Table). p-values are calculated with two-sided Chi-square test with Yates correction and annotated in figure. (Veh n=14268 cells, Enz n=15149 cells), sgTP53/RB1 (Veh n=12267 cells, Enz n=9850 cells), sgTP53/RB1/JAK1 (Veh n=25200 cells, Enz n=11096 cells). b-f, UMAP plot of single cell transcriptomic profiles colored by expression of selected AR target genes (z-score, AR Score genes) for each cell (dot). LNCaP/AR cells were transduced with Cas9 and annotated CRISPR guide RNAs and treated with vehicle or Enz for 5 days. Fields of different sample groups are labeled with different color. g, UMAP plot of single cells in cluster 4, colored by unsupervised clustering of 3 sub-clusters. h, Bar plot presents the percentage distribution of each single cell in different cell cycle phases from subcluster 4-1, 4-2 and 4-3. n of cells in each cluster: C4-1 n=3680 cells, C4-2 n=3459 cells, C4-3 n=2886 cells. p-values are calculated with two-sided Fisher's Exact Test. i-r, UMAP plot of single cell transcriptomic profiles colored by expression of canonical JAK-STAT target genes (z-score) for each cell (dot) of LNCaP/AR cells in Cluster 4. For panel i-r, distribution area of subcluster 4-1, 4-2, 4-3 are labeled with red, blue, and black. For all panels, color density of each cell is scaled by the color bar and p-values were annotated in figures.

Reporting Summary

Nature Portfolio wishes to improve the reproducibility of the work that we publish. This form provides structure for consistency and transparency in reporting. For further information on Nature Portfolio policies, see our [Editorial Policies](#) and the [Editorial Policy Checklist](#).

Statistics

For all statistical analyses, confirm that the following items are present in the figure legend, table legend, main text, or Methods section.

n/a Confirmed

- The exact sample size (n) for each experimental group/condition, given as a discrete number and unit of measurement
- A statement on whether measurements were taken from distinct samples or whether the same sample was measured repeatedly
- The statistical test(s) used AND whether they are one- or two-sided
Only common tests should be described solely by name; describe more complex techniques in the Methods section.
- A description of all covariates tested
- A description of any assumptions or corrections, such as tests of normality and adjustment for multiple comparisons
- A full description of the statistical parameters including central tendency (e.g. means) or other basic estimates (e.g. regression coefficient) AND variation (e.g. standard deviation) or associated estimates of uncertainty (e.g. confidence intervals)
- For null hypothesis testing, the test statistic (e.g. F , t , r) with confidence intervals, effect sizes, degrees of freedom and P value noted
Give P values as exact values whenever suitable.
- For Bayesian analysis, information on the choice of priors and Markov chain Monte Carlo settings
- For hierarchical and complex designs, identification of the appropriate level for tests and full reporting of outcomes
- Estimates of effect sizes (e.g. Cohen's d , Pearson's r), indicating how they were calculated

Our web collection on [statistics for biologists](#) contains articles on many of the points above.

Software and code

Policy information about [availability of computer code](#)

Data collection	Benchling guide RNA designing tool was used for CRISPR guide RNA sequences. Attune Nxt software (version 4.2.1627.1) was used for collecting FACS-based competition assay data.
Data analysis	All analysis in the work was done using open-source software. Bulk RNA-seq analysis was done using the QBRC Bulk RNA-seq pipeline (https://github.com/QBRC/QBRC_BulkRnaSeqDE). Alignment, quantification, and differential analysis were performed using the QBRC_BulkRnaSeqDE pipeline (https://github.com/QBRC/QBRC_BulkRnaSeqDE). Briefly, Alignment of reads to human reference genome (GRCh38, https://www.ncbi.nlm.nih.gov/assembly/GCF_000001405.26) was done using STAR (v2.7.2b) ⁶⁰ . FeatureCounts (v1.6.4) ⁶¹ was used for gene counts, biotype counts, and rRNA estimation. Differential expression analysis was performed using the R package DEseq2 (v1.26) ⁶² . Cutoff values of absolute fold change greater than 2 and FDR<0.1 were used to select for differentially expressed genes. Gene Set Enrichment Analysis (GSEA) was carried out with the R package fgsea (v1.14.0) using the 'KEGG' and 'Hallmark' libraries from MsigDB. 10x scRNA-seq data was preprocessed using the Cell Ranger software (5.0.0). Demultiplexing, alignment and read counting of the single-cell RNA-seq data were carried out using the 10x Genomics Cell Ranger 5.0.0. scRNA-seq data analysis was performed with the 'Scanpy' (v1.6.0) package in Python. To evaluate and model lineage plasticity as a function of cell genotype, we performed trajectory analysis using the R package 'Monocle 3'. We provided the single cell gene expression matrix containing only the highly variable genes defined as previously discussed as input and used PCA and UMAP during preprocessing steps. The trajectory was built using default parameters with the root defined from the 'loser' cluster. Custom codes for the analysis in the paper have been deposited to Github and can be accessed at https://doi.org/10.5281/zenodo.6888969 . Graph Pad Prism (V9.3.1, Graph Pad) is used for data graphing and statistical analysis. ImageJ (version 2.0.0) was used to quantify images of organoids, migration, invasion and prostasphere formation assay. FlowJo (version 10.8.0) software was used for the analysis of FACS result.

For manuscripts utilizing custom algorithms or software that are central to the research but not yet described in published literature, software must be made available to editors and reviewers. We strongly encourage code deposition in a community repository (e.g. GitHub). See the Nature Portfolio [guidelines for submitting code & software](#) for further information.

Data

Policy information about [availability of data](#)

All manuscripts must include a [data availability statement](#). This statement should provide the following information, where applicable:

- Accession codes, unique identifiers, or web links for publicly available datasets
- A description of any restrictions on data availability
- For clinical datasets or third party data, please ensure that the statement adheres to our [policy](#)

All the described bulk and single cell RNA-seq data that support the findings of this study have been deposited in the Gene Expression Omnibus under the accession numbers GSE175975. The human CRPC tumor biopsies single cell data was downloaded from and available in the Gene Expression Omnibus (GEO) under the accession number GSE137829. Patients genomic and transcriptomic data were derived from the TCGA research network and SU2C cohort, which were queried using cbiportal (http://www.ncbi.nlm.nih.gov/assembly/GCF_000001405.26/) and the Genomic Data Commons Data Portal (<https://portal.gdc.cancer.gov/>). SOX2 ChIP-Seq data were downloaded from and available under GSE166185. Source data for Fig. 1-6 and Extended Data Fig. 2-10 have been provided as Source Data files. Source data for Extended Fig 1 has been provided in Supplementary Table. RNA-seq Alignment of reads to human reference genome (GRCh38, https://www.ncbi.nlm.nih.gov/assembly/GCF_000001405.26/). All other data supporting the findings of this study are available from the corresponding author on reasonable request. Custom codes for the analysis in the paper have been deposited to Github and can be accessed at <https://doi.org/10.5281/zenodo.6888969>.

Field-specific reporting

Please select the one below that is the best fit for your research. If you are not sure, read the appropriate sections before making your selection.

Life sciences Behavioural & social sciences Ecological, evolutionary & environmental sciences

For a reference copy of the document with all sections, see nature.com/documents/nr-reporting-summary-flat.pdf

Life sciences study design

All studies must disclose on these points even when the disclosure is negative.

Sample size	Sample sizes are described in the methods and/or figure legends. The selection of sample sizes were described in Methods: "Statistics & Reproducibility" section. Specifically, for all in vitro experiments, three biological triplicates were used, no statistical method was used to predetermine sample size, but our sample sizes were similar to those reported in previous studies using those cell lines. For in vivo experiments, no statistical method was used to predetermine sample size, but our sample sizes were selected based on and similar to those reported in previous studies using the same LNCaP/AR xenograft models (Arora et al., Cell 2013, PMID 24315100; Mu et al., Science 2017, PMID 28059768; Zhang et al., Cancer Cell 2020, PMID 32220301). Based on those previous studies, sample size of 8-10 tumors per group would be sufficient to detect xenograft tumor growth differences.
Data exclusions	No excluded data points
Replication	All in vitro experiments were repeated at least 2 times and achieved similar conclusions. Replicates are described in methods and/or figure legends, and the representative results are shown. All attempts at replication were successful. For in vivo experiment, the LNCaP/AR xenograft model is a highly well-credential model from which enzalutamide and apalutamide were originally discovered, demonstrating its clinical relevance (Tran et al., 2009, PMID: 19359544; Arora et al., Cell 2013, PMID 24315100; Mu et al., Science 2017, PMID 28059768; Zhang et al., Cancer Cell 2020, PMID 32220301). However, due to the time-consuming nature of this model, and budget/time limitation, in vivo xenograft studies using LNCaP/AR xenograft model were only performed once.
Randomization	All 6-7 weeks old SCID mice were purchased from Taconic Biosciences and separated into each experimental group randomly, without prior designation. For in vitro experiments, randomization of cell lines was not possible. However, all cell lines were transduced with guide RNAs either targeting the gene of interest, or non-targeting sgNT control. All comparisons were between sgGeneX and sgNT to control the covariates. All cell lines were treated and analyzed in an identical fashion and the results of three biological replicates were analyzed concurrently.
Blinding	For all in vivo studies, the tumor cell injection and followup tumor treatment was performed by one researcher, while tumor measurement and data analysis were performed by a different researcher to ensure the studies were run in a blinded manner. For all in vitro experiments, blinding is impossible as the same researcher need to treat the cells and run the analysis. However, the cell numbers were automatically measured by FACS in the competition assay or by SpectraMax iD3 automatic plate reader in cell viability assay to ensure prior knowledge of the treatment groups had no impact on results. For the quantification of migration, invasion and prostasphere assays, as well as IHC and IF staining, the pictures were coded to blind researchers to treatment or genotype groups prior to data analysis to avoid bias.

Reporting for specific materials, systems and methods

We require information from authors about some types of materials, experimental systems and methods used in many studies. Here, indicate whether each material, system or method listed is relevant to your study. If you are not sure if a list item applies to your research, read the appropriate section before selecting a response.

Materials & experimental systems

n/a	Involved in the study
<input type="checkbox"/>	<input checked="" type="checkbox"/> Antibodies
<input type="checkbox"/>	<input checked="" type="checkbox"/> Eukaryotic cell lines
<input checked="" type="checkbox"/>	<input type="checkbox"/> Palaeontology and archaeology
<input type="checkbox"/>	<input checked="" type="checkbox"/> Animals and other organisms
<input checked="" type="checkbox"/>	<input type="checkbox"/> Human research participants
<input checked="" type="checkbox"/>	<input type="checkbox"/> Clinical data
<input checked="" type="checkbox"/>	<input type="checkbox"/> Dual use research of concern

Methods

n/a	Involved in the study
<input checked="" type="checkbox"/>	<input type="checkbox"/> ChIP-seq
<input type="checkbox"/>	<input checked="" type="checkbox"/> Flow cytometry
<input checked="" type="checkbox"/>	<input type="checkbox"/> MRI-based neuroimaging

Antibodies

Antibodies used

For western blot, antibodies used are JAK1 (Cell Signaling Technology, Cat # 3332S, Lot#6), STAT1 (Cell Signaling Technology, Cat #9172S, Lot#26), p-STAT1(58D6) (Cell Signaling Technology, Cat #9167S, Lot#25), Rb1(4H1) (Cell Signaling Technology, Cat #5230, Lot#11), P53(DO1) (Leica Biosystems, Cat# NCL-p53-DO1, Lot#6023804), Actin(8H10D10) (Cell Signaling Technology, Cat #3700, Lot#20). JAK2(C-10) (Santa Cruz, Cat# sc-390539, Lot#C0822), JAK3 (Cell Signaling Technology, Cat# 3775, Lot#6), STAT2(D9J7L) (Cell Signaling Technology, Cat# 72604, Lot#4), STAT3(D1B2J) (Cell Signaling Technology, Cat# 30835, Lot#4), Vimentin(D21H3) (Cell Signaling Technology, Cat# 5741, Lot#8), ASCL1(EPR19840) (Abcam, Cat# ab211327, Lot#GR3368513-4), Peroxidase AffiniPure Goat Anti-Mouse IgG (H+L)(AB_10015289) (Jackson ImmunoResearch, Cat# 115-035-003), Peroxidase AffiniPure Goat Anti-Rabbit IgG (H+L)(AB_2313567) (Jackson ImmunoResearch, Cat# 111-035-003).

Dilutions of all primary antibodies are 1:1000 and secondary antibodies are 1:5000.

For ChIP-qPCR experiment, antibodies used are Sox2 (D9B8N) (Cell Signaling Technology, Cat #23064S, Lot #1), Anti-Histone H3 (acetyl K27) antibody-ChIP Grade (Abcam, Cat# ab4729, Lot# GR3357415-1) and Tri-Methyl-Histone H3 (Lys27) (C36B11) Rabbit mAb (Cell Signaling Technology, Cat #9733S, Lot #8). Dilutions of all antibodies are 1:100.

For IHC and IF antibodies used are: Jak1 (Cell Signaling Technology, Cat #3332, Lot#6), Stat1 (Cell Signaling Technology, Cat #14994, Lot#26), Stat3(D1B2J) (Cell Signaling Technology, Cat #30835, Lot#4), Alexa Fluor® 647 Anti-Cytokeratin 8(EP1628Y) (Abcam, Cat #ab192468, Lot#GR198609-1), Alexa Fluor® Anti-Cytokeratin 18(E431-1) (Abcam, Cat #ab194125, Lot#GR-200266-1), Alexa Fluor® 647 Anti-Cytokeratin 5(EP1601Y) (Abcam, Cat #ab193895, Lot#GR-219431-2), Alexa Fluor® 647 Anti-Cytokeratin 14(EP1612Y) (Abcam, Cat #ab192056, Lot#GR-201705-1), Nkx3.1(4H4) (Abcam, Cat #ab96482, Lot#GR-165836-2), PSA/KLK3(D6B1) (Cell Signaling Technology, Cat #5365, Lot#4), NDRG1(D8G9) (Cell Signaling Technology, Cat #9485, Lot#4), Vimentin(D21H3) (Cell Signaling Technology, Cat #5741, Lot#8), Synaptophysin(D8F6H) (Cell Signaling Technology, Cat #36406, Lot#1), Alexa Fluor® 647-conjugated AffiniPure Goat Anti-Mouse IgG (H+L)(AB_2338902) (Jackson ImmunoResearch, Cat# 115-035-003), Alexa Fluor® 647-conjugated AffiniPure Goat Anti-Rabbit IgG (H+L)(AB_2338078) (Jackson ImmunoResearch, Cat# 111-035-144), Donkey Anti-Mouse IgG Antibody (Biotin-SP (long spacer))(AB_2307438) (Jackson ImmunoResearch, Cat# 715-065-150), Donkey Anti-Rabbit IgG Antibody (Biotin-SP (long spacer))(AB_2340593) (Jackson ImmunoResearch, Cat# 711-065-152).

Dilutions of all primary antibodies are 1:200 except for JAK1 (1:100). Dilutions of all secondary antibodies are 1:1000

Validation

All antibodies were recommended for the specific application by the manufacturer or had previously been published for the application used in this study. Relevant validation/manufacturer/citation information:

Jak1: Cell Signaling Technology, Cat # 3332S, Lot#6; Citation: PMID: 34556638; PMID: 35024200

REACTIVITY: H M; SENSITIVITY: Endogenous; MW (kDa): 130; SOURCE: Rabbit

Application-Dilution: Western Blotting-1:1000

Jak1 Antibody detects endogenous levels of total Jak1 protein. Polyclonal antibodies are produced by immunizing animals with a synthetic peptide corresponding to residues surrounding Tyr1022/1023 of human Jak1. Antibodies are purified by protein A and peptide affinity chromatography.

<https://www.cellsignal.com/products/primary-antibodies/jak1-antibody/3332>

STAT1: Cell Signaling Technology, Cat #9172S, Lot#26; Citation: PMID: 34925319; PMID: 34724828

REACTIVITY: H M R Mk; SENSITIVITY: Endogenous; MW (kDa): 84, 91; SOURCE: Rabbit

Application-Dilution: Western Blotting-1:1000; Immunoprecipitation-1:50; Chromatin IP-1:50

Stat1 Antibody detects endogenous levels of total Stat1 protein. The antibody detects both Stat1alpha (91kDa) and Stat1beta (84 kDa) isoforms. Polyclonal antibodies are produced by immunizing animals with a synthetic peptide corresponding to the sequence of human Stat1. Antibodies are purified by protein A and peptide affinity chromatography.

<https://www.cellsignal.com/products/primary-antibodies/stat1-antibody/9172>

p-STAT1(Tyr701) (58D6): Cell Signaling Technology, Cat # 9167S, Lot#25; Citation: PMID: 34992585; PMID: 34420035

REACTIVITY: H M; SENSITIVITY: Endogenous; MW (kDa): 84, 91; Source/Isotype: Rabbit IgG

Application-Dilution: Western Blotting-1:1000; Immunoprecipitation-1:100; Immunohistochemistry (Paraffin)-1:400 - 1:1600; Immunofluorescence (Immunocytochemistry)-1:200 - 1:800; Flow Cytometry-1:100 - 1:400; Chromatin IP-1:100; Chromatin IP-seq-1:100

Phospho-Stat1 (Tyr701) (58D6) Rabbit mAb detects endogenous levels of Stat1 only when phosphorylated at tyrosine 701. The antibody detects phosphorylated tyrosine 701 of p91 Stat1 and also the p84 splice variant. It does not cross-react with the corresponding phospho-tyrosines of other Stat proteins.

<https://www.cellsignal.com/products/primary-antibodies/phospho-stat1-tyr701-58d6-rabbit-mab/9167>

Rb1(4H1): Cell Signaling Technology, Cat #5230, Lot#11, Citation: PMID: 8939849; PMID: 9315635; PMID: 11134518

REACTIVITY: H Mk B Pg; SENSITIVITY: Endogenous; MW (kDa): 110; Source/Isotype: Mouse IgG2a

Application-Dilution: Western Blotting-1:2000; Immunoprecipitation-1:100; Immunohistochemistry (Paraffin)-1:400 - 1:1600;

Immunofluorescence (Immunocytochemistry)-1:800 - 1:3200; Flow Cytometry-1:200 - 1:800; Chromatin IP-1:200

Rb (4H1) Mouse mAb can be used in high throughput kinase assays and drug discovery applications. It detects Rb but does not recognize the Rb homologues p107 or p130. Monoclonal antibody is produced by immunizing animals with a fusion protein (Rb-C

Fusion Protein #6022) containing residues 701-928 of human Rb.
<https://www.cellsignal.com/products/primary-antibodies/rb-4h1-mouse-mab/5230>
 P53 (DO1): Leica Biosystems, Cat# NCL-p53-DO1, Lot#6023804; Citation: PMID: 28059768; PMID: 21533191
 This monoclonal antibody recognizes both wild type and mutant forms of human p53 protein under denaturing and non-denaturing conditions. The epitope recognized by clone DO-7 can be destroyed by prolonged fixation in buffered formalin. The heat induced epitope retrieval technique may improve staining in some cases.
<https://shop.leicabiosystems.com/us/ihc-ish/ihc-primary-antibodies/pid-p53-protein>
 β-Actin (8H10D10): Cell Signaling Technology, Cat #3700, Lot#20; Citation: PMID: 35301087; PMID: 35387176
 REACTIVITY: H M R Hm Mk Dg; SENSITIVITY: Endogenous; MW (kDa): 45; Source/Isotype: Mouse IgG2b
 Application-Dilution: Western Blotting-1:1000; Immunohistochemistry (Paraffin)- 1:8000 - 1:32000; Immunofluorescence (Immunocytochemistry)- 1:2500 - 1:10000; Flow Cytometry (Fixed/Permeabilized) 1:200 - 1:800
 β-Actin (8H10D10) Mouse mAb detects endogenous levels of total β-actin protein. Due to the high sequence identity between the cytoplasmic actin isoforms, β-actin and cytoplasmic γ-actin, this antibody may cross-react with cytoplasmic γ-actin. It does not cross-react with α-skeletal, α-cardiac, α-vascular smooth, or γ-enteric smooth muscle isoforms.
<https://www.cellsignal.com/products/primary-antibodies/b-actin-8h10d10-mouse-mab/3700>
 Stat3(D1B2J): Cell Signaling Technology, Cat #30835, Lot#4; Citation: PMID: 35326545; PMID: 35151317; PMID: 35157848
 REACTIVITY: H M R; SENSITIVITY: Endogenous; MW (kDa): 79, 86; Source/Isotype: Rabbit IgG
 Application-Dilution: Western Blotting-1:1000; Immunoprecipitation-1:200; Immunohistochemistry (Paraffin)-1:100 - 1:400; Immunofluorescence (Immunocytochemistry)-1:400 - 1:800
 Stat3 (D1B2J) Rabbit mAb recognizes endogenous levels of total Stat3 protein. Some unclear staining has been observed in rodent. Species reactivity for IHC-P and IF-IC is human preferred. Monoclonal antibody is produced by immunizing animals with a synthetic peptide corresponding to residues surrounding Pro695 of human Stat3 protein.
<https://www.cellsignal.com/products/primary-antibodies/stat3-d1b2j-rabbit-mab/30835>
 JAK2(C-10): Santa Cruz, Cat# sc-390539, Lot#C0822; Citation: PMID: 35455080; PMID: 35265208
 JAK2 (C-10) is recommended for detection of JAK2 of mouse, rat and human origin by Western Blotting (starting dilution 1:100, dilution range 1:100-1:1000), immunoprecipitation [1-2 µg per 100-500 µg of total protein (1 ml of cell lysate)], immunofluorescence (starting dilution 1:50, dilution range 1:50-1:500) and solid phase ELISA (starting dilution 1:30, dilution range 1:30-1:3000).
 JAK2 (C-10) is a mouse monoclonal antibody specific for an epitope mapping between amino acids 752-780 of JAK2 of mouse origin.
<https://www.scbt.com/p/jak2-antibody-c-10?requestFrom=search>
 JAK3: Cell Signaling Technology, Cat# 3775, Lot#6; Citation: PMID: 34286840; PMID: 32639993
 REACTIVITY: H; SENSITIVITY: Endogenous; MW (kDa): 115; SOURCE: Rabbit
 Application-Dilution: Western Blotting-1:1000
 Jak3 Antibody detects endogenous levels of total Jak3 protein. No cross-reactivity was detected with other family members at physiological conditions. Polyclonal antibodies are produced by immunizing animals with a synthetic peptide corresponding to residues at the carboxy-terminus of Jak3. Antibodies are purified by protein A and peptide affinity chromatography.
<https://www.cellsignal.com/products/primary-antibodies/jak3-antibody/3775>
 STAT2(D9J7L): Cell Signaling Technology, Cat# 72604, Lot#4; Citation: PMID: 34725437; PMID: 35301282
 REACTIVITY: H M; SENSITIVITY: Endogenous; MW (kDa): 97, 113; Source/Isotype: Rabbit IgG
 Application-Dilution: Western Blotting-1:1000; Immunoprecipitation-1:50; Immunofluorescence (Immunocytochemistry)-1:100 - 1:400; Flow Cytometry-1:50 - 1:200; Chromatin IP-1:50; Chromatin IP-seq-1:50; CUT&RUN-1:50
 Stat2 (D9J7L) Rabbit mAb recognizes endogenous levels of total Stat2 protein. Monoclonal antibody is produced by immunizing animals with a synthetic peptide corresponding to residues surrounding Leu706 of human Stat2 protein.
<https://www.cellsignal.com/products/primary-antibodies/stat2-d9j7l-rabbit-mab/72604>
 ASCL1(EPR19840): Abcam, Cat# ab211327, Lot#GR3368513-4; Citation: PMID: 31883968; PMID: 33547076
 Host species: Rabbit; Suitable for: IHC-P, WB, ICC/IF, IP; Reacts with: Mouse, Human
 Immunogen: Recombinant full length protein. This information is proprietary to Abcam and/or its suppliers.
<https://www.abcam.com/mash1achaete-scute-homolog-1-antibody-epr19840-ab211327.html>
 Sox2(D9B8N): Cell Signaling Technology, Cat #23064S, Lot#1; Citation: PMID: 34934057; PMID: 34619150; PMID: 34686327
 REACTIVITY: H M; SENSITIVITY: Endogenous; MW (kDa): 35; Source/Isotype: Rabbit IgG
 Application-Dilution: Western Blotting-1:1000; Immunoprecipitation-1:100; Immunofluorescence (Frozen)-1:400; Immunofluorescence (Immunocytochemistry)-1:400; Flow Cytometry-1:100; Chromatin IP-1:50; Chromatin IP-seq-1:50; CUT&RUN-1:50
 Sox2 (D9B8N) Rabbit mAb recognizes endogenous levels of total Sox2 protein. The abundant nonspecific cytoplasmic labeling was observed in adult brain by immunofluorescence (IF). However, the specific staining was observed in embryonic tissue, including brain, by IF. Monoclonal antibody is produced by immunizing animals with a synthetic peptide corresponding to residues surrounding Ala188 of human Sox2 protein.
https://www.cellsignal.com/products/primary-antibodies/sox2-d9b8n-rabbit-mab/23064?site-search-type=Products&N=4294956287&Ntt=23064s&fromPage=plp&_requestid=659745
 Anti-Histone H3 (acetyl K27) antibody-ChIP Grade, Abcam, Cat# ab4729, Lot# GR3357415-1; Citation: PMID: 33147444; PMID: 32592040
 Rabbit polyclonal to Histone H3 (acetyl K27) - ChIP Grade; Host species: Rabbit; Suitable for: ICC/IF, WB, IHC-P, ChIP, PepArr; Reacts with: Mouse, Rat, Cow, Human, Recombinant fragment
 Predicted to work with: Chicken, Xenopus laevis, Arabidopsis thaliana, Drosophila melanogaster, Monkey, Zebrafish, Plasmodium falciparum, Rice, Cyanidioschyzon merolae
 Immunogen
 Synthetic peptide corresponding to Human Histone H3 aa 1-100 (acetyl K27) conjugated to keyhole limpet haemocyanin.
 (Peptide available as ab24404)
https://www.abcam.com/Histone-H3-acetyl-K27-antibody-ChIP-Grade-ab4729.html?gclid=Cj0KCQjwtvqBhCVARIsAFUxcRscatj6ayli9g1JB61bfrTKabsO7yOQ1H0cOblwUsuUqPcd9DQwZfcAkrLEALw_wcB
 Tri-Methyl-Histone H3 (Lys27) (C36B11) Rabbit mAb, Cell Signaling Technology, Cat #9733S, Lot #8; Citation: PMID: 35399730; PMID: 35405016
 REACTIVITY: H M R Mk; SENSITIVITY: Endogenous; MW (kDa): 17; Source/Isotype: Rabbit IgG
 Application-Dilution: Western Blotting-1:1000; IHC-Leica® Bond™-1:200 - 1:800; Immunohistochemistry (Paraffin)-1:100 - 1:400; Immunofluorescence (Immunocytochemistry)-1:800 - 1:3200; Flow Cytometry-1:100 - 1:400; Chromatin IP-1:50; Chromatin IP-seq-1:50; CUT&RUN-1:50

Tri-Methyl-Histone H3 (Lys27) (C36B11) Rabbit mAb detects endogenous levels of histone H3 only when tri-methylated on Lys27. The antibody does not cross-react with non-methylated, mono-methylated or di-methylated Lys27. In addition, the antibody does not cross-react with mono-methylated, di-methylated or tri-methylated histone H3 at Lys4, Lys9, Lys36 or Histone H4 at Lys20. Monoclonal antibody is produced by immunizing animals with a synthetic peptide corresponding to the amino terminus of histone H3 in which Lys27 is tri-methylated.
https://www.cellsignal.com/products/primary-antibodies/tri-methyl-histone-h3-lys27-c36b11-rabbit-mab/9733?Ntk=Products&Ntt=9733&gclid=Cj0KCQjwtvqVBhCVARIsAFUxcRtK6k55Qe_aQaKRlyDOqapNftlhMm9xuW6LqlhGzwSJ7IctyCFRvVoaAqENEALw_wcb&gclsrc=aw.ds

Alexa Fluor® 647 Anti-Cytokeratin 8(EP1628Y): Abcam, Cat #ab192468, Lot#GR198609-1; Citation: PMID: 29096715
 Host species: Rabbit; Conjugation: Alexa Fluor® 647. Ex: 652nm, Em: 668nm; Suitable for: ICC/IF, Flow Cyt (Intra); Reacts with: Human Immunogen: Synthetic peptide. This information is proprietary to Abcam and/or its suppliers.
<https://www.abcam.com/alexa-fluor-647-cytokeratin-8-antibody-ep1628y-ab192468.html>

Alexa Fluor® Anti-Cytokeratin 18(E431-1): Abcam, Cat #ab194125, Lot#GR-200266-1; Citation: PMID: 23966837
 Host species: Rabbit; Conjugation Alexa Fluor® 647. Ex: 652nm, Em: 668nm; Suitable for: Flow Cyt, ICC/IF; Reacts with: Human Immunogen: Full length native protein (purified) corresponding to Human Cytokeratin 18.
<https://www.abcam.com/cytokeratin-18-antibody-e431-1-alexa-fluor-647-ab194125.html>

Alexa Fluor® 647 Anti-Cytokeratin 5(EP1601Y): Abcam, Cat #ab193895, Lot#GR-219431-2; Citation: PMID: 31839569; PMID: 33025905; PMID: 32747751
 Host species: Rabbit; Conjugation: Alexa Fluor® 647. Ex: 652nm, Em: 668nm; Suitable for: Flow Cyt (Intra), ICC/IF; Reacts with: Human Immunogen: Synthetic peptide. This information is proprietary to Abcam and/or its suppliers.
<https://www.abcam.com/alexa-fluor-647-cytokeratin-5-antibody-ep1601y-ab193895.html>

Alexa Fluor® 647 Anti-Cytokeratin 14(EP1612Y): Abcam, Cat #ab192056, Lot#GR-201705-1; Citation: PMID: 27762336
 Host species: Rabbit; Conjugation: Alexa Fluor® 647. Ex: 652nm, Em: 668nm; Suitable for: ICC; Reacts with: Human Does not react with: Mouse, Rat
 Immunogen: Synthetic peptide. This information is proprietary to Abcam and/or its suppliers.
<https://www.abcam.com/alexa-fluor-647-cytokeratin-14-antibody-ep1612y-ab192056.html>

Nkx3.1(4H4): Abcam, Cat #ab96482, Lot#GR-165836-2
 Host species: Mouse; Suitable for: WB, ELISA, IHC-P, Flow Cyt; Reacts with: Human
 Immunogen Recombinant fragment, corresponding to amino acids 1-234 of Human Nkx3.1
<https://www.abcam.com/nkx31-antibody-4h4-ab96482.html>

PSA/KLK3 (D6B1): Cell Signaling Technology, Cat #5365, Lot#4; Citation: PMID: 34698359; PMID: 35402240
 REACTIVITY: H; SENSITIVITY: Endogenous; MW (kDa): 29; Source/Isotype: Rabbit IgG
 Application-Dilution: Western Blotting-1:1000; Immunoprecipitation-1:50; Immunofluorescence (Immunocytochemistry)-1:200; Flow Cytometry-1:50
 PSA/KLK3 (D6B1) XP® Rabbit mAb recognizes endogenous levels of total PSA/KLK3 protein. Monoclonal antibody is produced by immunizing animals with a synthetic peptide corresponding to residues surrounding Phe165 of human PSA/KLK3 protein.
<https://www.cellsignal.com/products/primary-antibodies/psa-klk3-d6b1-xp-rabbit-mab/5365>

NDRG1 (D8G9): Cell Signaling Technology, Cat #9485, Lot#4; Citation: PMID: 33499898; PMID: 33334021
 REACTIVITY: H Mk; SENSITIVITY: Endogenous; MW (kDa): 46, 48; Source/Isotype: Rabbit IgG
 Application-Dilution: Western Blotting-1:1000; Immunoprecipitation-1:100; Immunohistochemistry (Paraffin)-1:800; Immunofluorescence (Immunocytochemistry)-1:200
 NDRG1 (D8G9) XP® Rabbit mAb recognizes endogenous levels of total NDRG1 protein. Monoclonal antibody is produced by immunizing animals with a synthetic peptide corresponding to residues near the carboxy terminus of human NDRG1 protein.
<https://www.cellsignal.com/products/primary-antibodies/nrdg1-d8g9-xp-rabbit-mab/9485>

Vimentin (D21H3): Cell Signaling Technology, Cat #5741, Lot#8; Citation: PMID: 35428310; PMID: 35414768
 REACTIVITY: H M R Mk; SENSITIVITY: Endogenous; MW (kDa): 57; Source/Isotype: Rabbit IgG
 Application-Dilution: Western Blotting-1:1000; IHC-Leica® Bond™-1:200 - 1:800; Immunohistochemistry (Paraffin)-1:100 - 1:400; Immunofluorescence (Immunocytochemistry)-1:50 - 1:200; Flow Cytometry-1:50 - 1:200
 Vimentin (D21H3) XP® Rabbit mAb detects endogenous levels of total vimentin protein. Monoclonal antibody is produced by immunizing animals with a synthetic peptide corresponding to residues surrounding Arg45 of human vimentin protein.
<https://www.cellsignal.com/products/primary-antibodies/vimentin-d21h3-xp-rabbit-mab/5741>

Synaptophysin (D8F6H): Cell Signaling Technology, Cat #36406, Lot#1; Citation: PMID: 34572962; PMID: 34671017
 REACTIVITY: H M R; SENSITIVITY: Endogenous; MW (kDa): 38; Source/Isotype: Rabbit IgG
 Application-Dilution: Western Blotting-1:1000; Immunohistochemistry (Paraffin)-1:200; Immunofluorescence (Frozen)-1:100
 Synaptophysin (D8F6H) XP® Rabbit mAb recognizes endogenous levels of total Synaptophysin protein. Monoclonal antibody is produced by immunizing animals with a synthetic peptide corresponding to residues surrounding Gly299 of human Synaptophysin protein.
<https://www.cellsignal.com/products/primary-antibodies/synaptophysin-d8f6h-xp-rabbit-mab/36406>

Peroxidase AffiniPure Goat Anti-Mouse IgG (H+L)(AB_10015289): Jackson ImmunoResearch, Cat# 115-035-003 Citation: PMID: 35240918; PMID: 35017439
 Based on immunoelectrophoresis and/or ELISA, the antibody reacts with whole molecule mouse IgG. It also reacts with the light chains of other mouse immunoglobulins. No antibody was detected against non-immunoglobulin serum proteins. The antibody may cross-react with immunoglobulins from other species.
 Whole IgG antibodies are isolated as intact molecules from antisera by immunoaffinity chromatography. They have an Fc portion and two antigen binding Fab portions joined together by disulfide bonds and therefore they are divalent. The average molecular weight is reported to be about 160 kDa. The whole IgG form of antibodies is suitable for the majority of immunodetection procedures and is the most cost effective.
<https://www.jacksonimmuno.com/catalog/products/115-035-003>

Peroxidase AffiniPure Goat Anti-Rabbit IgG (H+L)(AB_2313567): Jackson ImmunoResearch, Cat# 111-035-003 Citation: PMID: 35017439; PMID: 35761940
 Based on immunoelectrophoresis and/or ELISA, the antibody reacts with whole molecule rabbit IgG. It also reacts with the light chains of other rabbit immunoglobulins. No antibody was detected against non-immunoglobulin serum proteins. The antibody may cross-react with immunoglobulins from other species.
 Whole IgG antibodies are isolated as intact molecules from antisera by immunoaffinity chromatography. They have an Fc portion and two antigen binding Fab portions joined together by disulfide bonds and therefore they are divalent. The average molecular weight is reported to be about 160 kDa. The whole IgG form of antibodies is suitable for the majority of immunodetection procedures and is

the most cost effective.

<https://www.jacksonimmuno.com/catalog/products/111-035-003>

Alexa Fluor® 647-conjugated AffiniPure Goat Anti-Mouse IgG (H+L)(AB_2338902): Jackson ImmunoResearch, Cat# 115-605-003
Citation: PMID: 35310356; PMID: 35595807

Based on immunoelectrophoresis and/or ELISA, the antibody reacts with whole molecule mouse IgG. It also reacts with the light chains of other mouse immunoglobulins. No antibody was detected against non-immunoglobulin serum proteins. The antibody may cross-react with immunoglobulins from other species.

Whole IgG antibodies are isolated as intact molecules from antisera by immunoaffinity chromatography. They have an Fc portion and two antigen binding Fab portions joined together by disulfide bonds and therefore they are divalent. The average molecular weight is reported to be about 160 kDa. The whole IgG form of antibodies is suitable for the majority of immunodetection procedures and is the most cost effective.

<https://www.jacksonimmuno.com/catalog/products/115-605-003>

Alexa Fluor® 647-conjugated AffiniPure Goat Anti-Rabbit IgG (H+L)(AB_2338078): Jackson ImmunoResearch, Cat# 111-605-144
Citation: PMID: 35442190; PMID: 35721135

Based on immunoelectrophoresis and/or ELISA, the antibody reacts with whole molecule rabbit IgG. It also reacts with the light chains of other rabbit immunoglobulins. No antibody was detected against non-immunoglobulin serum proteins. The antibody has been tested by ELISA and/or solid-phase adsorbed to ensure minimal cross-reaction with human, mouse and rat serum proteins, but it may cross-react with immunoglobulins from other species.

Whole IgG antibodies are isolated as intact molecules from antisera by immunoaffinity chromatography. They have an Fc portion and two antigen binding Fab portions joined together by disulfide bonds and therefore they are divalent. The average molecular weight is reported to be about 160 kDa. The whole IgG form of antibodies is suitable for the majority of immunodetection procedures and is the most cost effective.

<https://www.jacksonimmuno.com/catalog/products/111-605-144>

Donkey Anti-Mouse IgG Antibody (Biotin-SP (long spacer))(AB_2307438): Jackson ImmunoResearch, Cat# 715-065-150
Citation: PMID: 35402512; PMID: 35579705

Based on immunoelectrophoresis and/or ELISA, the antibody reacts with whole molecule mouse IgG. It also reacts with the light chains of other mouse immunoglobulins. No antibody was detected against non-immunoglobulin serum proteins. The antibody has been tested by ELISA and/or solid-phase adsorbed to ensure minimal cross-reaction with bovine, chicken, goat, guinea pig, syrian hamster, horse, human, rabbit and sheep serum proteins, but it may cross-react with immunoglobulins from other species.

Whole IgG antibodies are isolated as intact molecules from antisera by immunoaffinity chromatography. They have an Fc portion and two antigen binding Fab portions joined together by disulfide bonds and therefore they are divalent. The average molecular weight is reported to be about 160 kDa. The whole IgG form of antibodies is suitable for the majority of immunodetection procedures and is the most cost effective.

<https://www.jacksonimmuno.com/catalog/products/715-065-150>

Donkey Anti-Rabbit IgG Antibody (Biotin-SP (long spacer))(AB_2340593): Jackson ImmunoResearch, Cat# 711-065-152
Citation: PMID: 35530297; PMID: 35521515

Based on immunoelectrophoresis and/or ELISA, the antibody reacts with whole molecule rabbit IgG. It also reacts with the light chains of other rabbit immunoglobulins. No antibody was detected against non-immunoglobulin serum proteins. The antibody has been tested by ELISA and/or solid-phase adsorbed to ensure minimal cross-reaction with bovine, chicken, goat, guinea pig, syrian hamster, horse, human, mouse, rat and sheep serum proteins, but it may cross-react with immunoglobulins from other species.

Whole IgG antibodies are isolated as intact molecules from antisera by immunoaffinity chromatography. They have an Fc portion and two antigen binding Fab portions joined together by disulfide bonds and therefore they are divalent. The average molecular weight is reported to be about 160 kDa. The whole IgG form of antibodies is suitable for the majority of immunodetection procedures and is the most cost effective.

<https://www.jacksonimmuno.com/catalog/products/711-065-152>

Eukaryotic cell lines

Policy information about [cell lines](#)

Cell line source(s)

Parental LNCaP/AR and CWR22Pc prostate cancer cell lines were obtained from Dr. Charles Sawyers' laboratory at MSKCC, Du145 (#HTB-81) and PC3 (#CRL-1435) cell lines were purchased from ATCC. CWR-R1 and WA01 cells were maintained in the Donald J. Vander Griend laboratory and were not directly used in this study. The existing SOX2 ChIP-Seq data generated from those two cell lines were downloaded from GSE166185. Trp53loxP/loxP, Rb1loxP/loxP murine organoids were generated from Trp53loxP/loxP, Rb1loxP/loxP mice. Human organoids were obtained from Dr. Yu Chen's laboratory at MSKCC (Tang et al., 2020, <https://doi.org/10.1101/2020.10.26.355925>; Mao et al., PMID: 202134417459). The organoids are cultured in 3D Matrigel according to protocol previously described (Gao et al., 2014, PMID: 25201530). Further information and requests for resources and reagents should be directed to and will be fulfilled by the corresponding author, Dr. Ping Mu (ping.mu@utsouthwestern.edu). All cell lines, plasmids and other reagents generated in this study are available from the corresponding author with a completed Materials Transfer Agreement if there is potential for commercial application.

Authentication

STR analysis (DNA fingerprinting) were performed to validate the identity of the cell lines every year and compared to ATCC cell line profiles to ensure that all the cell identities remain stable throughout the entire proposed studies. For all prostate organoids, the morphologies were assessed under microscope and their growth and mycoplasma contamination were also be tested monthly.

Mycoplasma contamination

All cell cultures were assessed for mycoplasma monthly via the highly sensitive MycoAlertTM PLUS Mycoplasma Detection kit (Lonza, Cat #LT07-710) and all results were negative.

Commonly misidentified lines
(See [ICLAC](#) register)

No commonly misidentified cell lines were used in this study.

Animals and other organisms

Policy information about [studies involving animals](#); [ARRIVE guidelines](#) recommended for reporting animal research

Laboratory animals

Male C.B-1g-1b/lcr Tac-Prkdcscid SCID (Severe Combined Immunodeficient) mice of 6-7 week-old were used for xenograft experiments, which were purchase from Taconic Biosciences. All animals were housed in humidity and temperature-controlled conditions with a 12h light 12h dark cycle in the pathogen free facilities at the University of Texas, Southwestern by the Animal Resource Center (ARC), and monitored closely to minimize discomfort, distress, pain or injury throughout all the course of in vivo experiments. Animal would be removed from the study and euthanized if any signs of pain and distress were detected, or the tumor volume reaches 2000mm³. The maximal tumor size was not exceeded in all reported studies.

Wild animals

This study did not use wild animals

Field-collected samples

This study did not use field collected samples

Ethics oversight

All procedures were performed in accordance with the recommendations of the Panel on Euthanasia of the American Veterinary Medical Association and the animal protocol was approved by Institutional Animal Care and Use Committee (IACUC) of UT Southwestern Medical Center (protocol #2019-102493).

Note that full information on the approval of the study protocol must also be provided in the manuscript.

Flow Cytometry

Plots

Confirm that:

- The axis labels state the marker and fluorochrome used (e.g. CD4-FITC).
- The axis scales are clearly visible. Include numbers along axes only for bottom left plot of group (a 'group' is an analysis of identical markers).
- All plots are contour plots with outliers or pseudocolor plots.
- A numerical value for number of cells or percentage (with statistics) is provided.

Methodology

Sample preparation

For FACS-based competition assay, the LNCaP/AR cells from different genotypes were digested to single cells, then were washed with PBS by centrifugation. Then the competition cell mixture of sgTP53/RB1-RFP cells and sgNT-GFP cells were previously cultured *in vitro* before starting the competition assay.

Instrument

Attune NxT Acoustic Focusing Cytometer by Thermo Fisher

Software

Attune Nxt software (version 4.2.1627.1) and FlowJo software (version 10.8.0) .

Cell population abundance

The cell mixtures of sgNT-GFP and sgTP53/RB1-RFP were treated in CSS medium with 10µM enzalutamide for 8 days and the number of GFP/RFP positive cells were measured by FACS on Day0, 4 and 8. Relative cell number fold change was calculated and normalized to veh treated group as previously described (Zhang et al., 2020, PMID: 32220301).

Gating strategy

LNCaP/AR cells were first gated based on SSC-H/FSC-A@FSC-H before measuring the RFP/GFP signals for the percentage of positive cells

Tick this box to confirm that a figure exemplifying the gating strategy is provided in the Supplementary Information.